Multi-material and multi-structural optimisation for generative design of controlled property domains

A THESIS SUBMITTED TO THE AUCKLAND UNIVERSITY OF TECHNOLOGY

IN FULFILMENT OF THE REQUIREMENTS FOR THE DEGREE OF

DOCTOR OF PHILOSOPHY

Supervisors

Prof. Sarat Singamneni

A/Prof. Loulin Huang

April 2022

By

Wuxin Yang

School of Engineering, Computer and Mathematical Sciences

Auckland University of Technology Auckland New Zealand

Abstract

Most naturally evolved structures exhibit the highest level of optimisation in terms of the material properties through carefully selected and adopted compositional and structural variations resulting in the functional grading of the highest order in the materiality of the continuum. Engineered designs and products lack such finer adjustments in the material attributes, mainly due to the limitations of the manufacturing processes, which have by far been suitable for bulk material consolidation mostly. With the advent of additive manufacturing technologies, the point-by-point material consolidation realm has become a reality, giving renewed opportunities to revisit the functional material grading regimes. Considering the immense benefits of being able to design and manufacture products with varying material characteristics to suit to specific performance attributes, the multi-material design and manufacturing opportunities have attracted significant research attention in recent years.

In particular, the multi-material printing based on the multi-jetting UV cured polymer processing theoretically allows for close control of the material composition and properties within a given printed part domain, allowing to design the material rather than designing a part with a given material for the target functionality. Based on these unique qualities, multi-material printing has been evaluated significantly, exploring the generative design dream to fabricate parts with carefully controlled material properties. However, the digitally mixed acrylic resins being inferior in mechanical properties, these promising developments were restrained to theoretical studies in most cases. The point-by-point or line-by-line material consolidation mechanics typical of all additive technologies can be further exploited to derive a step-change in the pursuit of generative material design to achieve tailored performance attributes.

The current research addresses this gap by extending the multi-material dispersion problem to optimise the structural forms of voxelised geometries developed by

discretising the problem domains of the design task. The challenge is still a generative design task and needs the use of multi-objective evolutionary algorithms integrated with the numerical evaluation schemes to explore the multi-material or multi-structural continuum mechanics. Beginning with the standard genetic algorithm, a variety of other evolutionary algorithms are used for the optimisation schemes, while the numerical simulations of the multi-material or multi-structural domains are implemented in COMSOL Multiphysics. The initial focus was on establishing the relative merits of different evolutionary algorithms development of the MATLAB coding that integrates the iterative interactions and evolutionary progress based on the optimisation and numerical simulation schemes. The multi-material case was solved during this stage, with a greater focus on the computational algorithms and processes. Once this was achieved, the structural manipulation of voxelised domains was undertaken for single material printing of generatively designed structural shapes using more advanced optimisation algorithms. The outcomes of the research are positive as an effective computational workflow was developed that will allow to generatively design a structural form with either multi-material or multi-structural optimised topologies for pre-set frequency, deflection, or other mechanical property responses.

Contents

List of Abbreviations

FDM	Fused Deposition Modelling
SLS	Powder Bed Fusion Based Selective Laser Sintering
SLM	Selective Laser Melting
EBM	Electron Beam Melting
GA	Binary Genetic Algorithms
NEAT	Neuro-Evolution Of Augmenting Topologies
CPPN-NEAT	Compositional Pattern Producing Networks With Neuro-Evolution Of Augmenting Topologies
CMA-ES	Covariance Matrix Adaptation Evolution Strategy
CMC	Ceramic Matrix Composites
FRP	Fibre-Reinforced Polymer
FGM	Functionally Graded Materials
DED	Direct Energy Deposition
MMAM	Multi-Material Additive Manufacturing
AM	Additive Manufacturing
CAD	Computer-Aided Design
BSSRDF	Bidirectional Scattering-Surface Reflectance Distribution Function
AM	Additive Manufacturing
MMAM	Multi-Material Additive Manufacturing
CAD	Computer-Aided Design

PSO	Particle Swarm Optimisation
ANN	Artificial Neural Network
SIMP	Solid Isotropic Material With Penalisation
ESO	Evolutionary Structural Optimisation
PDE	Partial Differential Equation
FEM	Finite Element Method
FEA	Finite Element Analysis
ML	Machine Learning
CNN	Convolutional Neural Network
FOS	Factor Of Safety
DNN	Deep Neural Network
ASTM	American Society for Testing and Materials
TS	Target Set
TVA	Tuned Vibrational Absorber
TMD	Tuned Mass Damper
SSM	Single Structured Material
MM	Multi-Material
NSGA-II	Non-Dominated Sorting Genetic Algorithm II
CUDA	Compute Unified Device Architecture

List of Figures

List of Tables

Attestation of Authorship

I hereby declare that this submission is my own work and that, to the best of my knowledge and belief, it contains no material previously published or written by another person nor material that to a substantial extent has been accepted for the qualification of any other degree or diploma of university or other institution of higher learning.

April 25 2022

-- -----------------------

Signature of candidate Date

Publications

In Refereed Journals

Yang, W., Calius, E., Huang, L., & Singamneni, S. (2020). Artificial Evolution and Design for Multi-Material Additive Manufacturing. *3D Printing and Additive Manufacturing, 7(6).*

Yang, W., Huang, L., & Singamneni, S. (2022). Generative Design of Structured Materials for Controlled Frequency Responses. *3D Printing and Additive Manufacturing*.

Yang, W., Huang, L., & Singamneni, S., Topology optimisation for controlled structural deflections, Currently communicated.

Yang, W., Huang, L., & Singamneni, S. Evolutionary algorithms for generative design of materiality, a perspective, to be communicated shortly.

Chapter 1

Introduction

1.1. Biomimicking design and engineering

Whether it is the bone constructions of the fauna or the stem structures of the flora, nature has abundant examples of controlled arrangements of materials attained through evolution to impart functionally graded performance attributes to different parts. The beak of a Humboldt squid gradually changing its internal structure to functionally grade the properties from a stiff tanned tip to a soft untanned base is an example of the level of evolution and adaptation biological systems strive to go through to attain controlled material property variations. While size, shape and compositional variations are the obvious means of achieving controlled functional property variations within structural systems, variations in the density and meso-structural intensities are also common in bones to achieve differential responses to varied stress and stain intensities due to applied loads.

Engineering design, however, depends mostly on optimising the overall shape of the system to achieve the functional attributes based on the bulk properties of a single material option. Metals, polymers and ceramics are by far the most common material types available as immediate options. Different combinations of these material systems also have evolved over the years due to the constant developments in materials science and technology. Different alloy systems as combinations of a metal with other elements, composites made possible by adding particulate and fibrous inclusions in polymer matrices, metal plus ceramic composites and metal matrix composites are examples where the good properties of different ingredients are combined in a material option with an overall better performance under given conditions. The advent of these new material classes added great opportunities for designers to choose from a wide range of materials to suit different application targets.

Despite these developments, the modern materials options are still homogeneous in terms of their nature and performance within a designed and fabricated component. Polymer and metal matrix composites definitely give rise to the possibility of achieving some amount of control over the heterogeneous property variation, albeit to a limited extent. For example, in fibre reinforced polymers, the size, distribution, and direction of orientation of the fibres can be used to control the nature of the material responses to loading in different directions. Also, cold worked components of different alloy systems can be made to have grain orientations in preferred directions to achieve directional properties. However, these responses are still at a relatively uniform level and do not really allow to achieve the true biomimicking dream, where engineering designs can exploit the point-by-point variation of material properties to match the component attributes to specific functional requirements. Limitations in the traditional manufacturing methods are central to these shortcomings.

1.2. Manufacturing hurdles and additive advances

Traditional manufacturing is mostly based on subtractive methods where the required design form is carved out of bulk by removing unwanted material portions. Some casting processes are to some extent additive in nature, but confined to specific forms of rigid moulds and are mostly used as methods to achieve the preliminary shapes requiring further processing by the subtractive means. Processes like welding also are additive in nature but at a much larger scale and by no means qualify to satisfy the point-by-point control over the consolidation required for the material design targets mentioned above. Other processes used for fibre reinforced composites or powder metallurgy methods for metal matrix composites are also bulk methods and do not actually provide means of closely controlling the dispersion and orientations of the filler phases. The recent advances leading to the layered manufacturing methods appear to provide better means of controlling the constitution of the material within a given part domain.

Commonly known as 3D printing, the additive processing methods are a set of technologies that evolved based on the point-by-point and line-by-line material consolidation mechanics. From being mere rapid prototyping solutions with a couple of polymeric material options, a few of these technologies grew rapidly in the past couple of decades and advanced to the stages of being able to produce complex functional components with many different material options, including metals and alloys. From 3D printing to rapid prototyping and then rapid tooling and manufacturing, the evolution has been quite rapid, and the technologies are now considered industrially acceptable and referred to as additive manufacturing. While there are a variety of additive processing technologies, the UV cured acrylic resin-based stereolithography or multi-jet printing, polymer filament based fused deposition modelling (FDM), powder bed fusion based selective laser sintering (SLS) or selective laser melting (SLM) and the electron beam melting (EBM), and the binder jetting based ceramic 3D printing are the most successful ones commonly used now. While all these technologies offer opportunities for point-by-point control over the material make-up, the multi-jet and multi-material printing methods directly offer immediate solutions, albeit with great limitations, as discussed next.

1.3. Multi-material printing promises and problems

The Stereolithography process was the first of the layer-wise printing methods that had evolved from the very early years of the additive realm. UV curable polymers in the liquid form are treated with a flash of light to cure the liquid selectively into solid sections, and the stacking of the solid sections one over the other leads to the building of the 3D forms. The slicing of the solid CAD models, the sequential exposure to the UV light and the feed movements along the build direction are all coordinated through the hardware and software systems. A relatively recent version of material consolidation by this method involves polymer jetting through nozzles onto a build platform and scanning by a UV light to consolidate layer after layer. The more advanced Connex Systems by Stratasys or the Multi-jet printing systems such as ProJet MJP 5600 by 3D systems use two different liquid polymers simultaneously and mix them in different proportions to constitute polymeric materials with varying properties as they are deposited on the building substrate, point-by-point.

Both these systems use two different polymeric materials, one soft and the other one stiff. During the printing process, the liquid polymers A and B can be mixed in varying proportions before being jetted through the multiple nozzles to be deposited at different locations on the building substrate. The CAD model can be discretised into small volume elements or voxels, and each voxel volume can be filled with a particular combination of soft and stiff polymer options to achieve controlled property variation. There is a certain limitation on the minimum size of the voxels, but this process definitely helps to achieve the seamlessly controlled variation of material properties from one point to the other within the domain of any given part.

Evidently, the multi-jet printing by UV cured polymeric material options is the ultimate dream coming true for designers to use the material property variation as yet another avenue to achieve the functional targets from material objects. Instead of designing a component for functionality based on a given material of fixed properties, the material itself is designed to match the component performance with the target functionality. This is a radically different approach to engineering design, and the ability to vary the material attributes programmatically will allow for a plethora of new opportunities. Naturally, multi-material printing has attracted significant research attention in the recent past as many attempts were made to explore the use of the material dispersion mechanisms to tailor the properties of printed components to meet multi-objective targets.

While this is all seemingly wonderful in terms of playing with material compositions and the ensuing property variations within a given part domain, the downside is that the materials options are of inferior quality in terms of mechanical and other properties. The acrylic resins digitally mixed in the injection print heads and subsequently cured by UV light are not truly engineering polymers. They will allow simulating the variation of properties from very soft to very stiff and in many different combinations within a given part domain. However, the mechanical properties and the overall performance of the printed parts are of no real engineering significance. These multi-material solutions became successful avenues to practically test the analytical and numerical predictions of the performance attributes of computationally designed product concepts. Beyond that, the solutions are not really practical for any engineering application, as these materials are not really load-bearing. Beginning with the multi-material solutions, the current research addresses these shortcomings through the development of a novel cellular structural solution.

1.4. The research context and objectives

The main focus of this research is on the exploration of the multi-dimensional functional responses possible through closely controlled material property variations in engineered product component domains. As was the case with numerous other approaches reported earlier, the study begins with the multi-material printing option as a possible practical solution. This is the first stage of this research, which will allow exploring the design space with continuously varying material compositions and properties within the set limits, paving the way for the establishment of the optimisation schemes and their integration with the analysis tools such as the finite element solutions. Further, instead of just solving for either minimisation or maximisation of a certain response, simultaneously satisfying a set of conflicting property responses will be sought through the optimisation of the material composition and properties. For example, converging on the material distribution pattern will allow a beam to attain a selected set of values for the first six natural frequencies.

In the next stage of the research, the limitations of the multi-material printing options that result in the lack of practical applications to the optimised material solutions explored in the first stage are resolved. For this, the problem domain is discretised into voxelised cellular structures, and the point-wise property variation is achieved by individually altering the geometries of the unit cells. Though limited in the range of properties possible compared to the multi-material solutions, the optimised voxel structural geometries are amenable for direct fabrication from the digital data, using different additive manufacturing technologies by printing with a single homogeneous material. Once again, the multi-objective optimisation and generative design schemes are to be applied to the problem of optimising the geometrical combinations of the voxel structures to achieve the pre-set first six natural frequency responses of the six degrees of freedom.

The third and final stage of the research is to evaluate the possible optimisation of the material distribution schemes for achieving multi-dimensional responses under mechanical loading conditions. Optimisation of the voxel structural geometries is again the avenue for controlling the material property variations. Deflections at specific points of a beam under point loading are considered as the set of responses for the multi-objective target. With the beam's overall dimensions and the base material properties remaining the same, the beam deflection patterns are to be matched with pre-set conditions, purely based on the identification of the optimum geometries of the individual unit cells used as the voxels in making up the overall structure of the beam. Together with the variation in the location of the external loading, simultaneously controlling the beam deflections at multiple points truly becomes a multi-objective optimisation problem.

1.5. Research plans, methods, and organisation of the thesis

Three definite objectives drive the research planning and methodologies used in this thesis. They are: 1) evaluation of the multi-material solution for multiple frequency responses, 2) evaluation of the controlled variations of macro geometries of cellular arrangements for controlled frequency responses and finally, 3) optimisation of the voxel geometries for selected mechanical property responses within a multi-objective generative design scheme. The analytical and numerical modelling are to be developed and implemented to achieve these objectives in the same order, as the progress from one stage prepares the base for the next stage. Research methods need to be developed for the optimisation schemes and their integration with the analysis of the mechanics of the multi-material and multi-property continuum.

Considering the varying schemes proposed for achieving the material property variations, different optimisation algorithms become necessary to be employed based on their relative strengths and weaknesses. The generative design method based on binary genetic algorithms (GA) was found to be the best option for solving the multi-material optimisation problem. Once the problem domain is discretised into finite volumes, the multi-material dispersion solution can be handled through topological optimisation by the searching algorithm. More advanced search algorithms such as neuro-evolution of augmenting topologies (NEAT) and compositional pattern producing networks with neuro-evolution of augmenting topologies (CPPN-NEAT) will also be used to further ascertain the optimised material distributions to satisfy the multi-dimensional frequency responses. A further extension of the multi-material optimisation scheme by GA will also be considered to achieve a pre-set multi-component mechanical property response such as the toughness of a uniaxially loaded specimen.

Exploring the geometrical forms of cellular voxel structures for matching frequency responses needs a more flexible optimisation scheme than the genetic algorithm based search algorithms. After careful consideration of different methods, the covariance matrix adaptation evolution strategy (CMA-ES) algorithm was identified and implemented. Apart from the generative design of the cellular structure of the beam for pre-set eigenfrequency response constraints under free vibrations, the algorithm has also been able to solve for the optimum structure of the beam for selected frequency responses under forced vibrations. The same methodology based on the CMA-ES algorithm is also implemented for the optimisation of the cellular beam structure to achieve specific deflection profiles as evaluated by the deflection responses at specific points under specific loading conditions.

Central to all these tasks is the use of a numerical scheme for analysing the continuum mechanics of the multi-material domains. Essential for the evaluation of the fitness functions, numerical simulations are implemented in the COMSOL Multiphysics commercial finite element package. All the optimisation algorithms and their integration with the finite element evaluation schemes are achieved through computational codes implemented in MATLAB, version R2017B. A detailed literature review is presented next in Chapter 2, which allows converging on the research gaps and specific questions to be addressed. Chapters 3 to 5 present the analytical and numerical experiments conducted to fulfil objectives 1 to 3, respectively and the ensuing results and discussions.

Chapter 2

Literature Review

2.1. Engineering materials and functional grading

Engineering materials are the material that makes up structures and devices that are used to maintain and improve our living conditions. Over the past 200 years, the techniques of processing the materials have been studied and improved through various methods in order to obtain desired properties. Engineering materials have become an essential part of modern industry. Amongst all the materials, metals, ceramics, polymers and their composites are the most commonly used and studied in for industrial use(Budinski & Budinski, 2009). Individual materials in their original form are often not able to provide satisfactory performance. Therefore, different methods of improving the characteristics of the material were in common use.

For example, to improve the inferior properties of metals, alloys are formed by adding a few elements together in combinations that work as per the material science principles. The iron-carbon alloys, commonly called as steels, are a great example of how alloys changed our lives. To further enhance the corrosion resistance, stainless steel is developed by adding chromium(Budinski & Budinski, 2009). Moreover, heat treatments can also be used for controlling the performance of metals or alloys for different tasks by microstructural transformations. Methods such as annealing, which is slowly cooling down the metal after being heated to a critical temperature and quenching, which rapidly cools down the metal, have been widely used to tune the mechanical properties to the end-use requirements (Fuller, Baker, & Pape, 1940).

For ceramic materials, the main weakness is brittleness. To improve the toughness of the conventional ceramic materials, ceramic matrix composites (CMC) using continuous or discontinuous metal or polymer fibre have evolved, reinforcing the ceramic matrices (Chawla, 2013). Similar to ceramics, polymers can be strengthened by blending different compositions together and forming polymer composites. Fibre-reinforced polymer (FRP) is made of a polymer matrix reinforced with fibres. The fibres are usually glass, carbon or aramid. Compared with traditional polymers, FRP can have superior performance in creep, wear, fracture toughness and thermal stability depending on the combinations and requirements (Michael F Ashby & Jones, 2012). Different methods, materials, and their combinations evolved involving metal, polymer, and ceramic composites to achieve desired mechanical, chemical, and other performance attributes, some immediate examples being cermets, reinforced cement concrete, iron-poly, and cobalt-poly combinations (Michael F Ashby & Jones, 2012; Wizel et al., 1999). A simple classification of engineering materials can be illustrated as shown in Figure 2.1. The focus of the current research is on exploiting the composite materials further, targetting controlled variations in properties.

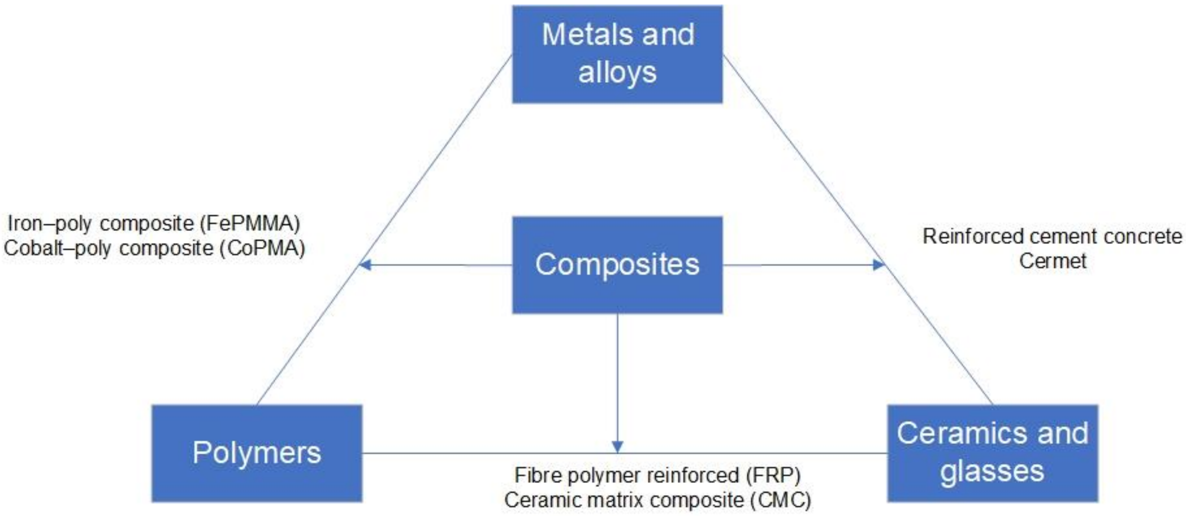

Figure 2.1. A general classification of engineering materials

The science of materials engineering has been evolving for thousands of years, as may be evident from the classification of the time periods of the growth of the human species and societies as the Stone Age, Bronze Age and the Steel Age (Almer, 2017). In particular, the composite reinforcement techniques can be dated back to 1500 BC. For example, the mud walls in houses were reinforced with bamboo short and laminated wood in ancient Egypt (Taj, Munawar, & Khan, 2007). The solutions for all these strengthening mechanisms often involve combining different materials with different scales, varying from basic elemental level to macro mixing. In terms of composite materials, nature is full of examples of biological structures that use heterogeneous composite materials in a closely controlled manner. The composite structures of specific organs of certain biological species have been optimised through the process of natural selection for millions of years.

For instance, the beak of the squid is a gradually changing structure from a stiff tanned tip to a soft untanned base, as shown in Figure 2.2. The structure allows the soft base of the beak to absorb the shock when it is biting hard materials such as the carb shell (X. Gu et al., 2016). In addition, the armour structure of the nacre shells is layers of polygonal aragonite platelets in a soft organic matrix, which can endure high hydrostatic pressures in the deep ocean while remaining lightweight (Huang & Wang, 2011). In addition, there are several examples in nature that show superior stiffness and toughness, such as bones and scales, which are the hierarchical composites of the organic and inorganic materials on the microscopic scale (Launey, Buehler, & Ritchie, 2010; Menig, Meyers, Meyers, & Vecchio, 2000).

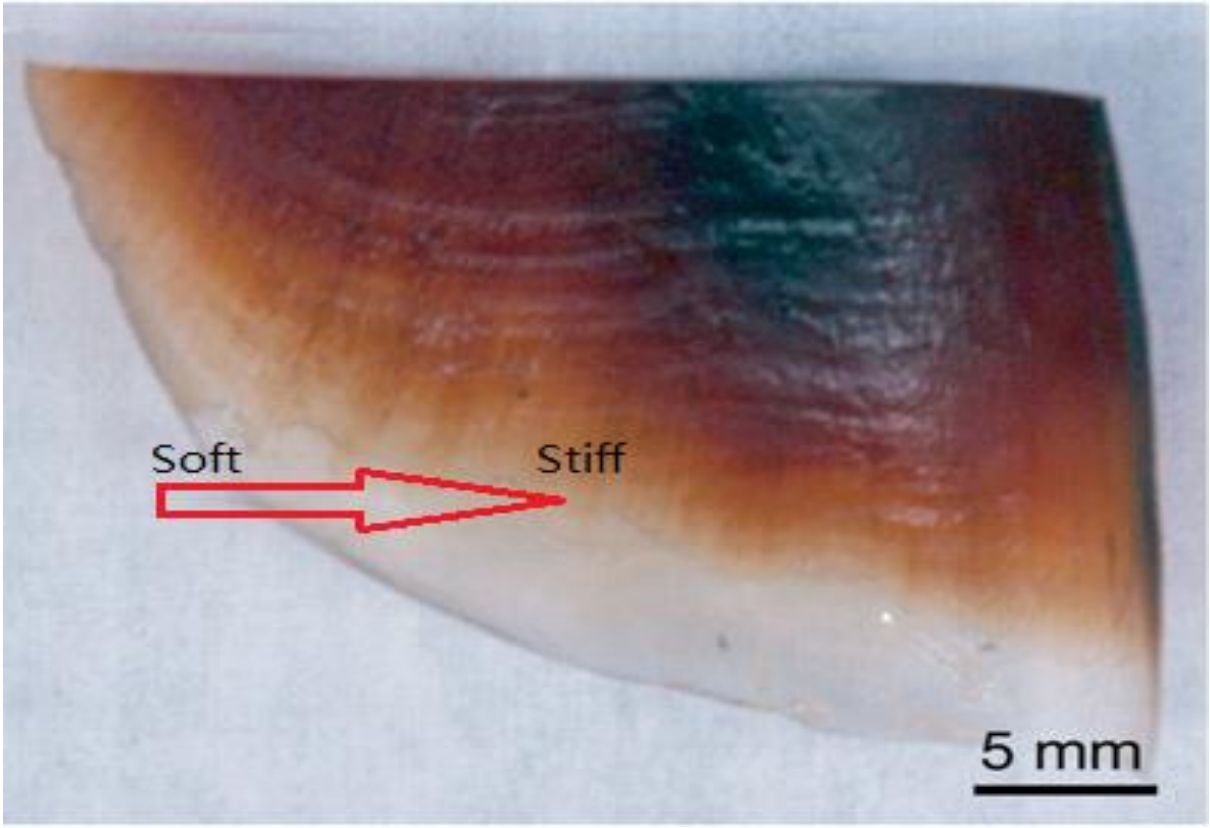

Figure 2.2. The composite material structure of the beak of the Humboldt squid

In the context of engineering materials, this leads up to functionally graded materials (FGM). The FGM is an inhomogeneous material that consists of two or more different materials and is engineered to continuously vary the composition profile. It is a solution to practical problems where high-performance and multi-functional responses are needed (Delfosse, 1998). FGMs have been used in various applications for improving performance, such as thermal resistance, corrosion resistance, hardness and toughness (Udupa, Rao, & Gangadharan, 2014). However, in most cases, there is no control over the design of the mixed materials that can accurately provide the desired variations in property responses.

Traditional manufacturing methods usually fabricate components with homogeneous compositions of heterogeneous structures on a large scale. Few methods can accurately provide the desired property without changing the geometrics in the design phase. Modern additive manufacturing (AM) technologies offer opportunities to fabricate components with selected properties by creating heterogeneous voxelated structures. This gives the designer the ability to accurately control the property variation within a given component, which vastly expands the application potentials of FGM. By using multi-material additive manufacturing (MMAM), the selective material assignment can be accurately deployed to provide the desired property without altering the original geometry. Moreover, single-material additive manufacturing can create cellular structures that allow controlling the properties by the design of the external or internal macro dimensions of the cells. The desired performance can be achieved by identifying the optimal dimensions and structures of the cells. Such designs can not be achieved by the traditional subtractive manufacturing methodologies.

Once the capability of AM to produce components with a controlled variation of properties is achieved, a plethora of new opportunities arise for designing components utilising the controlled gradation of material properties. In fact, instead of playing with the geometry of a structure with a given material, a calculated response of the material can be achieved by carefully designing the property variation within the given component domain. This is the premise based on which the research gaps and questions are formulated for this research. Varying material properties within a given domain can be achieved by using multi-material distributions or by creating cellular structures that will allow controlling the properties based on the macro dimensions of the cells. Both these approaches are evaluated in the current thesis. The following sections briefly review the current literature on the topic of functional grading of material properties and topology optimisation based on both multi-material and cellular geometric structures to achieve controlled property variations. Considering that 3D printing or AM are the essential technologies to achieve these, a quick overview of these technologies is presented first.

2.2. 3D printing or additive manufacturing technologies

Additive manufacturing (AM) refers to the technology of fabricating a three-dimensional object directly from a computer-aided design (CAD) model (Zhai, Lados, & LaGoy, 2014). Opposed to the traditional subtractive manufacturing methodologies, additive manufacturing (AM) is a process of fabricating objects by joining layers or voxels of homogeneous material or multiple materials(W. Gao et al., 2015; Mueller, 2012). Modern AM technology has been applied in a variety of 3D printing systems, and they are capable of fabricating different materials from photo resins to stainless steel(J. Hiller & H. Lipson, 2009). Though used mainly for prototyping initially (Wong & Hernandez, 2012), the AM technologies grew rapidly through applications in tooling and manufacturing with applications in widespread fields, including medical(Stansbury & Idacavage, 2016), aerospace(Lyons, 2014) and construction (Stansbury & Idacavage, 2016; Wu, Wang, & Wang, 2016). Several different methods of additive manufacturing evolved during the past two decades. The most commonly used methods are fused deposition modelling (FDM), selective laser sintering (SLS) and melting (SLM) based on the powder bed fusion techniques (Boschetto & Bottini, 2014; Palermo, 2013; Utela, Storti, Anderson, & Ganter, 2008).

The standard method of FDM uses the filament of thermoplastic polymer to 3D print the object by layers. The filament is heated and distributed to the platform, or the layers printed previously. This method is relatively cheap and reliable, and there are various desktop applications available in the commercial market. The main advantages of FDM are low-cost, high speed and user friendly. However, due to the layer by layer structure, the FDM printed object often suffers from low surface quality and resolution as well as low mechanical strength(Boschetto & Bottini, 2014). The basic process of the powder bed fusion method is spreading a thin layer of fine powders and then fusing the powders with a laser beam or binder. Then the excess powder will be removed. With repeated cycles and detailing such as coating, sintering or infiltration, the object is formed (Utela et al., 2008). The SLS method is widely used in polymers, metals and alloy powders as SLS only increase the surface temperature without fully melting the powder. The SLM method will fully melt the printing material powder; therefore, it can be only applied to metals such as steel and aluminium. Due to the fully melted fusion after the laser scanning in SLM, compared with SLS, the SLM fabricated object can obtain better mechanical strength(Yap et al., 2015). The main advantages of the powder bed fusion method are the superior printing quality and resolution. It is widely used in several areas such as tissue engineering, lattices, aerospace and electronics (Boschetto & Bottini, 2014; Palermo, 2013; Utela et al., 2008). However, the main drawbacks of the powder bed fusion method are the low processing speed and the high cost of the equipment(Ngo, Kashani, Imbalzano, Nguyen, & Hui, 2018).

Inkjet printing is another widely used method in additive manufacturing. This method is used to fabricate ceramic structures such as scaffolds for tissue engineering(Ngo et al., 2018) and thin-film transistors such as light-emitting devices and solar cells(M. Singh, Haverinen, Dhagat, & Jabbour, 2010). This method pumps a ceramic suspension through the injection nozzle onto the printing platform. The drops of the suspension form the pattern and dry through evaporation. Then the next layer of printed material will be applied to the previous layer. Instead of using liquid suspensions, another inkjet printing method uses wax-based ink. The wax-based ink is melted and ejected on a low-temperature surface to solidify. The inkjet printing method is fast and efficient for printing complex structures. However, the lack of adhesion between layers is the main disadvantage of this method(Ngo et al., 2018).

The direct energy deposition (DED) method uses a laser or an electron beam to melt the feedstock material previously deposited on the substrate. The melted material is then fused within the substrate and solidified. Compared with the selective laser melting method, DED does not use the powder bed and has a layer-by-layer process similar to the FDM method. In a commercial printer, the DED method can handle large metal structures, up to approximately 6 meters × 1.2 meters × 1.2 meters, with satisfactory mechanical properties (Sciaky, 2019). Moreover, DED allows the processing of several metal materials such as titanium, Inconel and aluminium. Besides manufacturing, the DED method can also be used for repairing large components such as turbine blades and finds applications in the aerospace and automotive industries (Gibson, Rosen, & Stucker, 2015a). However, compared to selective laser sintering or melting, DED offers lower accuracy and surface quality responses and is normally used for large components with lower complexities(Gibson, Rosen, & Stucker, 2015b).

The recent multi-material 3D printing technology enabled the fabrication of 3D objects with heterogeneous compositions, which allows the object to be fabricated using two or more materials. The combination of materials with different physical and chemical properties can create distinct properties for the desired functionality. For example, a heterogeneous object built with a rigid and flexible material combination will allow for varying the property of the composition. Selectively placing rigid and flexible material structures within the same part domain can lead to topological amendments and exploitation of the multi-material mechanics for specific performance attributes (J. D. Hiller & H. Lipson, 2009). In the medical area, multi-material 3D printing was used to demonstrate the fabrication of facial prostheses. Mohammed et al. used different combinations of Tango and Vero materials to explore the possible production of prototypes with different colours and textures. For example, the cartilage of the ears was printed with stiffer material Vero, while the earlobe was printed with softer material Tango. The combinations of different materials allowed the prosthesis to have more natural colour and texture, as evident from the examples in Figure 2.3 (Mohammed, Tatineni, Cadd, Peart, & Gibson, 2016). While this example clearly elucidates the capability of AM technologies in further pushing the boundaries of functionally graded materials, a closer look at the progress made so far is essential before being able to converge on the opportunities that are unexploited as yet.

Figure 2.3. Printed prostheses with different material combinations (Tango Plus, VeroMagenta and VeroYellow)(Mohammed et al., 2016).

2.3. Multi-material functional grading

The multi-material 3D printing research has been gaining substantial momentum in recent years, considering the capabilities to fabricate innovative parts with distinct properties by functional grading. A variety of experimental trials were undertaken to examine the possibility of varying the mechanical properties and fabricating objects with desired material properties (Bickel et al., 2010; Hašan, Fuchs, Matusik, Pfister, & Rusinkiewicz, 2010; J. Hiller & H. Lipson, 2009; Hiller & Lipson, 2010, 2012; Kong et al., 2014; Momeni, Liu, & Ni, 2017). Furthermore, through the topological combination of of the placement of different materials, much better control over the properties of the fabricated object could be demonstrated beyond what is possible by the shape of the object and the properties of the single constituent material system. This created an opportunity to customise the mechanical, thermal and electrical properties of the 3D printed objects giving far more freedom in the design of the engineering product than what was possible otherwise.

The combination of the materials with different physical, chemical, mechanical, and other characteristics can create distinct properties for the object fabricated for the desired functionality. Jonathan and Hod (Jonathan & Hod, 2010) explored the possibility of obtaining control over the material properties such as density, elastic modulus, ductility, and the failure modes by using a voxel-based fabrication process. Several trials were made to fill the voxels with aluminium and acrylic with different topological assignments to control the variation of the mechanical properties. This research demonstrated that various topological assignments such as layers, dither, mesh, and longitudinal could obtain dramatically different properties. For example, with the same 50% aluminium and 50% acrylic, the elastic modules with the longitudinal structures were tripled compared to the layer-wise allocation. (Jonathan & Hod, 2010). This was a preliminary work, mainly intended to demonstrate the opportunity to change the properties by changing the topological assignment of the materials. The focus of this research was limited to proving the ability to alter the properties rather than precisely controlling the properties to a desired set of values. However, this research has confirmed that the mechanical properties can be governed by the topological design of the materials, which is the main focus of the research leading up to this thesis.

A variety of works in topology optimisation based on selective material assignment have been undertaken in the past, considering surface scattering, thermal conductivity, resonant responses to stiffness variation(Cheney, Ritz, & Lipson, 2014; Hašan et al., 2010; J. Hiller & H. Lipson, 2009; Hiller & Lipson, 2010, 2012; O. Sigmund & Torquato, 1997). For example, a heterogeneous object combined with rigid and soft materials can present soft structures and rigid structures in different areas of the object, which cannot be created through a single material fabrication. This material design capability of AM will dramatically reform the engineering design process. With the advent of multi-material additive manufacturing, designer composite materials have become a promising approach for achieving tailored mechanical responses, such as frequency responses bending behaviour and toughness (Abueidda et al., 2019; Almeida & Awruch, 2009; Cheney et al., 2014; Grace X. Gu, Dimas, Qin, & Buehler, 2016; Gurugubelli & Kallepalli, 2014; Krishna, Mahesh, & Sateesh, 2017; Naik, Gopalakrishnan, & Ganguli, 2008; Yu, Qin, & Buehler, 2019).

The work done by Grace X. Gu et al. explored the possibility of maximising and minimising the stiffness of a multi-material block structure by combining soft and rigid materials. Using a simple greedy algorithm to identify the optimal material distribution, the results showed quick convergence, and the stiffness responses of the optimised structures were either increased or decreased significantly within a small number of iterations (Grace X. Gu et al., 2016). Hiller and Lipson also attempted to optimise the topology of a voxel-based beam model to control the stiffness and mass by using three materials with different properties (stiff, flexible, and lightweight). By controlling the dispersion of different materials, the beam geometry could be optimised to obtain the desired stiffness and weight ratio(J. D. Hiller & H. Lipson, 2009). Ćurković evaluated the use of multi-material lattice structures for desired deformation behaviour. By combining stiff and soft materials and identifying the optimal material topology, the deflection behaviour of the optimised cantilever beam could be closely matched with the target deflection profile (Ćurković, 2021).

Functional grading based on multi-material dispersion was also evaluated in a variety of other areas also to obtain controlled property responses. Hašan et al. proposed a method to obtain a specified subsurface scattering by stacking layers of different materials. This method used the bidirectional scattering-surface reflectance distribution function (BSSRDF) as the functional evaluation to calculate the scattering profile of the material compounds that were used to fabricate the object (Standards & Nicodemus, 1977). A depth-first searching algorithm was used to specify the thickness of the material stack for each surface point for a specified subsurface scattering profile. The result showed that the 3D printed optimised sample was able to provide a close match in scattering and transparency profiles (Hašan et al., 2010). The 3D printed samples are shown in Figure 2.4. There were also several attempts to apply the material topological optimisation for frequency responses, such as the maximisation of the Eigen-frequencies and the gaps (Du & Olhoff, 2007; Tsai & Cheng, 2013), the maximisation of the fundamental frequency (X. Yang, Xie, Steven, & Querin, 1999), and the minimisation of the frequency responses (Vicente et al., 2016; Yan Zhang, Xiao, Gao, Gao, & Li, 2020). Cheney et al. showed that multi-material distributions could closely control the natural frequency spectrum in a multi-material structure of fixed geometry. It was demonstrated that a designed distribution of two materials with different stiffness in cantilever beams can successfully tailor multiple natural frequencies to match randomly selected target frequency sets, albeit within a limited frequency range (Cheney et al., 2014).

Figure 2.4. 3D printed example with specified subsurface scattering (Hašan et al., 2010).

2.4. Functional grading of material properties by optimising cellular structures

Multi-material-based topological optimisation methods have been proven as reasonable solutions to the problem of designing composite structures with pre-set mechanical responses. However, in practice, they suffer from the lack of real engineering material options in existing MMAM processes. Current MMAM systems are only able to offer digitally mixed acrylic polymer options consolidated with UV curing (Kumar & Kruth, 2010). Therefore, instead of optimising material distribution, the structural design also can be used to control the mechanical responses of an object. Various structural optimisation schemes have been used for different functional grading problems.

For example, the beam structural optimisation problems such as stiffness to weight ratio (Kandemir, Dogan, & Yaman, 2018; Krishna et al., 2017; Ole Sigmund, 2007) and weight minimisation with stress and displacement limitations (Kawamura, Ohmori, & Kito, 2002) reported earlier. Tang et al. optimised the thickness of struts for maximising the stiffness to weight ratio of the structure evaluated, based on an Artificial Neural Network (ANN) used as a meta-model to ensure the manufacturability of the voxelised structure. The results showed that the optimised structure can improve the stiffness and reduce the Vom-Mises stress and displacement without increasing the volume and mass (Tang, Dong, Zhou, & Zhao, 2018). The optimisation for desired beam deflection curve profile was also proposed earlier. By using the Particle Swarm Optimisation (PSO) algorithm to search for the optimal setups of the segment widths of the beam for the desired locus of the beam tip, the desired beam deflection curve was obtained. Although the result only used one sampling point located in the beam tip for deflection, the conducted experiments showed superior accuracy in matching the desired deflection under different loading conditions (F. Gao, Liu, & Liao, 2020).

Optimisation of cellular structures was also proposed for frequency optimisation problems. In some studies, the frequency response optimisation was achieved by varying the number of internal truss elements and their locations(Gholizadeh & Barzegar, 2013; Stanford & Dunning, 2015). Other research elucidates optimisation in tasks such as the maximisation of steady-state vibrations at the desired frequency (Tcherniak, 2002), the fundamental frequency(Tsai & Cheng, 2013), the gaps in the eigenfrequencies (Du & Olhoff, 2007), and maximising and minimising the fundamental frequencies (X. Huang, Zuo, & Xie, 2010; Picelli, Vicente, Pavanello, & Xie, 2015; X. Yang, Xie, et al., 1999). Vicente et al. presented a concurrent topology optimization methodology for minimizing frequency responses. By removing the redundant material and identifying the optimum layout for distributing the designed cellular material based on the structural sensitivity, the frequency responses could be minimised within a small number of iterations. The results showed the proposed method as capable of reducing the amplitude of the vibration and vertical displacement by 80% in some cases (Vicente et al., 2016). Teimouri and Asgari proposed a multi-objective optimisation method for stiffness and fundamental natural frequency maximisation. The stiffness and frequency problem was solved as a two-objective topology optimisation problem by optimising the internal cellular arrangements of a 2D continuum structure. The multi-objective bi-directional evolutionary structural optimisation based on the weighed coefficient method was implemented for identifying the optimal balance between both objective functions. The single objective stiffness optimisation problem and multi-objective stiffness and frequency optimisation problem were validated numerically, and the result showed a significant increment in both objectives (Teimouri & Asgari, 2019). The foregoing discussion clearly elucidated that material topological and cellular structural optimisation are efficient for designing complex multi-material objects with a given set of pre-programmed property responses. The optimisation schemes are central in all these efforts, the details of which are further elaborated in Section 2.5.

2.5. Optimisation algorithms for functional grading

Fabricating objects with controlled property dispersions based on the selective material assignment and structural design has been a topic of interest in the recent past and requires the use of efficient optimisation schemes. The optimisation problems range from surface scattering to stiffness variations (Bickel et al., 2010; Hašan et al., 2010; J. Hiller & H. Lipson, 2009; Hiller & Lipson, 2010, 2012). A variety of optimisation methods have been used in the optimisation of the desired property and behaviour, such as the density-based solid isotropic material with penalisation (SIMP)(Du & Olhoff, 2007; Tcherniak, 2002; Tsai & Cheng, 2013), the evolutionary structural optimisation (ESO), its later version, bi-directional evolutionary structural optimisation (BESO) (X. Huang & Xie, 2008; Picelli et al., 2015; Vicente et al., 2016; X. Yang, Xie, et al., 1999), Evolutionary algorithms such as genetic algorithm (GA) and the covariance matrix adaptation evolution strategy (CMA-ES) (Brackett, Ashcroft, &

Hague, 2011; X. Huang et al., 2010; Jakiela, Chapman, Duda, Adewuya, & Saitou, 2000)

SIMP was proposed by Bendsoe in 1989 (Bendsøe, 1989). This method transforms a topology optimisation problem into a problem of material density optimisation and then identifies whether each element is solid or void in a fixed domain of finite elements(Deaton & Grandhi, 2014). It has been widely applied in frequency optimisation, such as the maximisation of the steady-state vibrations in the desired frequency(Tcherniak, 2002); the maximisation of the first natural frequency(Tsai & Cheng, 2013) and the gap in the Eigen frequencies(Du & Olhoff, 2007) structural optimisation problems such as stiffness to weight ratio (Kandemir et al., 2018; Krishna et al., 2017; Ole Sigmund, 2007) and compliance minimisation (Chu et al., 2019). The hard-kill approaches, such as the evolutionary structural optimisation (ESO) method, allow the object structure to evolve to the optimum by gradually removing the redundant material(X. Huang & Xie, 2008). This method employs a design domain by the finite element method, and the optimal structure can be produced by gradually removing the ineffectively used material or elements from the design domain. This iterative procedure is repeated until the rejection criterion values of all the elements are within a given range (Tanskanen, 2002). Bi-directional evolutionary structural optimisation BESO is an extension of ESO, which allows efficient materials to be added to the structure at the same time as the inefficient materials to be removed (X Huang & Xie, 2010; X. Huang & Xie, 2007). ESO and BSEO are used in optimisation problems such as stiffness to weight ratio optimisation (Pais, Alves, & Belinha, 2021; X. Y. Yang, Xie, & Steven, 2005), dimension optimisation under multiple load cases

(Li, Yu, He, & Lin, 2018), multi-objective optimisation for stiffness and fundamental natural frequency (Teimouri & Asgari, 2019), and optimising fracture resistance(Da & Qian, 2020; Da, Yvonnet, Xia, & Li, 2018). They are also widely applied for frequency optimisation problems such as maximising natural frequencies, designing structures with prescribed frequencies(X. Yang, Xie, et al., 1999), and minimising the natural frequency responses(Vicente et al., 2016).

Evolutionary methods such as genetic algorithm (GA) use the survival-of-the-fittest mechanism and transform the topological optimisation problem into a searching problem(Goldberg & Holland, 1988). Similar to natural selection, the genetic algorithm creates a number of populations and swaps the "genetic code" to create new generations. Then the fittest individuals are selected for the next generation iteratively, which leads to the identification of the optimal combinations. The optimisation scheme of the genetic algorithm is shown in Figure 2.5. Numerous examples are evident such as the maximisation of the stiffness-to-weight ratio(Chapman, Saitou, & Jakiela, 1994; J. Hiller & H. Lipson, 2009; Hiller & Lipson, 2012), optimisation of the build orientation(Phatak & Pande, 2012; Yicha Zhang, Bernard, Harik, & Karunakaran, 2017), minimisation of the compliance of the object(Jakiela et al., 2000) and desired deformation curve (Cheney et al., 2014; J. Hiller & H. Lipson, 2009).

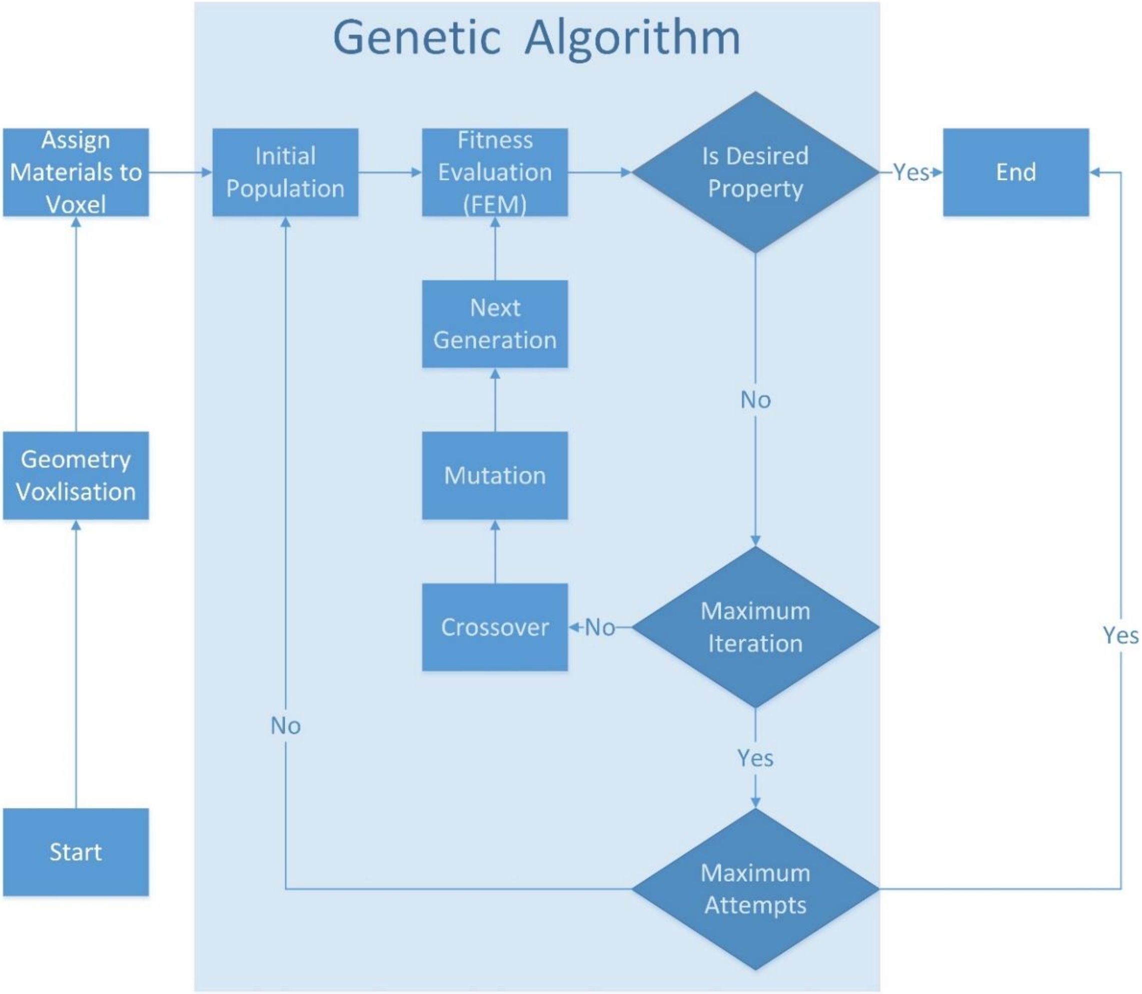

Figure 2.5. The flow chart of the genetic algorithm scheme in property optimisation.

The GA-based evolutionary algorithm, compositional pattern producing networks with neuro-evolution of augmenting topologies (CPPN-NEAT), uses a genetic algorithm to evolve an artificial neural network (ANN). By using multiple activation functions such as sine, cosine or exponential functions, CPPN-NEAT can produce complex topologies as output. (Kenneth O Stanley, 2007). Then ANN output can be used as the representation of the material distribution. By continually evolving the topology, the optimised ANN can generate material distribution as output that provides the desired property. It has been applied for geometry optimisation to increase the energy efficiency of the photovoltaic collector (Evins, Vaidyanathan, & Burgess, 2014), desired deflection profile (Ćurković, 2021), hardness maximisation (Richards, Abram, & Rennie, 2017) and matching frequency profile (Cheney et al., 2014).

Particle swarm optimisation (PSO) is a population-based optimisation algorithm. It is inspired by flocks of birds and shoals of fish and adapts the principle of social-psychological (Poli, Kennedy, & Blackwell, 2007). In PSO, a number of particles or artificial life are placed in the search space of a problem. Each particle has its own objective function and its own location. The particle evaluates its fitness at its current location and determines its movement based on its own fitness value and the fitness value of its neighbours. The swarm of the particle can interact with its social neighbourhood in the particle social network. The velocity of the particle is related to the fittest location so far encountered by the particle and the best location encountered by any neighbours in the swarm network(Poli, 2008). Through iterations, the swarm, like a flock of birds searching for food, is moving to the best location identified by the group. Unlike the genetic algorithm, PSO does not have a selection algorithm. The swarm is moving to the problem solution by interacting as a group(D. Wang, Tan, & Liu, 2018). The basic process of the PSO algorithm is shown in Figure 2.6. It has also been proposed for problems such as desired beam deflection curve by optimising the widths of each segment of the beam (F. Gao et al., 2020), maximisation of the tensile strength (Ming et al., 2012) and toughness optimisation (Mahfouf, Chen, & Linkens, 2005)

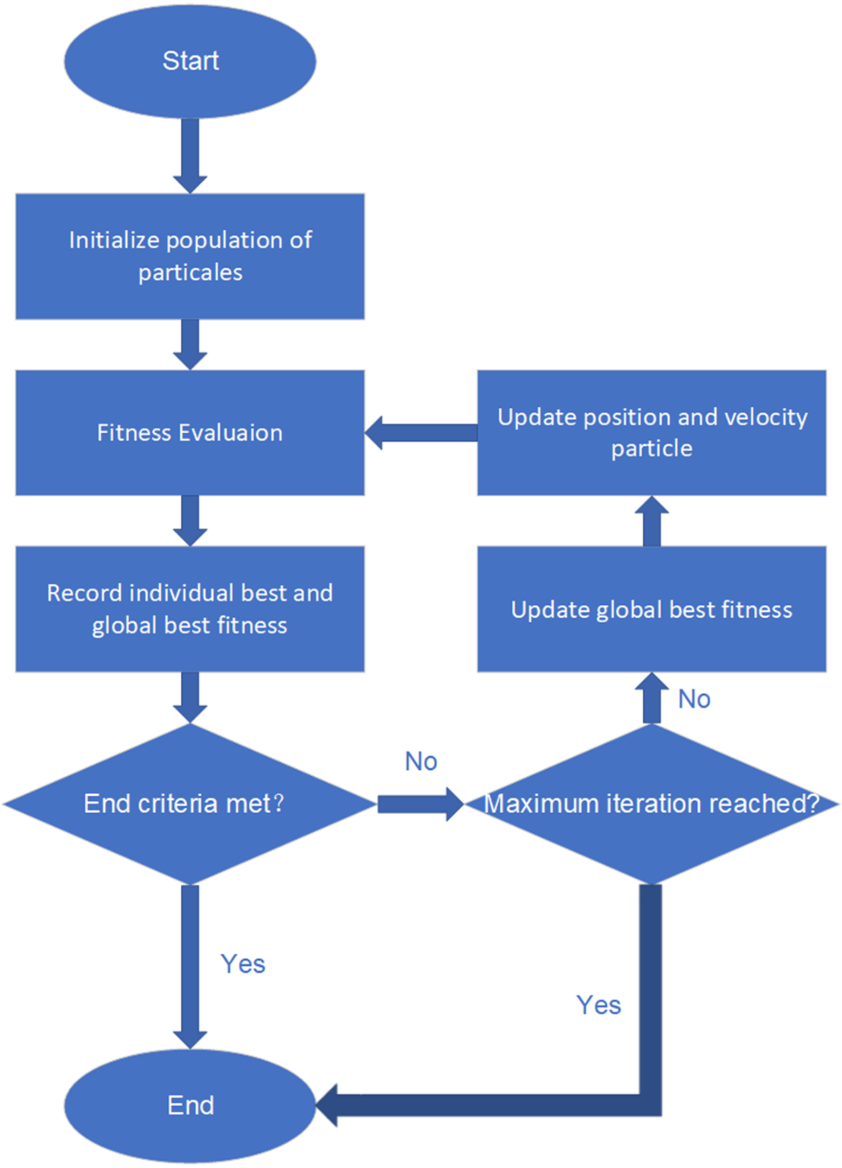

Figure 2.6. The flow chart of the particle swarm optimisation algorithm.

Covariance matrix adaptation evolution strategy (CMA-ES) (N. Hansen & Ostermeier, 2001) has become a popular tool for continuous black-box optimisation (N. Hansen, Müller, & Koumoutsakos, 2003) of complex, non-linear, and non-convex problems. It works by assembling a parametric distribution in the solution space. Then, it iteratively samples a population of solution candidates from a parametrised search distribution, and these candidates are evaluated by a black-box fitness function. In each iteration, a number of candidate solutions for the next generation are sampled from a normal distribution of multiple variables with a step size of the current generation base on the fitness value and the sampling distribution of the next generation is adjusted according to the fitness of each solution in the current generation(N. Hansen & Ostermeier, 2001).

CMA-ES was tested in various computer science and engineering studies. There were a number of notable examples, such as parameter tuning for neural networks (Jin, 2005; Loshchilov & Hutter, 2016) and ranking support vector machines (Kern, Hansen, & Koumoutsakos, 2006; Loshchilov, Schoenauer, & Sebag, 2012), structural optimisation for optimal truss layouts (Xiao, Wang, & Jin, 2013) and thermal cloaking performance (Fujii & Akimoto, 2019), topology optimisation for cloaking polarised light (Fujii, Takahashi, & Akimoto, 2018), identifying optimal metallic shapes and dielectric properties for desired electromagnetic scattering and radiation characteristics (Gregory, Wang, & Werner, 2011).

2.6. Numerical methods for graded materials and structures

To analyse the behaviour of a structure, a system of equations involving the equation of motion needs to be solved. For a simple homogeneous structure, this can be done manually with necessary parameters and numerical models. However, when solving heterogeneous or complex structured systems, the processes can be too complicated for a manual calculation. A numerical time-stepping method for the integration of differential equations needs to be used to obtain an approximation of the behaviour of such structures. The accurate analytical solutions of the system are usually impossible to obtain. The description of the laws of physics for space and time-dependent problems can be expressed in terms of partial differential equations (PDEs). For the vast majority of geometries and problems, these PDEs cannot be solved with analytical methods. Instead, an approximation of the equations can be constructed, typically based upon different types of discretisations.

The PDEs with different numerical model equations can be approximated by discretisation methods, which are solved using numerical methods. The solution to the numerical model equations can be considered as an approximation of the real solution to the PDEs. The finite element method (FEM) is used to compute such approximations(COMSOL, 2017). The FEM is a numerical technique used to subdivide mathematical models of an object into a mesh of elements. The responses of these elements is then calculated based on the number of degrees of freedom (DOF). The response of the model is approximated using the discrete response of all elements. The FEM can be used to perform finite element analysis (FEA) of any given physical phenomenon, such as structural, fluid behaviour, thermal transport and wave propagation etc. (Meshram & Pawar, 2015). FEM has been widely adopted in several well-tested engineering simulation software such as ANSYS (ANSYS, 2019) and COMSOL Multiphyics (COMSOL, 2019).

Machine learning (ML) is a statistical and predictive tool that helps to understand the behaviour and patterns of a particular set of data (Abueidda et al., 2019). ML methods such as artificial neural network (ANN) (Al-Assaf & Kadi, 2007; Hu, Feng, Meng, & Yang, 2021; M. O. Shabani & Mazahery, 2011; Vijaya Kumar, Lo Yin Kai, Arumugam,

& Karuppanan, 2021) deep neural network (DNN)(Do, Lee, & Lee, 2019; Lee, Ha, Zokhirova, Moon, & Lee, 2018; Nguyen, Kashani, Ngo, & Bordas, 2019) and convolutional neural network (CNN)(Grace X. Gu, Chen, & Buehler, 2018; Rao & Liu, 2020; Yu et al., 2019) have been employed as an alternative to FEM for identifying the properties of different structural and material systems. ANN is a computational model inspired by the architecture of biological neural networks, which is designed to simulate the processes of humans learning from given data (Do et al., 2019). It has been proved as an efficient universal computational model in many areas such as object recognition (Pohtongkam & Srinonchat, 2016), trajectory prediction (Cardenas, Rázuri, Sundgren, & Rahmani, 2013; Zissis, Xidias, & Lekkas, 2015) and medical diagnosis (Ahmad, Saeed, Saleem, & Kamboh, 2016; Koprinkova-Hristova, Mladenov, & Kasabov, 2014).

The typical ANN is a computational model that mimics the nervous system in its learning process. It is a universal computational model that can learn and adapt from the data and make a generalisation(Kasabov, 1996). The conventional multilayer NN structure consists of the input layer, output layer and hidden layer, as represented in Figure 2.7. ANN can be viewed as the weighted directed graphs, where the artificial neurons are the nodes, and the directed edges are the connections between neuron output and the input. Each neuron in the hidden layer runs independently (Jain, Mao, & Mohiuddin, 1996). ANN is a powerful statistical method that recognises the correlations and relations between the input parameters of a given problem and its output responses (M. Shabani, Mazahery, Rahimipour, Tofigh, & Razavi, 2012).

Compared with the FEM, the ANN method can compute the behaviour of a structure without actually building the simulation model. It can predict the target behaviour based on limited input parameters and the previous training data. As a universal computational model, ANN can be adapted to compute the behaviour of a structure. For example, a trained ANN has been used for the prediction of slope instability(Verma, Singh, Chauhan, & Sarkar, 2016). By using slope angle pore pressure cohesion and the friction of the slope as the input data, the ANN can calculate the Factor of Safety (FOS) index, which indicates how close a slope is to failure. Similarly, ANN is adapted to predict or simulate the yield stress and elongation percentage of the aluminium alloy (M. O. Shabani & Mazahery, 2011), failure prediction (Vijaya Kumar et al., 2021), buckling behaviour analysis (Hu et al., 2021), ultimate tensile strength(Santos, Nieves, Penya, & Bringas, 2009) and fatigue life prediction (Al-Assaf & Kadi, 2007). Similar to ANN, DNNs usually have an input layer, hidden layers, and an output layer. However, DNN is an artificial neural network (ANN) with multiple hidden layers between the input and output layers which allows DNN is able to handle non-linear relationships (Abueidda et al., 2019; Do et al., 2019). Several studies used DNNs to investigate the material and structural behaviour, such as the prediction of the compressive strength of foamed concrete, which is a complex composite material and difficult to calculate by standard FEM (Nguyen et al., 2019), the prediction of hysteretic behaviour under stochastic excitations (Kim, Kwon, & Song, 2019) pavement distress evaluation under earthquake excitations (Gopalakrishnan, Khaitan, Choudhary, & Agrawal, 2017).

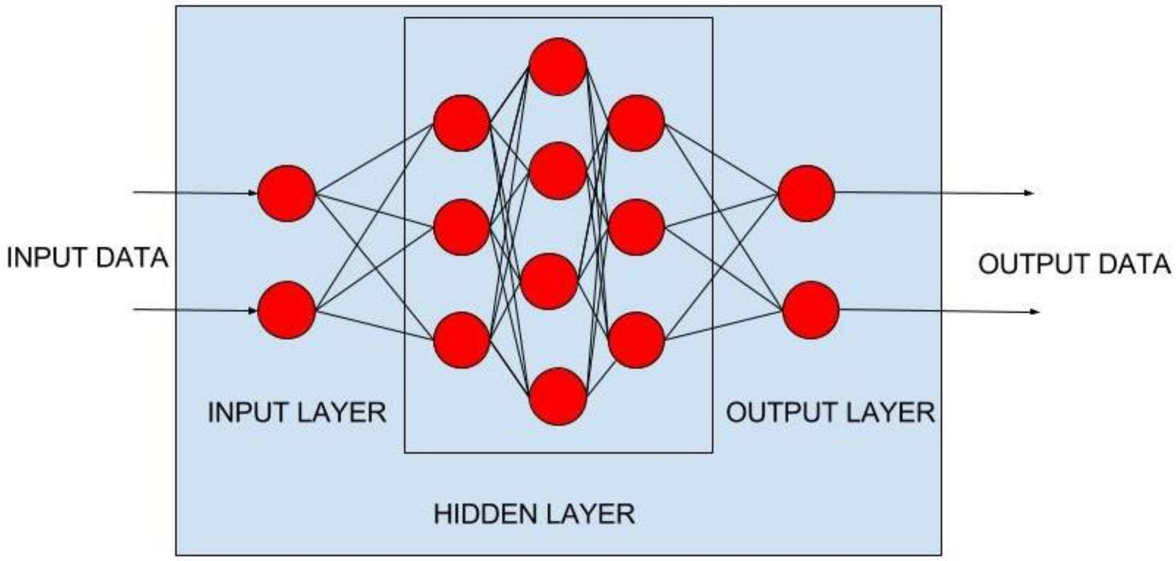

Figure 2.7. the standard multilayer neural network model, the red circles, represents the neurons

CNN is a type of neural network that consists of neurons that have evolvable weights and biases. Typically, it is a neural network used to classify images. CNN is usually composed of several convolutional layers followed by one or more fully connected layers, similar to a standard feed-forward multilayer perceptron, starting from the raw image pixels on one end and ending in a regressive value at the other. It preserves the spatial relationship by learning feature representations. Then features are learned and applied across the whole image, and design features can be captured at different scales (Yu et al., 2019). By handling the structural topology as an image, CNN can be used to capture the functional relationship and predict the property or behaviour of specific structural topology or material combinations by their patterns and features. Compared to the standard FEM solution, the pre-trained CNN can identify the property or behaviour by recognising the patterns and features without involving heavy computations for meshing and equation solving. It has been used as a numerical method for identifying the mechanical property or behaviour of a structure, such as identifying the multi-material distribution with maximum toughness (Grace X Gu, Chen, Richmond, & Buehler, 2018), predicting the elastic modulus of a porous structure (X. Liu, Yan, & Zhong, 2021), predicting compliance information (Lee, Kim, Lieu, & Lee, 2020) and predicting the stress fields in linear elastic cantilevered structure (Abueidda et al., 2019).

2.7. Research gaps and questions

Functional grading for desired behaviours and properties through multi-material topology optimisation or structural design have been studied comprehensively. Different optimisation schemes and methods were applied to various optimisation problems such as stiffness to weight ratios, frequency responses, bending and deformation behaviours, and toughness variations. Multiple optimisation schemes such as BESO SIMP and GA were proposed and widely used to handle specific problems for improving the behaviours and properties of the structural design (Abueidda et al., 2019; Almeida & Awruch, 2009; Cheney et al., 2014; Grace X. Gu et al., 2016; Gurugubelli & Kallepalli, 2014; Krishna et al., 2017; Naik et al., 2008; Yu et al., 2019). However, from the literature reviewed, it is evident that the focus of the majority of the functional grading methods was limited to either maximisation or minimisation rather than closely and accurately controlling a set of property responses, which is the next level of achievement from the multi-material or multi-property systems.

For example, with the optimisation of the frequency responses, most of the past papers focused on the maximisation and minimisation of the fundamental frequency and gaps in the resonate frequency rather than accurately controlling the frequencies to match desired target frequency sets (Cheney et al., 2014; Du & Olhoff, 2007; Tsai & Cheng, 2013; Vicente et al., 2016; X. Yang, Xie, et al., 1999; Yan Zhang et al., 2020). In the optimisation of the beam behaviour and responses, the maximisation of the stiffness to weight ratio (Kandemir et al., 2018; Krishna et al., 2017; Ole Sigmund, 2007), minimisation of the compliance and weight (Wang & Tai, 2005), weight minimisation with stress and displacement limitations (Kawamura et al., 2002) and beam segment dimension optimisation for desired beam deflection (F. Gao et al., 2020) have been studied. However, there was no evidence that the previous works can closely control the beam deflection to match a selected profile under different loading conditions. Multi-material distributions were also optimised to obtain the maximum toughness responses, but the true tensile responses of the specimens demonstrating the optimised toughness responses was not given sufficient attention (Abueidda et al., 2019; Grace X. Gu et al., 2018; Grace X. Gu et al., 2016).

The current research addresses these gaps and expands the scope of multi-material or property solutions to reach pre-set material attributes through multi-objective optimisation schemes. The overarching research question to be addressed is:

How can the point-wise material consolidation mechanics of the additive manufacturing methods be effectively utilised to achieve closely controlled material property variations within given product domains in order to match the selected property responses to pre-set conditions?

Two possible pathways can be taken, exploring the controlled property variations to find the answers to this research question. The first method is by considering the multi-material printing possibility, based on the multi-jet digitally mixed material printing technologies. This will allow for wide possibilities both for the number of materials as well as the range of property variations. The possibilities to find optimum solutions will be plenty, even with a two-material dispersion scheme. However, as already stated, the digital material mixing and multi-material solutions lead to non-engineering materials options that may not prove to be of great use in real-world engineering applications. An alternative to this is to go with a single material printing but alter the properties from one point to the other by means of adjusting the macro geometries of multi cellular arrangements used to define the part geometry. This pathway truly utilises the added design freedom arising from the use of additive technologies and paves ways to fabricate the optimised structural forms with real materials, including metals.

Different property responses can also be considered for the scientific exploration of the research premise leading to the answers to the key research question stated. A set of the first six natural frequencies is a popular choice as simultaneously satisfying the frequency responses of all the six degrees of freedom becomes a truly multi-objective optimisation problem. The effectiveness of the evolutionary algorithms in searching for the optimum points within the problem domain will truly be utilised in this approach, where the option of using only two materials will add a further challenge. The research scope can further be expanded by considering the mechanical responses. However, to bring the problem conditions into the multi-objective optimisation realm, responses such as beam deflections at multiple points, matching to pre-set conditions based on material property dispersion, is a great option. Other responses such as toughness can also be easily treated as multi-objective problems due to the dependency on both the strength and the ductility of the material. Analytical, numerical and experimental schemes necessary to be framed and integrated to scientifically investigate and find the answer to this question will lead to further sub-questions, but overall, the following objectives are set for the research undertaken as part of this study:

- Evaluate the possible design of a material structure with the controlled dispersion of two different materials selectively to conform to a set of selected natural frequencies for the first six degrees of freedom.
- Evaluate the possible design of a material structure with the controlled variation of the macro geometries of unit cells used to construct the problem domain to conform to a set of selected natural frequencies for the first six degrees of freedom. Controlling the cellular geometries should allow for the point-wise continuous variation of material properties within a pre-set range based on a structure printed using a single material.
- Evaluate the controlled deflection of a beam based on the optimisation schemes applied to the same single material cellular beam structure as defined in the above objective.

2.8. Research methods

For objective 1, a generative design method based on the binary GA, is proposed to be used to identify the optimal material distribution of a multi-material cantilever beam structure for the desired eigenfrequency responses. The finite element analysis method is to be used for the functional evaluation of the dynamic performance of the multi-material structure. For purposes of designing the material distribution, the 3-dimensional volume of the specimen is to be divided into a collection of brick-like hexahedral volume elements (voxels) through a process known as voxelisation. In the optimisation scheme of GA, the topological optimisation problem will be transformed into a searching problem. The GA will iteratively swap (crossover) and randomly alter (mutation) the genome representation and create offsprings for the next iterations. By evolving the offspring based on the fitness value, GA can gradually evolve the genome array or the material topology to the combination for higher fitness value, which leads to the identification of the optimal combinations in the final iteration. The overall optimisation scheme has to be implemented in MATLAB (R2017B, release date September 14, 2017, MathWorks, Natick, Massachusetts, USA), and the functional evaluation for the fitness function performed by COMSOL Multiphysics (Version 5.3, release date April 25, 2017, COMSOL Inc., Stockholm, Sweden), an off-the-shelf finite element analysis software package. The optimised results will be compared with alternative optimisation algorithms NEAT and CPPN-NEAT, which demonstrated superior accuracy for optimising the material topology for matching a selected evenly spaced eigenfrequency set.

The same binary GA optimisation scheme will also be used to optimise the material topology for maximising the toughness by identifying the optimal combination of rigid and soft materials. The geometry of the American Society for Testing and Materials (ASTM) D638-14 TYPE IV specimen will be used as the design domain. Through voxelisation, the material topology can be presented as the genome array for the binary genetic algorithm. The same external finite element analysis software COMSOL

Multiphysics (Version 5.5, release date April 1, 2020, COMSOL Inc., Stockholm, Sweden) can be used for the fitness value evaluation, which simulates a standard uniaxial tensile test for obtaining the toughness of the specimen. Presumably, the material distribution optimised by GA can provide a significant increment in toughness as compared to specimens of uniform or randomly generated material dispersions.

For objective 2, the frequency optimisation for a similar cantilever beam will be studied. However, to overcome the limitation of material options in MMAM, instead of using MMAM, the functional grading on the cellular structure with homogeneous material will be used to control the effective mechanical properties and mass, which leads to control over the overall eigenfrequency responses. In this approach also, voxelisation similar to the design used in objective 1 will be carried out on the cantilever beam. However, the solid voxels will be replaced by voxels with cellular structures that can provide effective variations in the distribution of effective stiffnesses and density. To tailor the frequency responses, the bending and torsional stiffnesses, as well as the mass of each voxel, will be indirectly controlled through geometrical parameters such as the overall dimensions of the voxel and the heights of the internal cellular structures, which are used as design variables by the generative design algorithm. After careful consideration of different methods, the CMA-ES algorithm was identified to be used to find configurations of the cellular structure of each voxel to achieve the eigenfrequencies closely matching the design targets. By comparing with the MMAM solution, the functional grading by the cellular structure can provide equal or better performance in matching multiple selected evenly spaced target frequency sets. The further objective is also to demonstrate that the CMA-ES optimisation scheme is able to cope with pre-loaded cases and different material settings while maintaining satisfactory accuracy.

For objective 3, the functional grading based on varying cellular structures with homogeneous material will be tested in the optimisation of the deflection behaviour of a cantilever beam. The cantilever beam structure will be voxelised into hexahedral volume elements (voxels). Once again, the CMA-ES algorithm will be adapted to optimise the beam deflection behaviour to the desired profile by varying the cellular structure of each voxel with a single material. The structural parameter of the voxels, such as the sizes, numbers and the location of the internal hollow structures, will be used as numerical parameter inputs for the CMA-ES algorithm. COMSOL Multiphysics COMSOL Multiphysics (is again the FEA platform for analysing the deflection behaviour. By varying the voxel structures, the deflection behaviour can be closely governed to match selected deflection profiles under different multiple load conditions. Considering the relatively easier measurements, an experimental verification plan is developed to build the optimum cellular beam structure by polymer 3Dprinting and subsequent three-point bending experiments. Different voxelisation and cellular structure settings will be tested under different load conditions. It is envisioned that the optimised cantilever beam with cellular structure can provide the desired deflection profiles under different load conditions with relatively lesser error levels in the convergence.

2.9. The organisation of the thesis

There are several research gaps in the current methods of functional grading for desired behaviours and properties. For instance, in the functional grading for frequency responses, the genetic algorithm is seldom used to optimise the structure for the desired natural frequency set. Chapter 3 fills this gap, demonstrating the ability of genetic algorithms to optimise the multi-material topology to match the selected natural frequencies closely. Chapter 3 also presents a further evaluation of the optimisation schemes to demonstrate the ability of the functional grading by multi-material printing for the optimisation of material properties such as toughness. The genetic algorithm will be used to optimise the material distribution of a standard dogbone specimen for the maximisation of the toughness.

The limitation that the MMAM solutions suffer from the lack of real engineering material options as the current systems can only offer digitally mixed acrylic polymer options consolidated by UV curing will be addressed in Chapter 4, presenting a novel solution as an alternative. Instead of altering the distribution of the materials, the overall structure is voxelised as a cellular structural form. Then the cellular structure of each voxel can be changed to alter its effective mechanical properties, which leads to the control of the overall frequency responses. The CMA-ES algorithm takes over subsequently, optimising the cellular structural form of each voxel to fulfil the desired natural frequency requirements. Compared with the MMAM solution, this approach expands the material readiness for the commercial AM technologies while maintaining satisfactory accuracy in matching the desired frequency sets.

It is evident that the CMA-ES has not yet been used in functional grading for desired deflection behaviour by optimising cellular structures. Chapter 5 illustrates how the generative design method CMA-ES is adapted for controlling the beam deflection behaviour by optimising a cellular system. The objective is to demonstrate the ability to closely control beam deflection behaviour under various conditions by optimising the cellular structures using CMA-ES. The results indicate that the beam with the optimised cellular structures can accurately match the beam deflection behaviour profile under different loading conditions. The proposed optimisation scheme was also shown to be capable of handling different cellular structure settings.

Chapter 3

Artificial evolution and multi-material generative design

3.1. Evolutionary computing and multi-material mechanics

Limitations of the traditional manufacturing methods often force engineered components to be made of single material systems. However, this is going through changes due to the advent of additive manufacturing methods as the point-by-point consolidation allows for a possible change of the material constitution within a given part domain. This will give rise to a plethora of new material and property options for the designers, where just human perception may fail to realise the full benefits. Automated design tools integrating material choice, dispersion, analysis, and optimisation algorithms need to be developed to assist in finding the optimal multi-material dispersion solutions achieving given performance criteria sets.

Considering the fact that the multi-material manufacturing systems are only recently coming into use, design solutions targeting optimal placement of multiple materials are not common. The current chapter addresses this gap, evaluating a numerical model integrated with different optimisation schemes to find the optimal material solutions achieving certain pre-set performance criteria such as combinations of natural frequencies in different degrees of freedom. Implementation of three different metaheuristic optimisation schemes based on genetic algorithms indicates, firstly, that it is possible to create a beam with six uniformly spaced natural frequencies and to change these frequencies without modifying the structural geometry; and secondly, that the basic genetic algorithm generally outperforms neural net based alternatives for this problem.

This tailoring of the structural resonance spectrum demonstrates that evolutionary computing combined with multi-material additive manufacturing can be used to unlock previously unavailable structural functionality. For further validation of the proposed material topology optimisation scheme, additional experiments involving the optimisation of the toughness response of a standard tensile specimen model are conducted. The results indicate that the optimised multi-material model attains a significant increase in toughness compared with the single material or the randomly generated multi-material model.

3.2. Multi-Materials solutions for frequency optimisation

Additive manufacturing (AM) refers to the technologies allowing to fabrication of three-dimensional objects directly from computer-aided design (CAD) models(Zhai et al., 2014). As opposed to the traditional subtractive manufacturing methodologies, additive manufacturing (AM) follows the point-by-point and layer-by-layer addition of single or multiple materials to build complex 3D forms(W. Gao et al., 2015; Mueller, 2012). The relatively recent multi-material 3D printing technologies enabled the fabrication of 3D objects with heterogeneous compositions, as a single object can be composed of two or more materials. The combination of materials with different physical and chemical properties can create customised composite properties tailored to the desired functionality. The materiality of an object provides additional design degrees of freedom beyond those available from shape optimisation. The design of the object's shape only affects its external boundary and is often limited by other considerations, while material heterogeneity design affects its entire volume. A heterogeneous object built by selectively placing rigid and soft materials within the same part domain then leads to the exploitation of multi-material mechanics for specific performance attributes such as the natural frequencies of mechanical parts, for example.

Natural frequencies play a vital role in determining the vibration and overall dynamic response of structures and machinery under time-varying loads. Vibrational motions can become intense in certain frequency ranges, leading to severe stress fields and subsequent weakening or even failure. There are well-known problems in fields ranging from civil engineering, such as London's Millennium Bridge, through rotating machinery to aerospace systems which require serious consideration and often tuning of natural frequencies(M. Hansen, 2003; Osiander, Darrin, & Champion, 2018). Stiffness, mass and damping increases are normally used to tune natural frequencies, which increase mass and size. Also, many mass damping structures can only affect the first or fundamental resonant frequencies(Cheney et al., 2014). The ability to control multiple natural frequencies with minimal changes to geometry and mass can significantly benefit many areas of engineering.

Natural frequencies can also be exploited to provide additional functionality. Energy harvesting from human motion and environmental vibrations, in general, is a case in point where more intense motion greatly improves energy conversion efficacy. Locally resonant mechanical metamaterials are another, where motions and phase changes are used to create dynamic behaviours that are not otherwise available and that can lie outside the range of existing material properties, such as effective negative density. In these cases, it is desirable to broaden the frequency bandwidth over which the system is effective, and clustering multiple natural frequencies in an ordered fashion can greatly increase that bandwidth.

Optimisation based on selective material assignment has been studied in the past, considering surface scattering to stiffness variations and fabricating objects with controlled property dispersions(Bickel et al., 2010; Hašan et al., 2010; J. Hiller & H. Lipson, 2009; Hiller & Lipson, 2010, 2012). Once the material topology is optimised, the properties of the final part are not completely dependent on the shape or the actual nature of the base materials but rather are closely associated with the mechanics of material dispersion. This creates opportunities to customise the mechanical, thermal, and electrical properties of the object, leading to material design freedom and dramatically reformed engineering design processes. While different material properties were targeted in specific, the optimisation of the frequency responses has been attempted by a variety of methods, such as the density-based solid isotropic material with penalisation (SIMP)(Du & Olhoff, 2007; Tcherniak, 2002; Tsai & Cheng, 2013), the hard-kill evolutionary structural optimisation (ESO), its later version, bi-directional evolutionary structural optimisation (BESO) (X. Huang & Xie, 2008; Picelli et al., 2015; Vicente et al., 2016; X. Yang, Xie, et al., 1999), and genetic algorithms (GA) (Brackett et al., 2011; X. Huang et al., 2010; Jakiela et al., 2000).

The basic idea of SIMP was proposed by Bendsoe in 1989 (Bendsøe, 1989). This method transforms a topology optimisation problem into a problem of material density optimisation and then identifies whether each element is solid or void in a fixed domain of finite elements(Deaton & Grandhi, 2014). It has been widely applied in the frequency optimisation, such as the maximisation of the steady-state vibrations in the desired frequency(Tcherniak, 2002); the maximisation of the first natural frequency(Tsai & Cheng, 2013) and the gap in the Eigen frequencies(Du & Olhoff, 2007). On the other hand, hard-kill approaches such as the evolutionary structural optimisation (ESO) method allow the object structure to evolve to the optimum by gradually removing the redundant material(X. Huang & Xie, 2008). BESO is an extension of ESO, in which materials are also added to the structure, apart from being removed(X Huang & Xie, 2010), and is widely used in the frequency optimisation problems such as maximising natural frequencies, designing structures with prescribed frequencies(X. Yang, Xie, et al., 1999), and minimising the natural frequency responses(Vicente et al., 2016).

Evolutionary methods such as genetic algorithms (GA) use the survival-of-the-fittest mechanism and transform the topological optimisation problem into a searching problem(Goldberg & Holland, 1988). Creating a number of populations, swapping the "genetic code" to create new generations and selecting the fittest individuals for the next generation iteratively leads to the identification of the optimal combinations.

Numerous examples are evident such as the maximisation of the stiffness-to-weight ratio(Chapman et al., 1994; J. Hiller & H. Lipson, 2009; Hiller & Lipson, 2012), optimisation of the build orientation(Phatak & Pande, 2012; Yicha Zhang et al., 2017), and minimisation of the compliance of the object(Jakiela et al., 2000). A variation on evolutionary algorithms known as compositional pattern producing networks with neuro-evolution of augmenting topologies (CPPN-NEAT), which uses a genetic algorithm to evolve the structure of a neural network, has been applied to automate the design and tune the natural frequencies of a multi-material cantilever beam(Cheney et al., 2014). However, only randomly selected distributions of target frequencies were tested in this work, and many of the implementation details were not reported.

The genetic algorithm (GA) is adopted in this work to optimise the three-dimensional topological distribution of the material in a cantilever beam of specific dimensions to meet selected ranges of natural frequencies. The outcomes clearly demonstrated the possibility of fabricating the object with the desired frequency properties closely matched, considering the optimum dispersion of two selected material systems currently used in specific commercial multi-material 3D printing facilities. Although frequency optimisation has been researched for several decades, the use of evolutionary genetic algorithms together with the consideration of materials for multi-material additive manufacturing has been limited. This chapter fills this gap, demonstrating the ability of genetic algorithms to optimise the material topology and numerically ascertain the achievement of the desired natural frequencies closely.

3.3. Generative design and evolutionary computing methods

Generative design can be defined as the process of using algorithms to find design solutions that satisfy functional requirements. The iterative nature, when implemented using modern computing, allows it to explore large numbers of permutations to arrive at more effective designs. Generative design methods are normally used to develop the shape of an object while keeping its material composition uniform. However, the development of multi-material additive manufacturing processes is enabling the material composition of an object to be tailored in ways that have not been practical before. Although fullest design freedom emerges from the interaction of shape and materiality, as shown in Figure 3.1, the latter has received little attention. When tailoring natural frequencies and overall dynamic responses, the material design allows an order of magnitude increase in freedom of choice relative to shape optimisation alone. The latter allows for one or at the most two natural frequencies to be tailored independently, based on design studies of resonant structures previously undertaken. The current study is focused on materiality, i.e. the design of effective composite properties and therefore, an existing structural geometry is assumed and kept constant throughout.

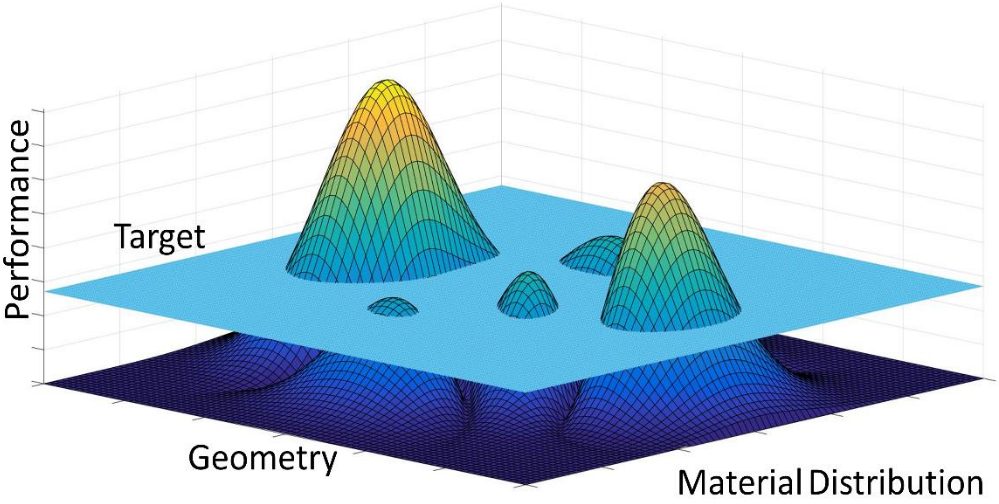

Figure 3.1. Interaction of the fitness surface generated by material distribution and geometry with a certain performance target

For purposes of designing the material distribution, the 3-dimensional volume of the structure is divided into a collection of brick-like hexahedral volume elements (voxels) through a process known as localisation. The voxel shape and dimensions cannot be smaller than the physical dimensions of the minimum material unit deposited by the additive manufacturing process (maxel) but may be considerably larger, depending on the mechanics of the structural system. A material is assigned to each voxel from a palette of two or more, and it is this assignment that is the subject of optimisation. The initial material distribution is a parameter that may have a significant influence on the final results, so in order to eliminate its complex effects in this study, all designs have the same initial material distribution.

3.3.1. Genetic algorithms

The baseline optimisation method uses a single objective binary genetic algorithm combined with finite element analysis for functional evaluation of the dynamic performance of the multi-material structure. The overall scheme is implemented in MATLAB (R2017B, release date September 14, 2017, MathWorks, Natick, Massachusetts, USA) and calls on an external finite element analysis tool to compute the desired number of eigenvalues. For each generation, once the fitness values have been established from the functional evaluation, the parents for the next generation are shortlisted by different selection strategies such as roulette wheel, tournament, and random selection(M. K. Heris, 2015). The process is continued generation iteratively after generation and finally terminated when either the fitness value converges to a steady-state or the limit on the number of iterations is reached. As this is a single objective optimisation, the fitness function is a scalar. In this study, it was defined as the weighted (w) mean square error, where the error is the difference between the desired or target natural frequencies and the frequencies calculated by eigenvalue analysis. The lower the error, the lower is the fitness value.

$$fitness = \sum_{i=1}^{N} w\left(freq_i^{target} - freq_i^{calc}\right)^2 \tag{3.1}$$

$$w = (N + 1 - i)/N \tag{3.2}$$

Where $freq_i^{target}$ and $freq_i^{calc}$ are the target and the calculated frequencies; N and i indicate the number of the eigenfrequencies and the current eigenfrequency calculated by eigenvalue analysis.

Three selection methods (roulette wheel, tournament, and random selection) were included in this implementation to allow for comparative trials.

1. The roulette wheel selection uses fitness to assign a probability of selection to each individual. If f_{worst} is the highest error attained, f_i is the fitness of any individual i, and pre is the selection pressure, the probability of selecting the individual i is calculated as

   $$probability_i = exp\ (-pre * f_i / f_{worst}) \qquad (3.3)$$

2. The tournament selection method is directly based on the fitness values of the individuals. In the current method, n candidates are chosen from the overall population for the tournament, and the top two candidates with the lowest error are chosen as the parents for the next generation.
3. The random selection is based on randomly selecting the parents from the population.

Three different crossover methods are used with selected crossover percentages (PC) to choose from, namely, single point, double point and uniform. In the crossover process, one of the three methods will be selected based on a roulette wheel selection. The probability of each of the methods being selected is 0.1, 0.2 and 0.7, respectively. In binary GA, the mutation is randomly replacing chromosome, usually with a low probability (0.001 to 0.01). The mutation process gives the genetic structure the possibility to jump out of the old loop and recover the "good" genetic materials that are lost in the previous crossovers(Chipperfield, Fleming, Pohlheim, & Fonseca, 1994a).

3.3.2. NEAT and CPPN-NEAT

Alternative optimisation methods based on two different types of Neuro-Evolution of Augmenting Topologies (NEAT) algorithms, basic NEAT(K. Stanley, 2014; Kenneth O Stanley & Miikkulainen, 2002) and Compositional Pattern Producing Networks (CPPN)-NEAT(Kenneth O. Stanley, 2015; Kenneth O Stanley, D'Ambrosio, & Gauci, 2009) were also used for comparison. Instead of using a genetic algorithm to directly evolve the binary representation of the structure, NEAT and its extension CPPN-NEAT use GA to evolve the structure of a neural network. The optimised neural net then becomes a representation of the material distribution in the beam. Instead of using the same activation function in all neurons, CPPN allows neurons to use different activation functions. By using multiple activation functions such as sine, cosine or exponential functions, CPPN-NEAT can produce more complex topologies as output. Then the fitness value is calculated for each topology produced and the genetic algorithm applies the crossover and mutation process to select and evolve the neural net.

3.3.3. Functional evaluation

The eigenvalue analysis needed for functional evaluation is carried out by COMSOL Multiphysics (Version 5.3, release date April 25, 2017, COMSOL Inc., Stockholm, Sweden), an off-the-shelf finite element analysis software package. It uses its standard quadratic solid elements, with one element being assigned to each voxel in the structure. The higher the number of voxels, the higher the number of degrees of freedom and the solving times.

3.4. Optimisation on frequency responses

To demonstrate its power, the method described in Section 2 was used to design cantilever beams with evenly and closely spaced natural frequencies, something that is impossible to achieve by conventional means. A beam with a uniform rectangular cross-section, as shown in Figure 3.2 (a), is one of the simplest structural forms, and its structural dynamics are well understood, at least when composed of either a single material or a regular arrangement of materials such as in laminated or bi-material beams. A beam is a structure rather than a material as its mechanical behaviour is driven as much by geometrical (e.g. the moment of inertia) as by material properties. Many of the more complex structural systems, ranging from ship hulls to bridge trusses, can be considered as beams or assemblies of beams. Consequently, a beam example is used here to demonstrate the power of materiality whilst moderating the computational costs. The dimensions chosen for these numerical experiments are 40 mm long by 10 mm wide and 1 mm thick. The natural frequency design targets used for the optimisation scheme are listed in Table 3.1 below. Note that the range of feasible target frequencies is constrained by the properties of the materials used in the construction of the beam.

Table 3.1. Frequency design targets for algorithm testing

Target groups	First natural frequency (Hz)	Natural frequency spacing (Hz)
1	10 - 50 in increments of 10	20
2	10	10 to 100 in increments of 10
3	50, 90, 110, 150	100

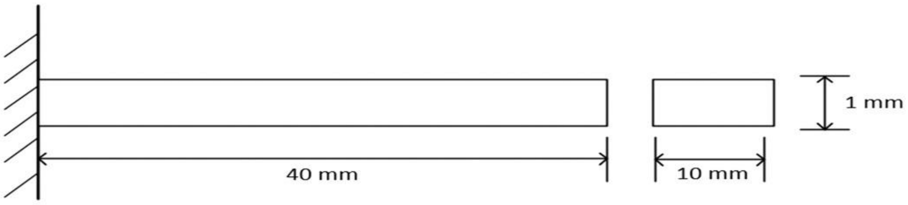

The cantilever domain

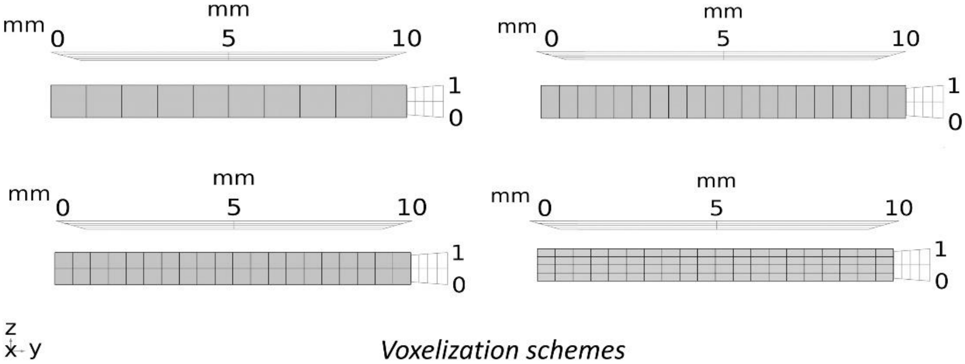

Voxelization schemes

Figure 3.2. The dimensions voxellisation of the cantilever beam used in the optimisation for the frequency responses

3.4.1. Voxelisation

Four different mesh configurations were tested, which divided the cantilever beam volume into 400, 1600, 3200, and 6400 voxels, respectively, as depicted in Figure 3.3. With the overall dimensions of the beam remaining the same, the unit voxels varied with the number of voxels, from 1 mm cubes for the 400 voxels configuration to 0.5 mm x 0.5 mm x 0.25 mm bricks for the 6400 voxel version.

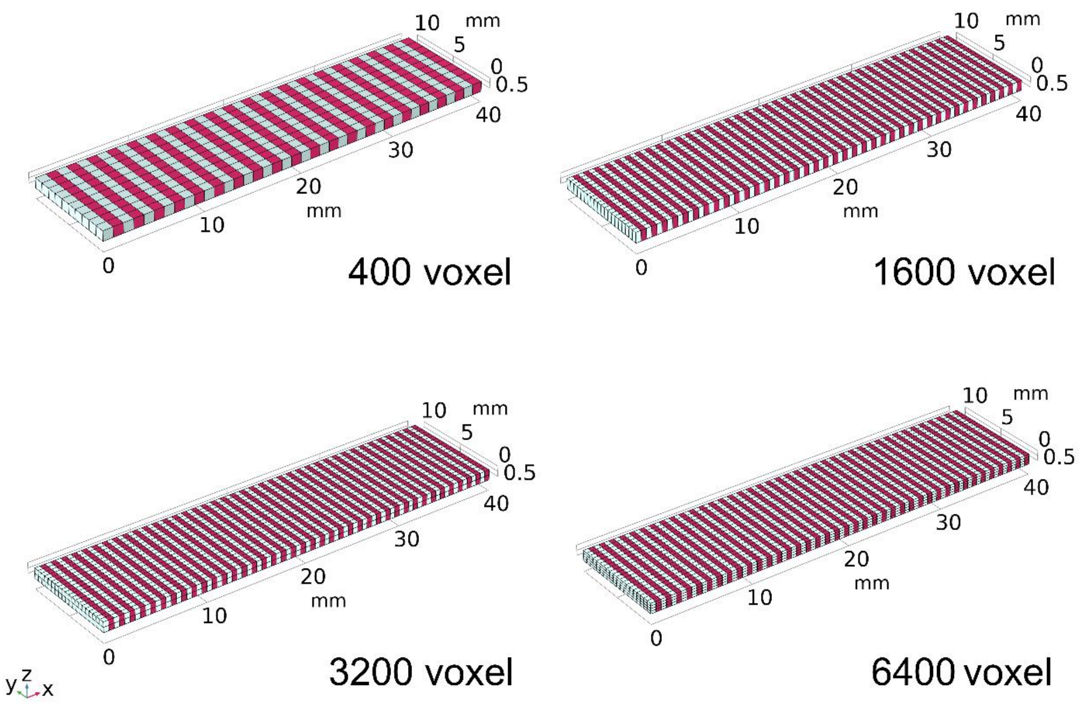

Figure 3.3. Initial material distribution for beams with the four different voxel numbers, showing the alternative bands of soft (white) and stiff (red) materials.

3.4.2. Materials

Two different linear elastic materials were used whose properties were based on those of the softest and stiffest polymers available in a commercial multi-material 3D system, such as the Stratasys Connex. These two materials are designated Vero White and Tango+ by the manufacturer, and their relevant properties are listed in Table 3.2. Note that their density is almost identical, but Young's modules differ by three orders of magnitude. Both these materials exhibit nonlinear stress-strain behaviour, but this complicating factor has been ignored in this initial analysis.

Table 3.2 Material Properties

Materials	**Density (*kg/m*^{3})**	**Young's modulus (*Pa*)**	**Poisson's ratio**
Tango+	1120	9.2×10^5	0.48
Vero White	1170	2.3×10^9	0.35

3.4.3. Initial distribution

The initial configuration was adopted where 50% of the voxels were assigned to each material, arranged in a regular pattern of alternating transverse rows. This was used as the initial point of the optimisation process for every analysis as discussed in the result section. The first six natural frequencies of the initial models are recorded in Table 3.3

Table 3.3. Natural frequencies of initial models

Modes of vibration	**1st**	**2nd**	**3rd**	**4th**	**5th**	**6th**
400 voxels	11.85	73.04	90.87	138.34	199.26	323.03
1600 voxels	11.82	72.733	91.674	132.01	198.02	324.97
3200 voxels	11.809	72.665	91.664	132	197.84	324.91
6400 voxels	11.804	72.638	91.659	131.17	197.77	324.84
Full soft material	4.5794	23.002	28.443	28.853	73.382	79.891
Full stiff material	183.64	1134.6	1144.7	1366.3	3203.7	3557.4

3.4.4. Genetic algorithm tuning

The efficacy of the genetic algorithm can be tuned by the following six parameters: crossover percentage mutation rate and mutation percentage; selection method; population size; and a number of voxels. A set of experiments were conducted to determine the effect of these parameters on the optimisation performance for this particular case. The baseline for comparison was a 400 voxel model, a population size of 100 and the roulette wheel selection method. The average mean square error is evaluated from 5 repeated trials to calculate the fitness value with each combination. Each trial is repeated five times to obtain an estimate of the magnitude of variance and make any random effects immediately apparent.

1) Combinations of three crossover percentages (0.5, 0.6 and 0.7) and four mutation rates (0.01, 0.02, 0.04 and 0.08) are tested with the mutation percentage fixed at 0.08.
2) Considering the best crossover percentage and mutation rates as fixed, further trials are conducted with mutation percentages of 0.02, 0.04 and 0.08.
3) The optimum combination of the above parameters are used to evaluate the relative performance of the three selection methods: random, tournament, and roulette wheel.
4) Four population sizes (20, 50, 100 and 150) are tested using the best selection method.
5) Four increasingly fine voxel meshes (400, 1600, 3200 and 6400) are tested.

The design target for these algorithm tuning trials is to have equally spaced natural frequencies every 20 Hz, starting at 10 Hz, something that is impossible to achieve by conventional means.

3.4.5. CPPN-NEAT algorithm tuning

Although natural frequency tailoring of a multi-material beam using CPPN-NEAT has been reported in the literature (Cheney et al., 2014), the values of the algorithm parameters used were not provided. For comparison purposes, the algorithm parameters in the NEAT and CPPN-NEAT experiments were set to values that were equivalent to those used for the direct GA experiments.

3.4.6. Generative design algorithm testing

The test matrix for the multi-material distribution algorithm consists of three groups of target natural frequency sets. In the first group, each target set has a different first natural frequency but the same uniform frequency spacing. In the second group, each target set has the same first natural frequency but different uniform frequency spacings. The third group has target sets with large gaps in the first natural frequency and a large uniform step size.

3.5. Results of the frequency optimisation

3.5.1. An example

As an example of the results produced by the generative composite material design process described above, Figure 3.4 illustrates a final distribution of soft and stiff material obtained for a cantilever with 6400 voxels. It is important to note that each run of the algorithm will produce a different result, but these results will be visually similar material patterns that can be said to form a family. More importantly, material patterns such as this are unlikely to be arrived at by a conventional design process. The mode shapes corresponding to each of this beam's first six natural frequencies are illustrated in Figure 3.5.

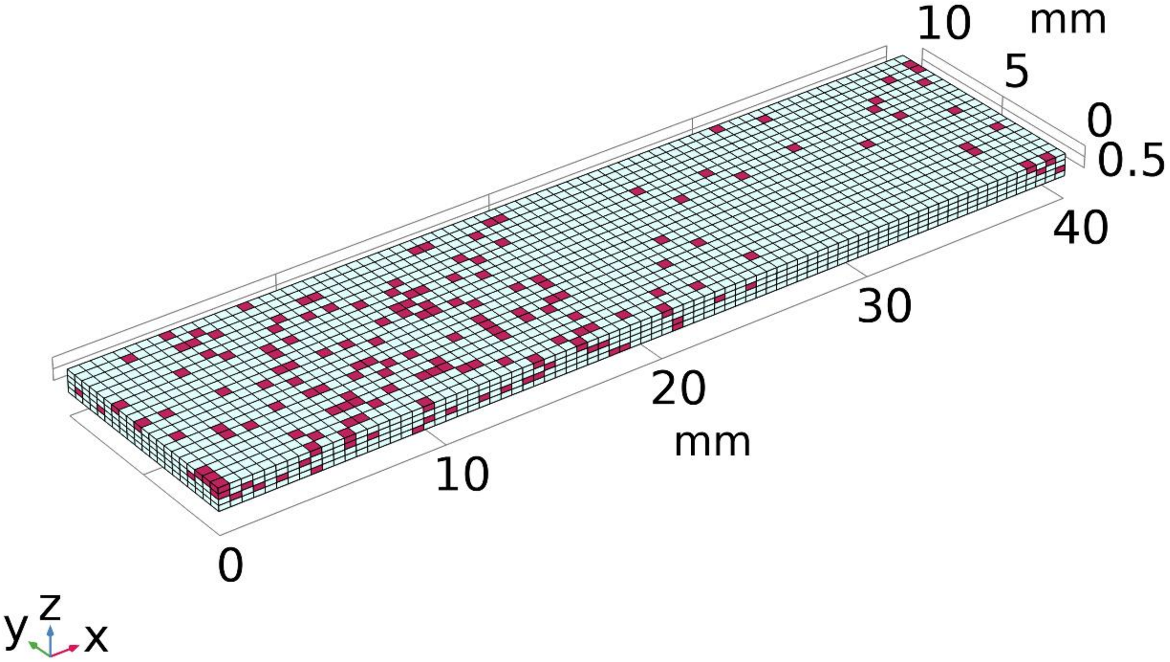

Figure 3.4. The distribution of stiff Vero White (red voxel) and soft Tango+ (white voxel) materials produced by a single run of the algorithm for a cantilever beam divided into 6400 voxels when targeting natural frequencies of 10, 30, 50, 70, 90 and 110 Hertz.

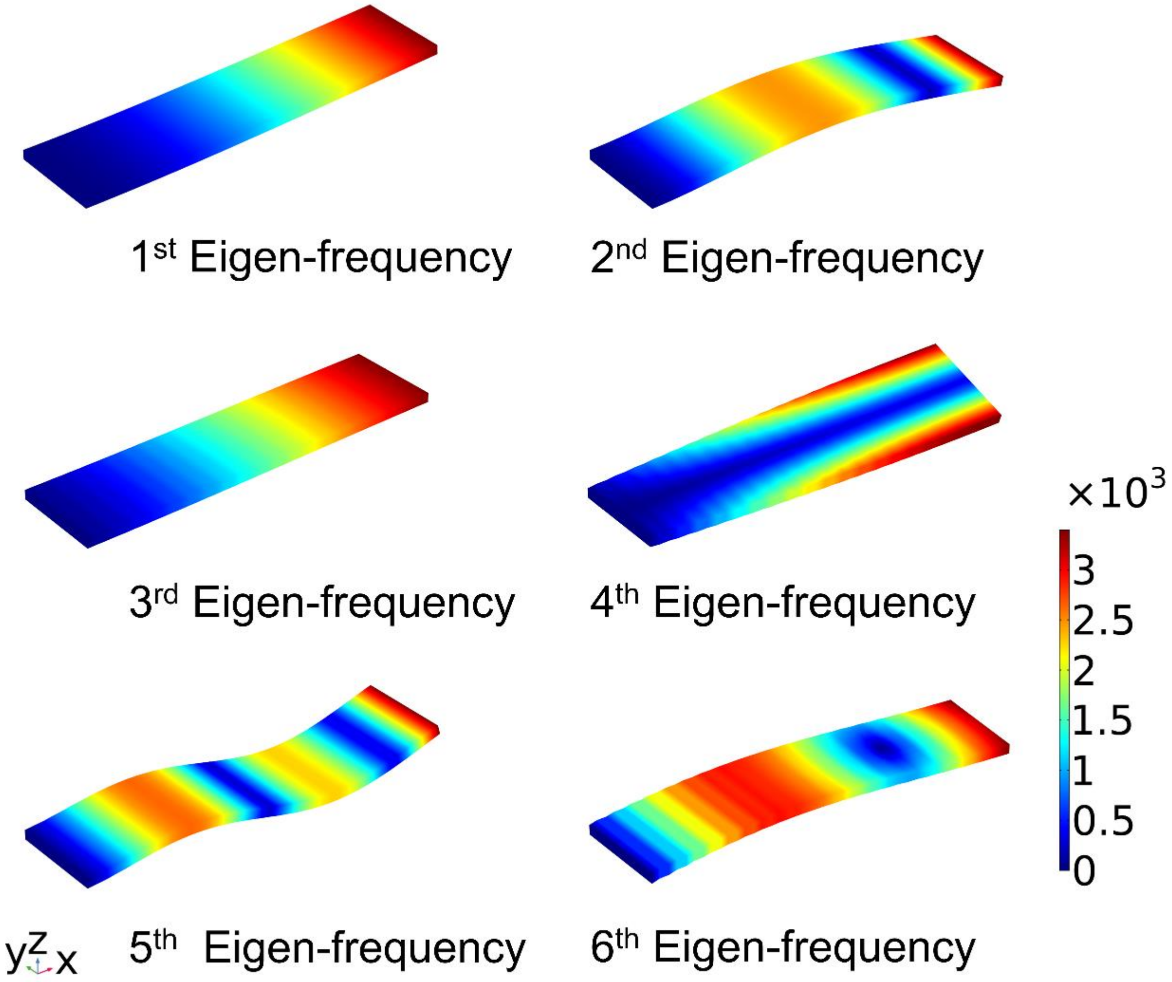

Figure 3.5. The mode shapes of the first six natural frequencies for the 6400 voxel beam, with the corresponding target frequencies (10Hz, 30Hz, 50 Hz, 70 Hz, 90 Hz, 110 Hz).

3.5.2. Algorithm tuning

The averaged fitness values for combinations of three crossover percentages and four mutation rates are listed in Table 3.4, from which it can be observed that the crossover percentage and the mutation rate have relatively little effect on GA performance for this case. The mutation percentage trial results are summarised in Table 3.5 and indicate that a mutation percentage value of 0.08 allows the GA to reach the lowest fitness value but with a high magnitude of variance. From these results, the optimal combination of crossover percentage, mutation rate and mutation percentage is identified to be 0.6, 0.08 and 0.08, respectively. Though the randomness is high, these settings are employed in the following trials.

Table 3.4. Average fitness value results for 12 different combinations of crossover percentage and mutation rate

Crossover Percentage	Mutation Rate	Fitness (average of 5 trials)
0.5	0.01 0.02 0.04 0.08	43.15 46.59 31.07 50.60
0.6	0.01 0.02 0.04 0.08	36.85 39.66 34.54 30.20
0.7	0.01 0.02 0.04 0.08	31.35 44.36 40.84 35.56

Table 3.5. Fitness value results for different mutation percentages

Mutation Percentage	Lowest fitness value	Highest fitness value
0.02	31.92	73.26
0.04	34.59	95.67
0.08	23.76	114

The fitness values and variances resulting from 5 independent trials for each of the selection methods, population sizes and the number of voxels are presented in Figure3. 6. The solid line denotes the median value, and the error bars represent the lowest and highest fitness values obtained during these trials. The three selection methods are compared in Figure 3.6a, and it is clear that the roulette wheel method is the best option for the current experimental setup. As evident from Figure 3.6b, the fitness rapidly improved as the population size was increased, up to a population size of 100 and then showed little change. Figure 3.6c and Table 3.6 show that as the number of voxels increases, both errors and scatter in frequency decrease significantly. The fitness value of the 400 voxel model varies from 35.58 to 54.2 over five independent runs, but for the 6400 voxel model, this becomes only 10.3 to 12.12. However, FEA solving times also increase by 5.5 times as the number of voxels in the model increases from 400 to 6400. The times to compute the first six eigenvalues are 2, 4, 6, and 11 seconds respectively, with 400, 1600, 3200, and 6400 voxels.

The functional evaluation time dominates the total computation time, so the overall computational expense is directly proportional to the number of voxels. Based on these results, high mutation rates from 0.02 to 0.08 and high mutation percentages from 0.02 to 0.08 are employed in subsequent runs of the algorithm.

Table 3.6. First 6 natural frequencies for different numbers of voxels.

Models	**1st**	**2nd**	**3rd**	**4th**	**5th**	**6th**	**Fitness Value**
400 voxels	8.3037	32.478	45.988	68.133	93.693	116.47	31.98
1600 voxels	8.7716	32.928	46.591	67.658	94.14	110.47	24.88
3200 voxels	7.0897	31.971	48.345	69.865	90.65	112.39	14.1
6400 voxels	6.99495	31.112	49.209	69.977	90.545	111.23	11.13
Target frequencies	10	30	50	70	90	110	

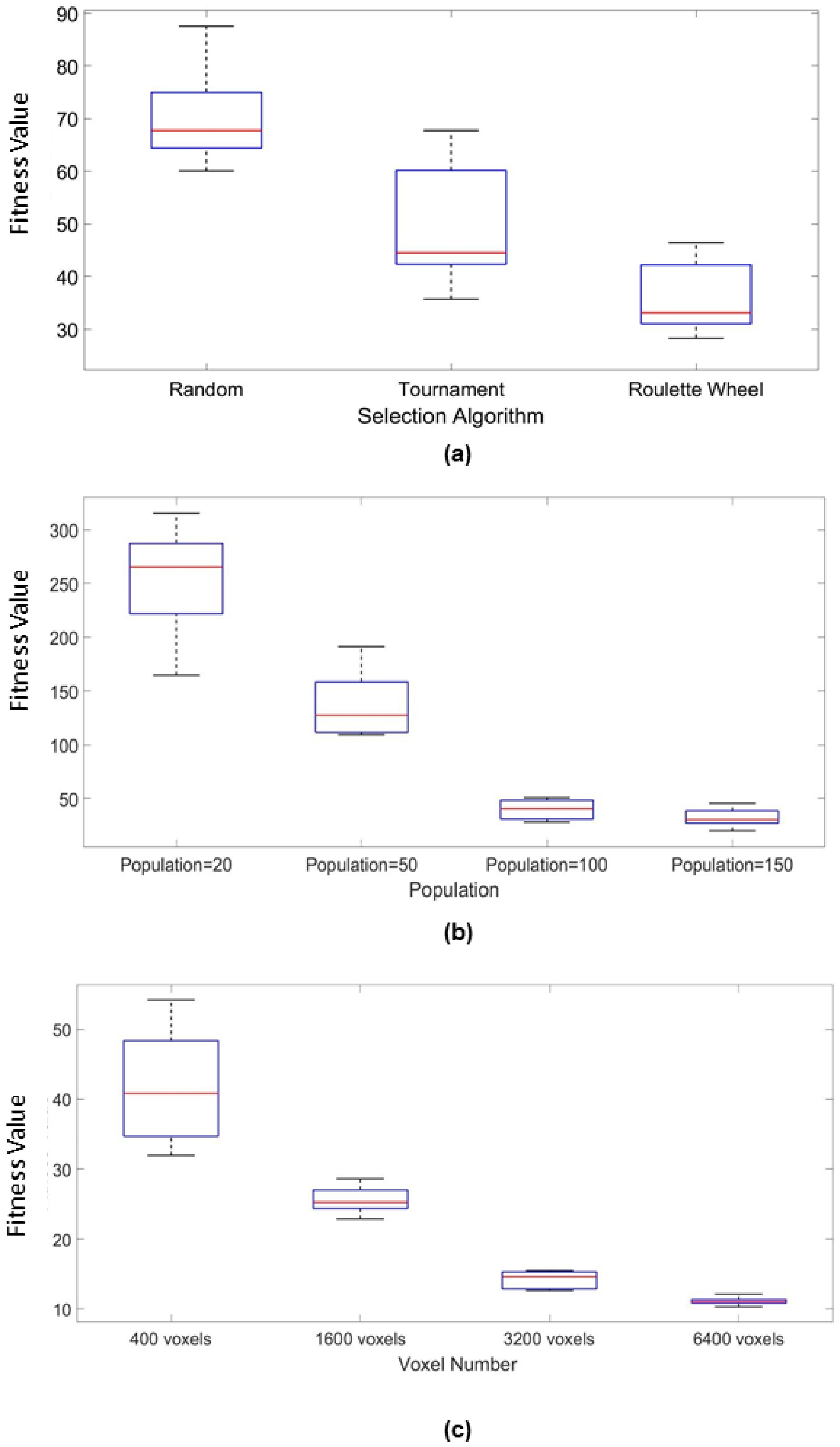

Figure 3.6. The effect of (a) selection method, (b) population size, and (c) the total number of voxels on the fitness value achieved by the algorithm. The lower the fitness value, the closer the beam's eigenvalues were to the target frequencies. The solid lines indicate the median fitness value, and the boxes represent the 25th and 75th percentiles.

3.5.3. Material design evolution with GA

Based on the results of the tuning of the generative design algorithm presented above, the GA parameters were set as; population 100, crossover percentage 0.6, mutation percentage 0.08, mutation rate 0.08, roulette wheel selection and maximum 150 iterations. To achieve the preferred balance of performance and computing time, the 1600 voxel model is used for all beam material design experiments. As outlined in Section 3.4, 17 different design frequency target sets were tested, and each test involved five independent evolution runs, resulting in 510 frequency values. Figures 3.6 and 3.7 provide a sampling of these values and an overall picture of how close they were to their targets.

The best result obtained from these 17 target sets is shown in Figure 3.7a. All of the first six eigenvalues are very close to the target frequency values, with errors of less than 1%. The worst results are shown in Figure 3.7b, where it is evident that the first eigenvalue has a large percentage error, which is an error of approximately 50%, the matching of the 2nd to 6th eigenvalues to the target natural frequencies is satisfactory. As the target of the first frequency of this target set (150Hz) is close to the first natural frequency of the first eigenfrequency of the full stiff material model (183.64Hz), which requires most of the material in the structure to be the stiff material. But for the 2nd to 6th eigenvalues, the target set (250Hz-650Hz) is far from the full stiff material model (1134.6Hz-3557.4Hz). In this dilemma, GA chooses to evolve the structure to match the 2nd to 6th eigenvalues during the selection, which causes a large error in the first eigenfrequency.

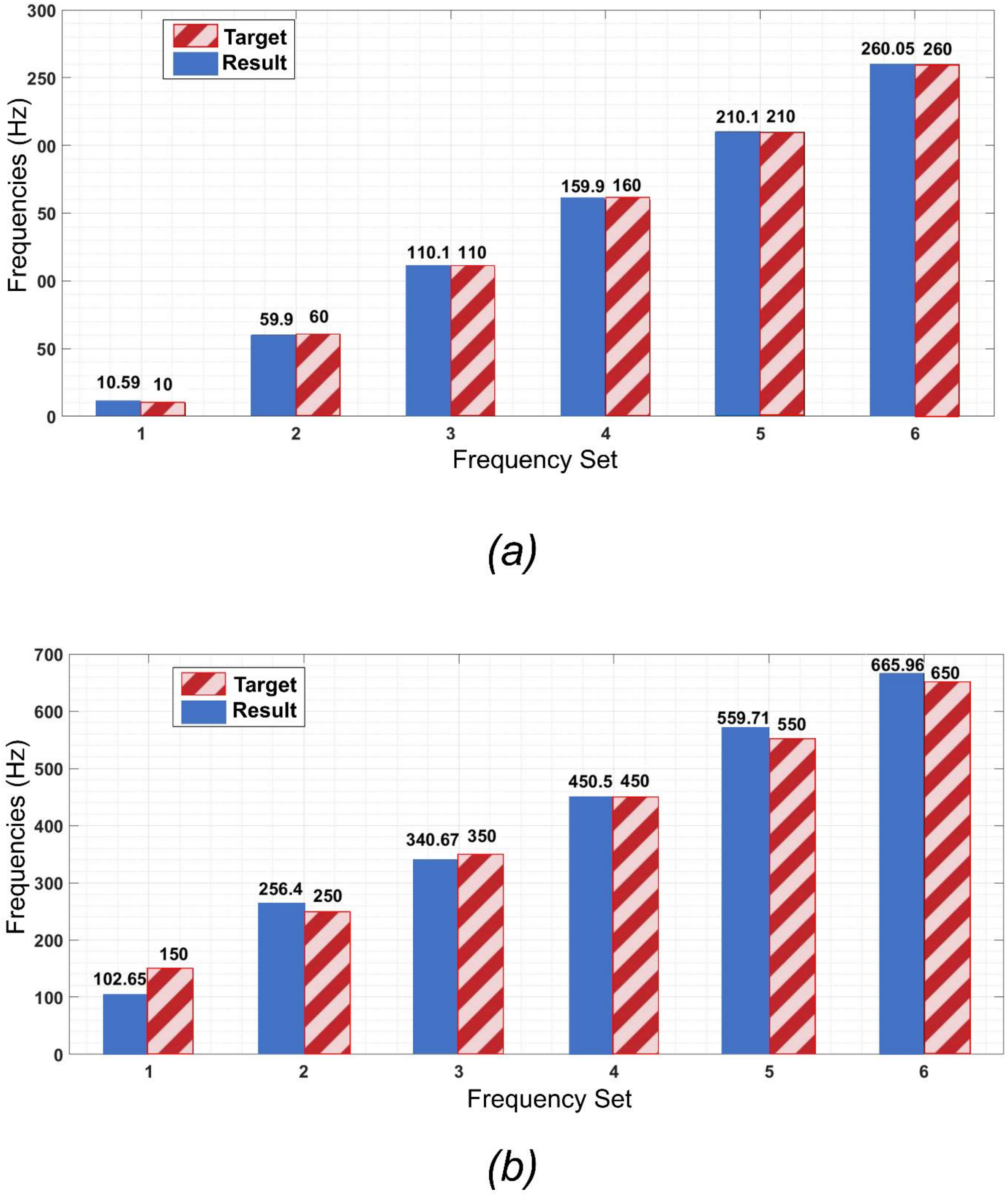

Figure 3.7. Comparison of the first six natural frequencies for the final evolved material design, as computed by finite element analysis, with the corresponding target frequencies for (a) the best result and (b) the worst result for a higher frequency target.

Figure 3.8 provides an overview of how close the design algorithm came to its targets for all six frequencies in the 17 test sets. The frequency error is defined as the difference between the eigenvalues of particular material architecture and the corresponding target frequencies. Both, when expressed as a percentage and as an actual value, the largest errors by a considerable margin are for the first natural frequency, but the other frequencies exhibit much less scatter. Overall the algorithm has produced natural frequencies that are close to the targets; the average error is less than 8%. For target frequency spacing between 30 and 100 Hz, the error is consistently less than 5 Hz; but for spacing of 10 and 20 Hz, the errors are much more variable with some high values. The errors decrease with increased target frequency spacing until a minimum is reached at 50 Hz spacing, after which errors increase again.

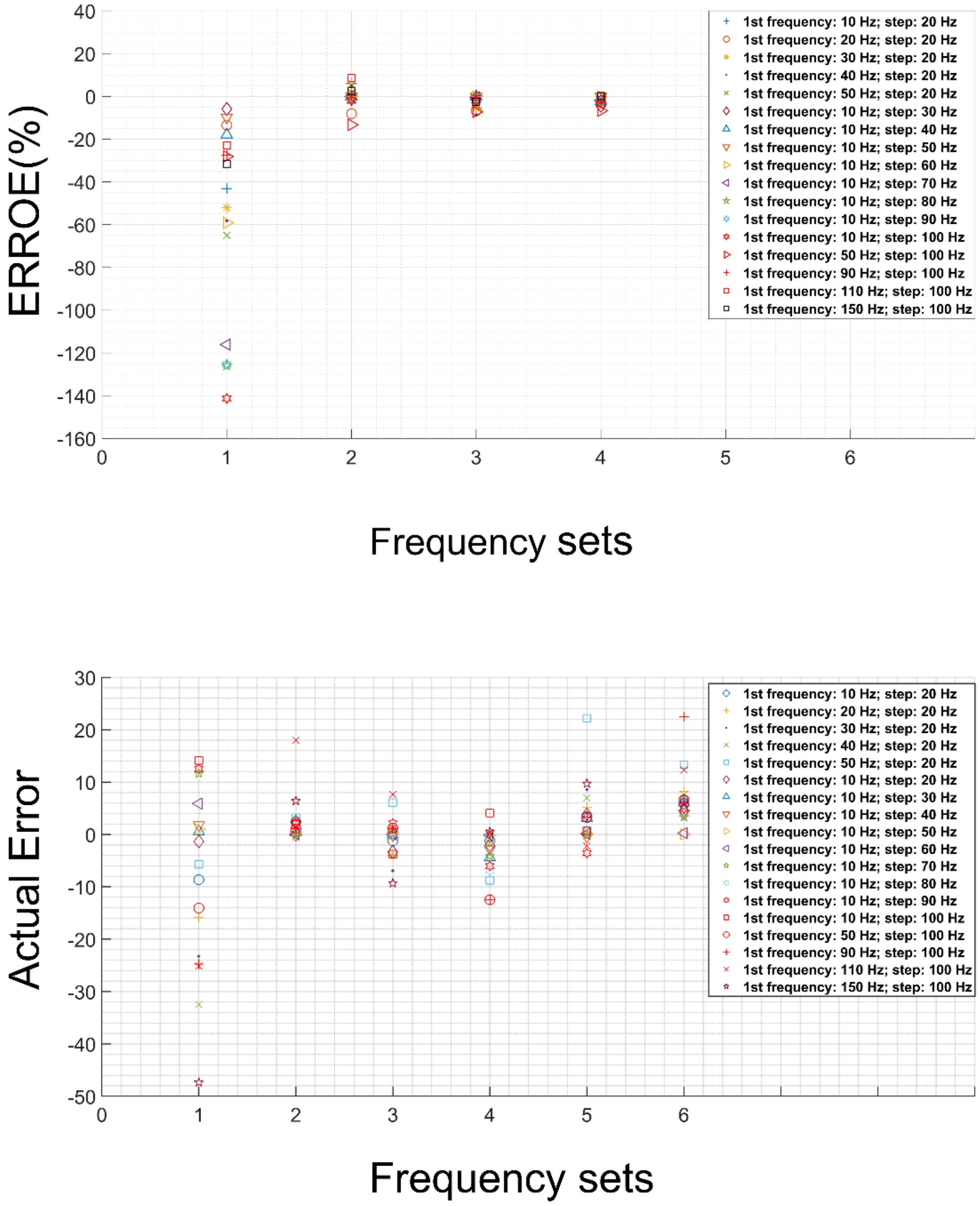

Figure 3.8. the percentage and actual difference or error between finite element model eigenvalues and corresponding target natural frequencies for the 17 test sets. Each data point is the average of 5 independent runs

3.5.4. Comparative performance of GA, NEAT and CPPN-NEAT

Based on the GA tuning results, the NEAT and CPPN-NEAT parameters were set as; population 100, crossover percentage 0.6, 0.08 mutation probability for adding nodes and connections and a maximum of 150 iterations. For CPPN-NEAT, sine, cosine and exponential functions were used as the activation function list. The 400 voxel beam model was used for the comparisons, and three groups of tests, with ten trials per target set, were conducted to test performance against three sets of natural frequency targets. These three sets correspond to those for which GA produced the best and worst results and the one that had the highest frequency range. The first two had a first natural frequency of 10 Hz and resonance spacings of 20 and 50 Hz, respectively, while the third had its first natural frequency at 50 Hz, and subsequent resonances were spaced 50 Hz apart.

As shown in Figure 3.9 (a)***,*** direct GA generated better results in both average and absolute fitness values than either NEAT or CPPN-NEAT in the two test groups with the lower first natural frequency. For the third test group, according to the paired t-test, GA and NEAT do not have significantly different mean fitness values (p-value 0.058). However, GA had a lower mean fitness value than CPPN-NEAT (p-value: 0.002 with a 95% confidence interval). While GA still obtained the lowest fitness value of all the trials for the target set 3, it also had higher variability than the other algorithms. Compared with NEAT and CPPN-NEAT, the classic genetic algorithm evolves the entire binary representation of the structure rather than evolving a neural network structure to represent the multi-material beam.

Therefore, GA has more freedom in arranging materials as it evolves, which provides a higher probability of approaching the optimal structure, i.e. one that fulfils the design target. Through the comparison of these different algorithms against three target groups, it can be observed that classic GA provided the most satisfying performance for natural frequency tailoring in a structural element with simple geometry but potentially complex material distributions. It was also found that for this problem, the computational times for all three algorithms were similar, as they are dominated by the computation of the finite element model's eigenvalues at each functional evaluation and add up to approximately 200 seconds per generation or 30000 seconds for a 150-generation run. All three algorithms were limited to 150 generations, as testing up to 1000 generations had shown that for all three algorithms, fitness improvements stopped within 150 generations. Figure 3.9(b) shows an example of the convergence of the three algorithms when optimising the structure with the target was a first natural frequency at 10 Hz and resonance spacings of 20 Hz.

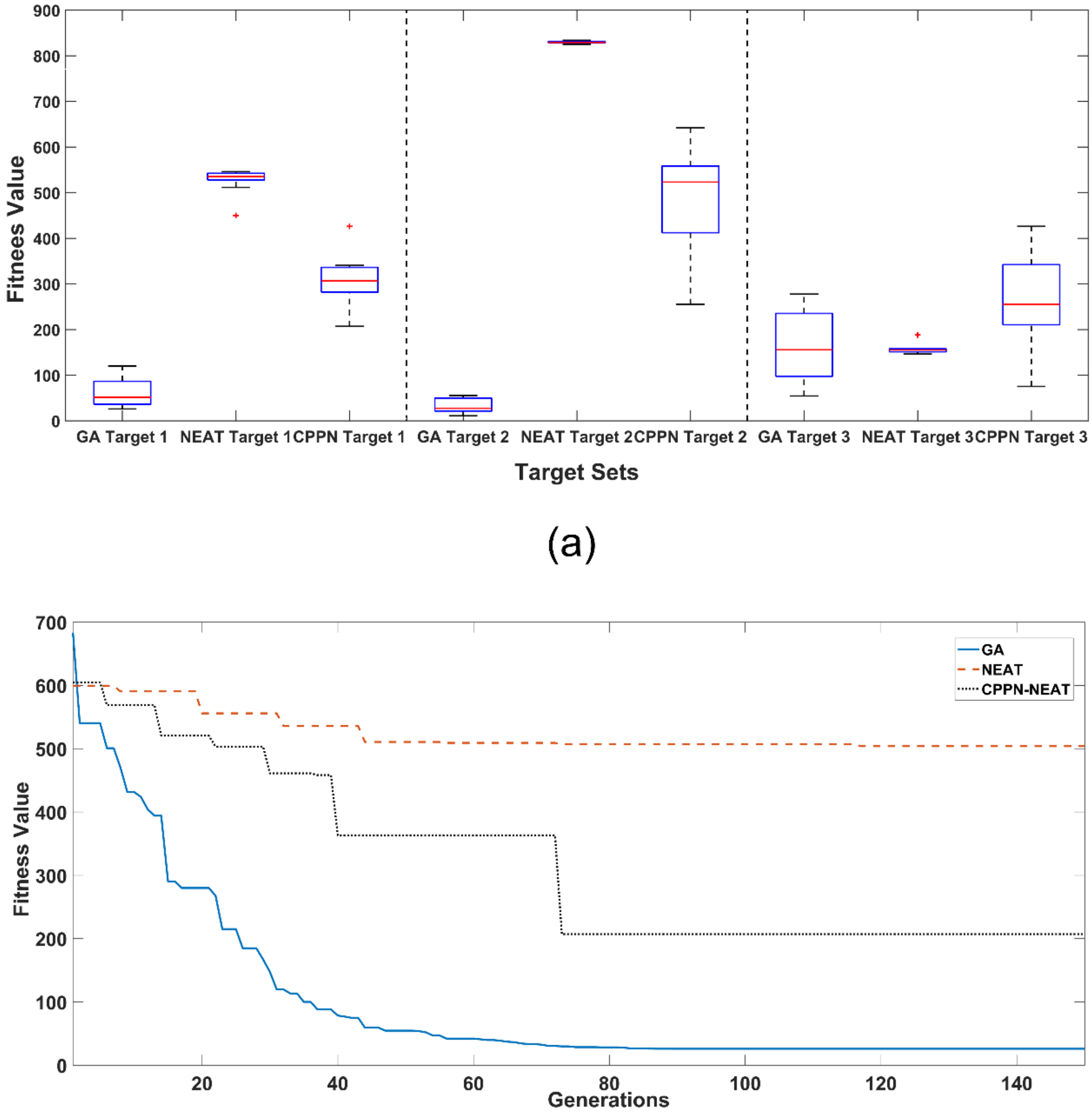

(a)

(b)

Figure 3.9. (a) Comparison of fitness values obtained by GA, NEAT and CPPN-NEAT for three target frequency sets, summarising the results of 10 trials for each target set. The lower the fitness value, the closer the beam's eigenvalues were to the target frequencies. The solid lines indicate the median fitness value and the boxes represent the 25th and 75th percentiles, and (b) An example of the fitness value improvement based on GA, NEAT and CPPN-NEAT algorithms, with optimisation target set [10, 30, 50, 70, 90, 110] Hertz.

3.6. Material topology manipulation for optimum toughness

To further validate the proposed material topology optimisation scheme, the optimisation of the material distribution for the maximum toughness is considered based on a standard dumbbell-shaped tensile test specimen. Compared with frequency optimisation, which is balancing the distribution of the soft and stiff materials for an exact eigenfrequency response, toughness uses the distribution of the soft and stiff materials to maximise both stress and strain, which are conflicting responses in the case of many common materials. The objective of this section is to verify the ability of the proposed GA optimisation scheme in handling multi-objective and conflictive targets, such as the maximisation of both stress and strain responses of a component for optimal toughness property. A standard American Society for Testing and Materials (ASTM) D638-14 TYPE IV specimen is used as the problem domain. The specimen geometry is illustrated in Figure 3.10, and the dimensions are listed in Table 3.7 (ASTM, 2022). The stress-strain relationships are established from the tensile tests simulated in COMSOL Multiphysics.

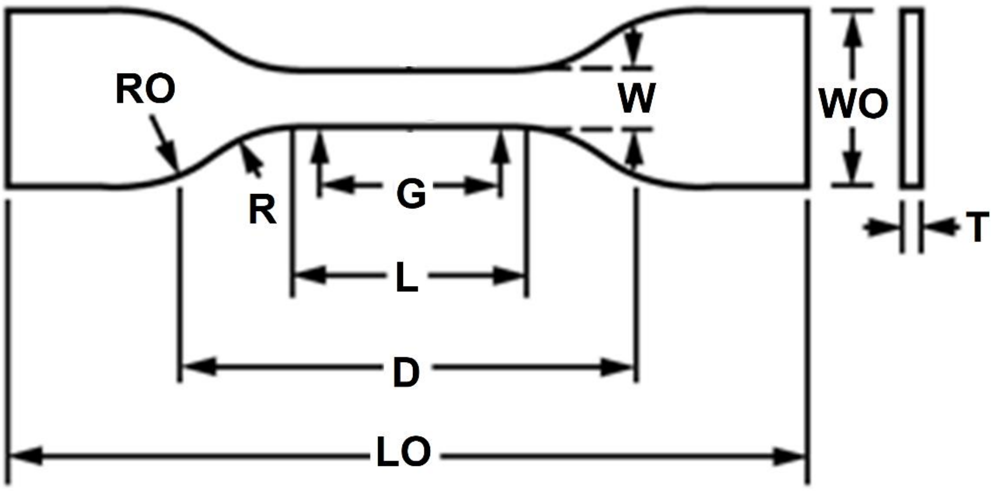

Figure 3.10. ASTM D638-14 TYPE IV specimen

Table 3.7. ASTM D638-14 TYPE IV specimen Dimensions

Dimensions (mm)	W	L	WO	LO	G	D	R	RO	T
D638-14 TYPE IV	6	33	19	115	25	65	14	25	3.2

3.6.2. Functional evaluation

The same finite element analysis software package COMSOL Multiphysics (Version 5.6, release date November 11, 2020, COMSOL Inc., Stockholm, Sweden) is used to simulate stress and strain behaviour. The standard quadratic solid elements are used for finite element discretisation and analysis. In the optimisation for toughness, the target is searching for the optimal material combination for maximum toughness. The stress and strain curve is retrieved from COMSOL Multiphysics to compute the resulting toughness as the area under the stress-strain curve of the structure, as shown in Figure 3.11, which is then used as the fitness function in the genetic algorithm. It is defined as the energy that the structure can absorb before fracture during the tensile test.

Stress is defined as the ratio of the force F to the original cross-sectional area A_o of the structure. And the strain is represented as the ratio of the stretched length of the structure in the body relative to the original length L_o. The expression of stress and strain are given by equation 3.4 and equation 3.5, where F is the applied force at the ends of the structure; A_o is subjected to the cross-sectional area of the structure; L_t and L_o represent the length of the structure under the applied force F and the original length and the structure, respectively.

$$\sigma_E = F/A_o \tag{3.4}$$

$$\varepsilon_E = L_t - L_o/L_o \tag{3.5}$$

The area under the stress-strain curve is computed via the standard trapezoidal approximation function in MATLAB. The target and fitness function is shown in equation 3.6. Where i indicates the index of the sampling point. σ_i and ε_i Indicates the stress and strain in the sampling point i. Then toughness value is used as the fitness value for the genetic algorithm optimisation.

$$Toughness_{max} = \sum_{i=0}^{i}(\sigma_i + \sigma_{i+1})(\varepsilon_{i+1} - \varepsilon_i)/2 \qquad (3.6)$$

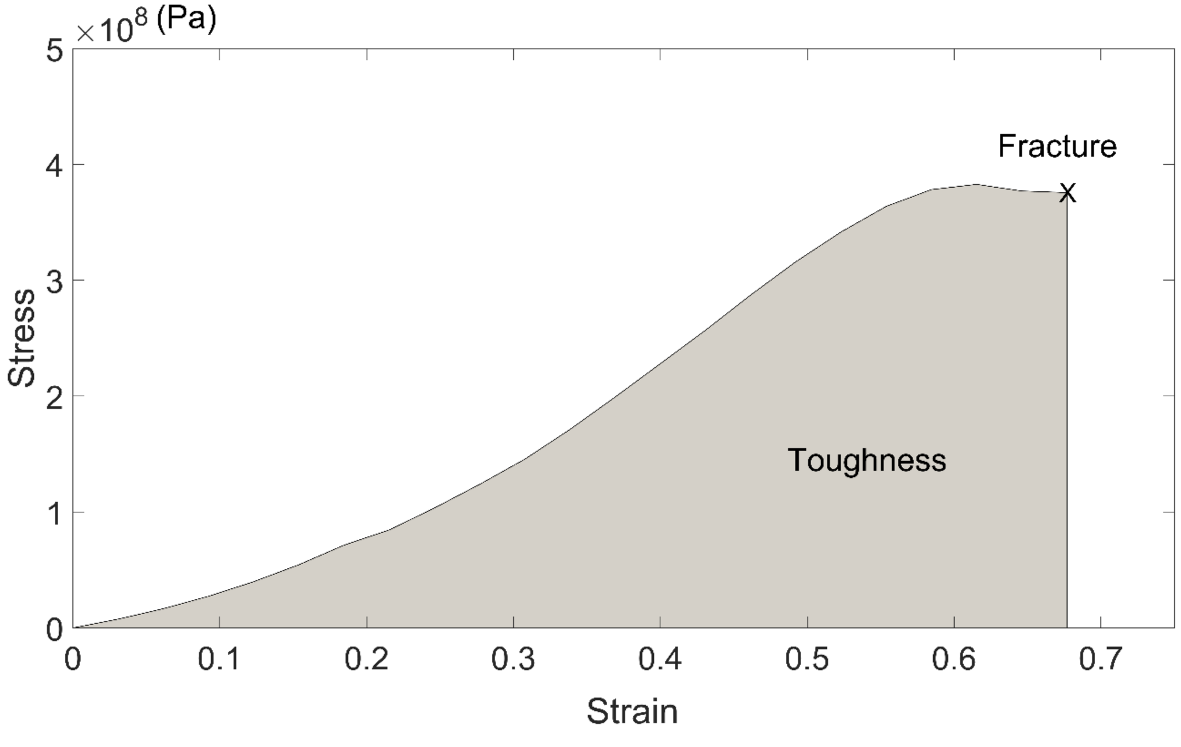

Figure 3.11. Toughness as defined by the area under the stress-strain curve

3.6.3. Experimental setup

ASTM D638-14 TYPE IV specimen and standard tensile test simulated in COMSOL Multiphysics for the relationship between stress and strain are used. Two mock materials are used in the simulation, as listed in Table 3.8, and the isotropic hardening model in COMSOL Multiphysics is used to simulate plasticity during the tensile test (COMSOL, 2021). As shown in Figure 3.12, a dumbbell-shaped specimen of 388 voxels is used. As the force is applied along the X-axis, the material topology is set symmetrical with the x-axis. Therefore, 156 designable domains are used as inputs in the optimisation scheme. As documented in section 3.5.2, the GA parameter combination of the population 100, crossover percentage 0.6, mutation percentage 0.08, mutation rate 0.08 and roulette wheel selection can provide the optimal result in balancing the performance and computing time. The same parameters are used in the optimisation for toughness maximisation. And the randomly generated material distribution is used as the initial model in the optimisation scheme.

Table 3.8 Mock material Properties for toughness optimisation

Materials	**Density (*kg/m*^{3})**	**Young's modulus (Pa)**	**Poisson's ratio**	**Initial yield stress (Pa)**
Soft material	1000	0.25×10^9	0.3	6×10^6
Stiff material	1000	25×10^9	0.3	6×10^8

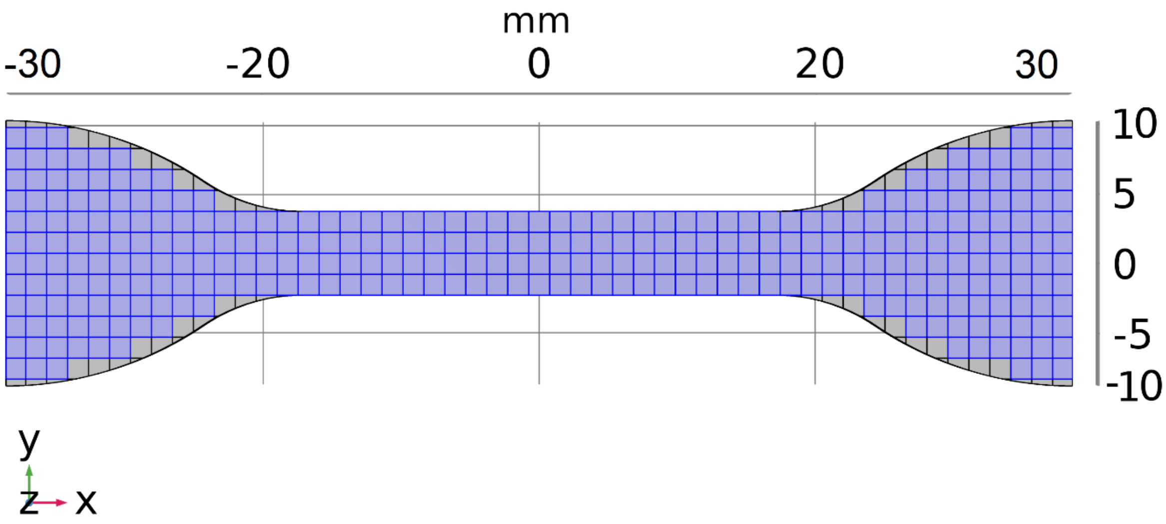

Figure 3.12. The ASTM D638-14 TYPE IV specimen and the designable domains (blue blocks)

3.6.4. Optimum toughness results

An example of the distribution pattern of the two material systems resulting from the proposed generative composite material design process is illustrated in Figure 3.13 (a). The overall deformation and the internal deflection patterns under the stress of the dumbbell-shaped specimen with the optimum material dispersion are shown in Figure 3.13 (b). The stress-strain curves constructed for different material distribution patterns are presented in Figure 3.14, and the toughness values obtained in all the cases are shown as the bar graphs in Figure 3.15. Based on the results in Figures 3.14 and 3.15, the stress-strain results of the single stiff and soft material cases are rather obvious and as expected. Striking differences are evident in the stress-strain responses of specimens filled with optimum distributions as obtained by the generative design methods and the randomly distributed cases. The two specimens with the two materials randomly distributed within the voxels have resulted in the least toughness values, with both stress and strain responses far inferior compared to the original material constituents. It is clearly indicative that randomly combining the soft and stiff materials destroys the overall material responses, and a carefully designed material distribution achieved by means of a carefully constructed search algorithm is essential to converge on the target material performance.

The specimens with the optimised material distribution have clearly sustained significantly higher stress and strain before fracture. The fracture points for the specimens with the optimum distribution patterns 1 and 2 reached almost similar ultimate stress levels as the fully stiff material specimen while also demonstrating significantly larger deformation or strain before fracture. The specimens with the optimum material dispersions attained almost four times higher toughness values compared with the all soft material model. These results indicate that the proposed GA topological optimisation can efficiently handle the optimisation of the stiff and soft material distribution for maximum toughness, increasing both stress and strain responses. It is also pertinent to point out that the topological optimisation schemes used for the toughness case only needed minimum changes from the version used for frequency optimisation, which demonstrates the versatility of the proposed optimisation schemes.

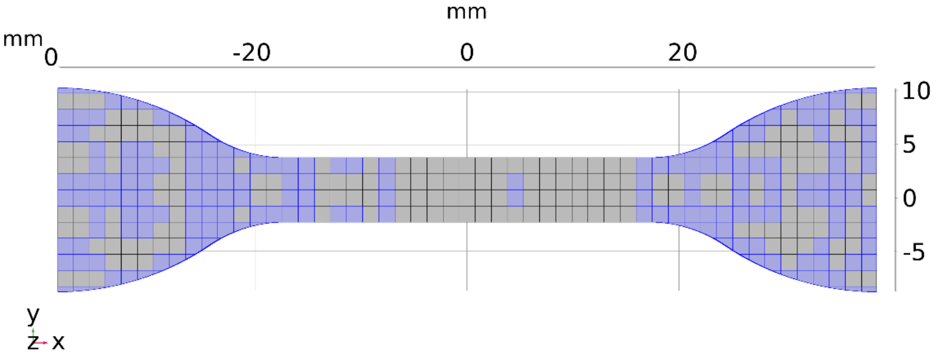

(a)

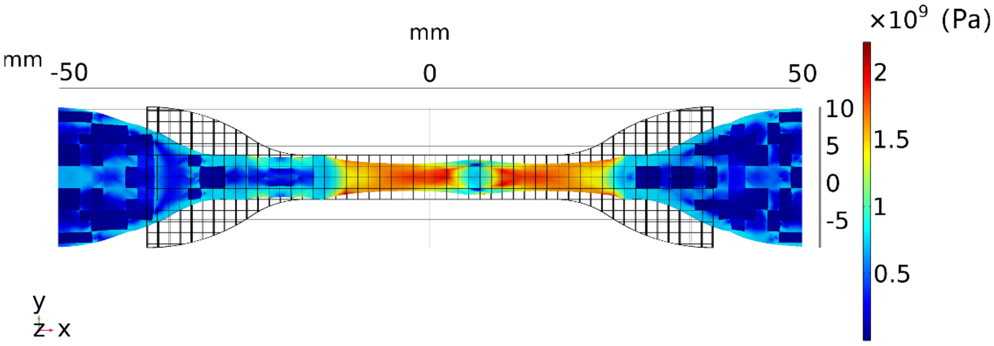

(b)

Figure 3.13. An example of the optimised dumbbell specimen (a). The distribution of stiff material (blue voxel) and soft material (grey voxel) is produced by the proposed topological optimisation scheme. The deformation of the specimen under stress is dispatched in (b).

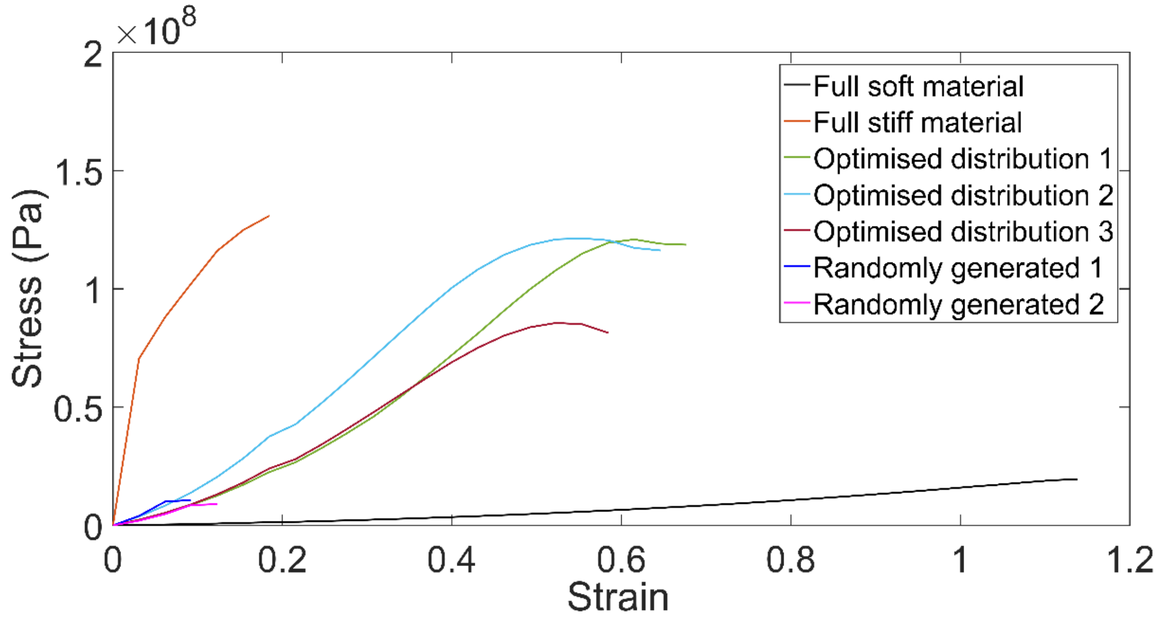

Figure 3.14. the stress and strain curves obtained from the FE simulations for single materials, random distribution of materials and other material distributions obtained at different levels of optimisation.

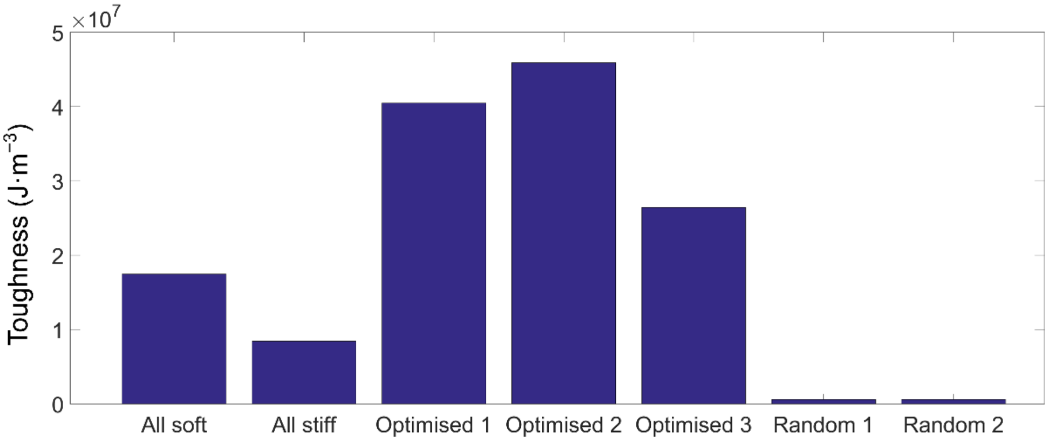

Figure 3.15. The toughness values for optimised specimens and specimens with randomly generated material distribution.

3.7. Summary of Chapter 3

A method for the automated design of material compositions to achieve a set of chosen dynamic performance targets is presented. Evaluations based on the optimisation of the natural frequencies of a cantilever beam that is composed of two different polymers are used to evaluate the performance of this method. As a test, it is given a target of generating a design where the first six natural frequencies match an evenly and closely spaced set of target frequencies. The results indicate that it is indeed possible to extract novel, unprecedented behaviours from well-known structural elements and existing materials, the physical implementation of which is now possible by taking advantage of the advances in multi-material additive manufacturing solutions.

A metaheuristic search using a binary genetic algorithm, as explored in this initial study, can tailor the natural frequencies of a beam structure to a good approximation of the customised target set, with less than 5% error in many cases. It provides an exciting approach to the solution of vibration problems and the optimisation of the dynamic performance of structures and machinery. The experiments conducted indicate that the design of materiality can produce desired natural frequencies with acceptable error margins. Though demonstrated with beams, this simple structural form is a building block for many structures and mechanisms across multiple engineering fields, which gives these findings considerable generality in their applications.

While the results are encouraging overall, there are interesting issues of error and variability, and the evolutionary process is extremely computationally expensive. For this problem, the binary genetic algorithm generated equal or better results in terms of both fitness value and computational cost than either NEAT or CPPN-NEAT, perhaps because it has more freedom in assigning materials to voxels than what is provided by the neural nets and that CPPN-NEAT was generally equal or better than NEAT. Further, the optimisation schemes applied to the toughness evaluation showed the proposed multi-material topology optimisation to be satisfactory maximisation of toughness. It demonstrated the versatility of the proposed method and proved that the proposed method is capable of handling different property optimisation tasks with minimum changes

Chapter 4

Generative design of structured materials

4.1. Multi-material dispersion vs spatial structural variations

Spatially-varying material properties allow the dynamic response of structural systems to be almost arbitrarily tailored, far beyond the first or fundamental natural frequency. Continuing advances in manufacturing technology are making it possible to achieve the necessary range of stiffness and density variations, but the design of these property distributions is a challenging task because of the complex, multi-dimensional nature of the problem. Generative design methods based on evolutionary optimisation algorithms have been successfully used to obtain solutions based on multi-material distributions. However, the applicability of these solutions is limited by their reliance on multi-material additive manufacturing, which currently only offers digitally mixed acrylic polymer options that are generally unsuitable for producing functional parts. A novel structured material solution is proposed here in which the problem domain is divided into several volume elements (voxels), each of which contains a structure whose geometrical form is altered to adjust its effective properties to desired values.

The single material structural solution will be amenable for ready fabrication by the powder-based selective laser sintering and melting processes with real engineering polymer and metal systems, thereby allowing for the realisation of the benefits in real-world applications. The resulting continuous design spaces are searched using a modern evolutionary algorithm, the covariance matrix adaptation evolution strategy (CMA-ES). A MATLAB implementation of this evolutionary design method, in conjunction with finite element simulations for fitness evaluation, showed good convergence for several different cantilever beam test cases when tested against several different sets of natural frequency targets. Correlations with the multi-material solutions show that the single structured material approach is on par or even better in some cases, even though the test domain was discretised into 80% fewer voxels than for the multi-material case. Furthermore, the voxel structures can be realised using current additive manufacturing technologies.

4.2. The background

The frequencies at which a body will vibrate after being disturbed from equilibrium, in the absence of any driving force, are known as the natural frequencies. When time-varying loads oscillate at a frequency that matches one of the natural frequencies, resonance occurs, and there is a peak in system response(Crowell, 2020). Resonance, with the associated natural frequencies, is one of the most important and familiar concepts in physics as it permeates the behaviour of oscillating systems, be they mechanical, acoustic, electromagnetic, atomic particles, etc. (Buchanan, 2019). Tuning the mechanical resonance or natural frequencies of structures, vehicles, and machines is an important aspect of mechanical engineering design, as these frequencies play a vital role in dictating vibrations and overall dynamic responses under time-varying loading. Vibrational motions can become intense around resonance, leading to severe stresses, fatigue, and subsequent weakening or even fracture in engineered systems. This can lead to catastrophic failures in rotating machinery, piping systems, and several aerospace disasters are immediate examples(M. Hansen, 2003; Osiander et al., 2018). The most recent instances are a series of resonance-driven uncontained engine failures in Airbus A220 airliners, as reported in the news in 2019 and 2020(Hepher, 2020). On the other hand, resonances can also be exploited to improve performance. The more intense motion and vibrations can provide increased energy conversion efficiencies in energy harvesting mechanisms in wearable devices(Saha, O'donnell, Wang, & McCloskey, 2008) or wave energy conversion systems(de la Villa Jaén, García-Santana, & Montoya-Andrade, 2014; Stappenbelt & Cooper, 2010). Resonances are also key to advances in wireless communications that depend on resonant vibroacoustic wave filters, the latest of which is known as 5G(Y. Liu et al., 2020)

The control of vibrations is a classic engineering design problem. The first engineering solution is to redesign the structure or mechanism so that the natural frequencies are well separated from the loading frequencies, as the latter is often tonal. If that is impractical or in the presence of a broadband loading spectrum, the solutions depend on transferring the vibrational energy into additional energy-absorption systems. For this purpose, different types of tuned vibrational absorber (TVA) solutions were designed(Sun, Jolly, & Norris, 1995; Tarng, Kao, & Lee, 2000; Vonflotow, Beard, & Bailey, 1994). Similarly, tuned mass damper (TMD) systems depend on increasing stiffness, mass, and damping to achieve control of the natural frequency(Hoang, Fujino, & Warnitchai, 2008; Kaynia, Biggs, & Veneziano, 1981). However, extra damping or energy-absorbing structures usually can only affect the first or fundamental resonant frequencies(Cheney et al., 2014). Furthermore, in many cases, the designed structure is integrated with pre-existing structures, with significant adverse effects on the size and weight of the final design.

On the other hand, several methods based on topology optimisation algorithms have been proposed for automating the redesign of the system to alter its natural frequencies. Some optimise the resonant response by varying the number of truss elements and their locations(Gholizadeh & Barzegar, 2013; Stanford & Dunning, 2015). Others use density-based approaches, like the solid isotropic material with penalisation (SIMP) method, which has been applied in tasks such as the maximisation of steady-state vibrations at the desired frequency(Tcherniak, 2002), the fundamental frequency(Tsai & Cheng, 2013), and the gaps in the eigenfrequencies(Du & Olhoff, 2007). Hard-kill techniques such as the evolutionary structural optimisation (ESO)(Y. M. Xie & Steven, 1993) and its extended version, bi-directional evolutionary structural optimisation (BESO, which enables the material to be added after removal)(Querin, Young, Steven, & Xie, 2000; X. Yang, Xei, Steven, & Querin, 1999) have also been widely applied to frequency design problems such as maximising and minimising the fundamental frequencies as well as a set of frequency responses(X. Huang et al., 2010; Picelli et al., 2015; Vicente et al., 2016; X. Yang, Xie, et al., 1999).

To search the optimal distribution of the materials for desired properties, generative design methods based on evolutionary algorithms, the classic genetic algorithm (GA) and the more recent variants based on neuroevolution of augmented topologies (NEAT) have been applied. This is solving the inverse problem of identifying the multi-material distributions that can produce the desired natural frequency spectrum in a multi-material structure of fixed geometry. It has been shown that this approach can be used to design the distribution of two materials in cantilever beams using a variant of NEAT known as compositional pattern-producing networks (CPPN-NEAT)(Kenneth O Stanley, 2007). The feasibility of successfully tailoring multiple natural frequencies to match randomly selected target frequency sets was demonstrated, albeit within a limited frequency range(Cheney et al., 2014). The current authors subsequently advanced state of the art through a generative design method that distributes materials so as to obtain equally and closely spaced natural frequencies, something that is of practical importance and impossible with conventional approaches(W. Yang, Calius, Huang, & Singamneni, 2020). The method used to identify combinations of two materials that closely match the first six desired frequencies of the beam was based on binary GA, but versions using NEAT and CPPN-NEAT were also tested for comparison. Some excellent results were obtained, but there were also significant challenges associated with certain target spectra that featured lower fundamental natural frequencies and larger resonance spacing(Cheney et al., 2014; W. Yang et al., 2020).

Evidently, generative design methods based on multi-material distributions provide possible solutions to the problem of designing composite structures with pre-set frequency responses. When it comes to fabricating multi-material structures, hybrid manufacturing was shown to be useful to achieve specific engineering responses by combining two or more materials with predetermined forms, structures, and methods (M. F. Ashby & Bréchet, 2003). This method was also adapted to design a damper system combining metallic additive manufacturing and polymer filling techniques, where the internal features of the damper system were designed to achieve the desired fundamental natural frequency responses(Betters et al., 2020). Additive manufacturing (AM) technologies take this much further, allowing to fabrication of three-dimensional (3D) objects directly from computer-aided design models achieving controlled material property variations, as opposed to subtractive manufacturing(Zhai et al., 2014). With the advent of the latest multi-material additive manufacturing, designable composite materials have become a promising approach for achieving tailored mechanical responses. A range of works indicated the possibility of varying the material properties and fabricating objects with desired material properties such as stiffness, deformation behavior, subsurface scattering, and frequency responses(Bickel et al., 2010; Cheney et al., 2014; Hašan et al., 2010; J. Hiller & H. Lipson, 2009; Hiller & Lipson, 2010, 2012).

However, in practice, the multi-material additive manufacturing (MMAM) solutions suffer from the lack of real engineering material options as the current systems are only able to offer digitally mixed acrylic polymer options consolidated by UV curing. They also deposit only one material at a time, so the structure is divided into volume elements, known as voxels, to each of which one material is assigned out of the total palette. This discretisation process is known as voxelisation. The voxel shape and dimensions cannot be smaller than the minimum material unit deposited by the MMAM process (maxel) but may be considerably larger, depending on the mechanics of the structural system.

A novel solution is presented in this chapter as an alternative, in which the solid voxels are replaced by cellular structures that can provide effective variations in the material responses as needed. In this approach, instead of changing the materials, each voxel is made as a structural form that can be changed in geometry to alter its effective mechanical properties and mass. As long as certain constraints are respected, it should then become possible to effectively control the properties of each voxel while also expanding the range of properties that can be assigned to it. This approach will eliminate the need for MMAM, allowing these structures to be built out of real engineering materials using existing additive manufacturing methods, in particular, the powder bed fusion technologies that are suitable for the production of functional parts of complex geometries. However, this approach also introduces the requirement for the voxels to be large enough to be manufacturable, thus limiting the total voxel count to a much smaller number than what is allowable when using MMAM. Nevertheless, the approach is envisioned to be far superior to the multi-material printing solutions with digitally mixed material options in terms of the readiness of applying the commercial printing technologies, the overall performance of the printed structures, and the ranges of variations possible. The research question of whether this approach can match the results that have been obtained with multi-material generative design solutions is addressed in this chapter.

4.3. Methodology for optimising voxellised structures

4.3.1. The generative design algorithm and its controlling parameters

Evolutionary design is an iterative methodology inspired by nature. The "survival of the fittest" mechanism drives each generation to move towards the targets or requirements specified by the objective function, with the solutions being chosen from the final generation(Fischer & Herr, 2001). With ever-increasing computational power and the advent of computational methods enabled by this power, different generative design methods have evolved for finding solutions to frequency response problems(Cheney et al., 2014; Du & Olhoff, 2007; Gholizadeh & Barzegar, 2013; Picelli et al., 2015; Stanford & Dunning, 2015; Tcherniak, 2002; Tsai & Cheng, 2013; Vicente et al., 2016; X. Yang, Xie, et al., 1999). While most of the current frequency response design schemes depend on multi-material solutions(Cheney et al., 2014; Picelli et al., 2015; Vicente et al., 2016), the approach proposed here is to locally alter the structure to vary the distribution of effective stiffnesses and density, while maintaining the base material the same. The problem domain is divided into multiple brick-like hexahedral volume elements (voxels) all with the same length and width. Each of the voxels has a structure defined by a number of geometrical parameters. To tailor the frequency response, the bending and torsional stiffnesses, as well as the mass of each voxel, are indirectly controlled through these geometrical parameters, which are used as design variables by the generative design algorithm instead of its material composition. This allows a considerable degree of independence between the bending and torsional stiffnesses and the density of each voxel. And since these design variables are continuous rather than discrete, as would be the case when using material selection, a modern evolutionary algorithm for continuous spaces known as the covariance matrix adaptation evolution strategy (CMA-ES)(N. Hansen et al., 2003) is used to find configurations that provide natural frequencies matching the design targets as closely as possible.

CMA-ES has become a popular tool for continuous black-box optimisation of difficult, non-linear, and non-convex problems and, to the best of the authors' knowledge, has not been used for materials-based tailoring of structural dynamics (N. Hansen et al., 2003). In each iteration, a number of candidate solutions for the next generation are sampled from a normal distribution of multiple variables with a step size of the current generation. The fitness of these solutions is evaluated, and the sampling distribution of the next generation is adjusted according to the fitness of each solution in the current generation(N. Hansen & Ostermeier, 2001). In this work, the original CMA-ES proposed by Hansen and Ostermeier(N. Hansen & Ostermeier, 2001) has been adapted.

The overall optimisation scheme was extracted from the existing CMA-ES solution system(N. Hansen & Ostermeier, 2001) and implemented in MATLAB (R2017B, release date September 14, 2017, MathWorks, Natick, Massachusetts, USA). The major analysis steps are presented in the form of the pseudo-code shown in Figure 4.1. The structural optimisation scheme is summarised in the flow chart as shown in Figure 4.2(N. Hansen & Ostermeier, 2001; S. M. K. Heris, 2015). COMSOL Multiphysics (Version 5.5, release date April 25, 2020, COMSOL Inc., Stockholm, Sweden), a commercial finite element analysis software package, is used to compute the desired eigenfrequency values. The standard quadratic solid elements are used for finite element discretisation and analysis.

```
Step 1: CMA-ES parameters setting
    FitnessFunction            //Fitness function evaluated by FEA
    VarSize                    //Decision variables matrix size
    Varboundary                //Boundary of decision variables
    MaxIt                      // Maximum Number of iterations
    Target                     // Desired Target frequency

Step 2: Initialize CMA-ES
    Initialize population      //Generating individuals within
    Apply boundaries
    Evaluating population      //Evaluating individuals by Fitness function
    Sorting population

Step 3 While MaxIt AND Target are not met do
        Updating step size
        Updating covariance matrix
        Evaluating individuals by Fitness function
        Sorting population
        Updating best solution
    End While
```

Figure 4.1. The pseudo-code of the major steps of the overall optimisation scheme

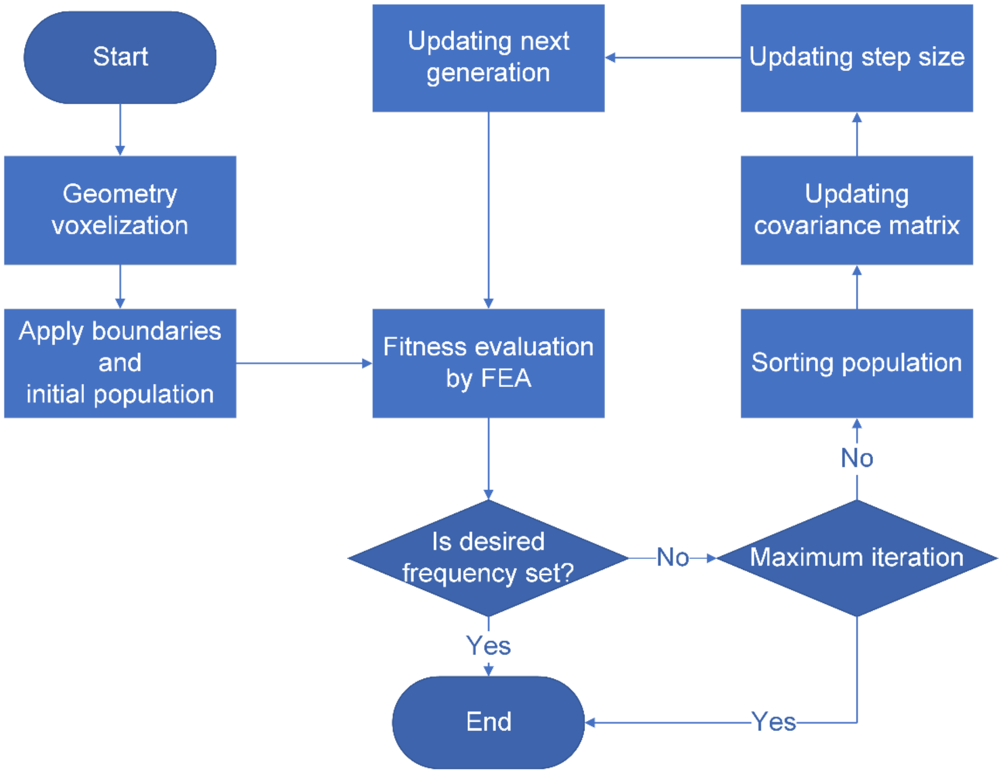

Figure 4.2. The flow chart of the overall optimisation scheme

The objective function minimises a single fitness value that is defined as the sum of the weighted (w_i) mean square errors of the frequency set. That errors are the differences between the first N desired or target frequencies and the corresponding natural frequencies or eigenfrequencies of the candidate solution.

$$fitness = \sum_{i=1}^{N} w_i \left(freq_i^{target} - freq_i^{calc}\right)^2 \tag{4.1}$$

$$w_i = (N + 1 - i)/N \tag{4.2}$$

Where $freq_i^{target}$ and $freq_i^{calc}$ are the target and the eigenfrequencies computed by the finite element analysis; N and i indicate the total number of the eigenfrequencies and the index of the current eigenfrequency.

4.3.2. Comparison to multi-material generative design with a binary genetic algorithm

The performance of the method described above is also comparatively assessed against the best of the multi-material generative design schemes based on a binary genetic algorithm (W. Yang et al., 2020). In the genetic algorithm, the material assignments in the voxelated structure are represented as a binary array, which is used as its genetic code. GA then uses a survival-of-the-fittest mechanism to search the multi-dimensional space of these binary array representations or material distributions for those that provide the best matches to the desired frequency responses. GA runs in an iterative manner; a population is created at each iteration, and the "genetic code" of each individual is exchanged according to rules of crossover and mutation. The parents of the next generation are selected based on fitness values and different selection strategies. The crossover process swaps the genetic representation of the "parents" to create the next generation. The mutation process will randomly switch the genetic representation, allowing the genetic structure to break the old loop, which could become trapped in the local extrema and induce randomness. The next generation is produced through crossover and mutation procedures, controlled by parameters that establish the balance between local exploitation and wider exploration(Chapman et al., 1994; Chipperfield, Fleming, Pohlheim, & Fonseca, 1994b). Best combinations are identified by evaluating their fitness values, calculated using Equations (1) and (2). This comparative assessment was carried out through numerical experiments, using a selection of the most interesting target frequency sets identified in the work by Yang et al. (W. Yang et al., 2020).

4.4. The cantilever beam settings for frequency response analysis

Tailoring the frequency responses of a cantilever beam with a fixed length and width was selected as the test case for the experiments to evaluate the strengths and weaknesses of structural variation as a generative design approach. The cantilever beam is one of the simplest structures in engineering. Its mechanics are well-known, keeping the research focus on the effectiveness of the proposed method in converging on solutions that match the design target. The cantilever beam has the same length (40 mm) and width (10 mm) as that used as the test domain in the multi-material generative design by Yang et al. (W. Yang et al., 2020). The principal differences lie in the thickness of the beam, which previously was fixed at 1 mm and is now allowed to vary, and in the structure of the voxels, which previously were uniform solids. As before, the first six natural frequency responses are used as the criteria for evaluation. Tests were conducted with three target sets. These target sets have their first frequency values at 10, 10, and 50 Hz and spacings of 20, 50, and 50 Hz, respectively, resulting in the target sets listed in Table 4.1, which will be referred to as Target Sets 1, 2, and 3 from here onwards.

Table 4.1. Frequency targets for testing the algorithm

Natural frequency number	Target Set 1 (Hz)	Target Set 2 (Hz)	Target Set 3 (Hz)
1st	10	10	50
2nd	30	60	100
3rd	50	110	150
4th	70	160	200
5th	90	210	250
6th	110	260	300

4.4.1. Voxel structure and boundaries of the design search space

Two different voxel structure designs were tested, depicted as type A and B voxels in Figure 4.3. Both are hollow rectangular blocks with open ends to allow unconsolidated powder to be removed if produced by a powder bed AM process. The type A voxel has a single void space located in the centre and runs the whole length of the voxel with two geometric design parameters and the voxel alters the voxel stiffness characteristics. For the type B voxel structure, the height H_b and the void height H_v that is adjusted by the CMA-ES algorithm to the central void is split into two identical lengthwise void spaces positioned symmetrically relative to the midplane of the voxel. This adds an extra geometric design parameter T_m representing the central cross-web thickness, which is additional to the two (voxel and void height), it shares with the type A voxel.

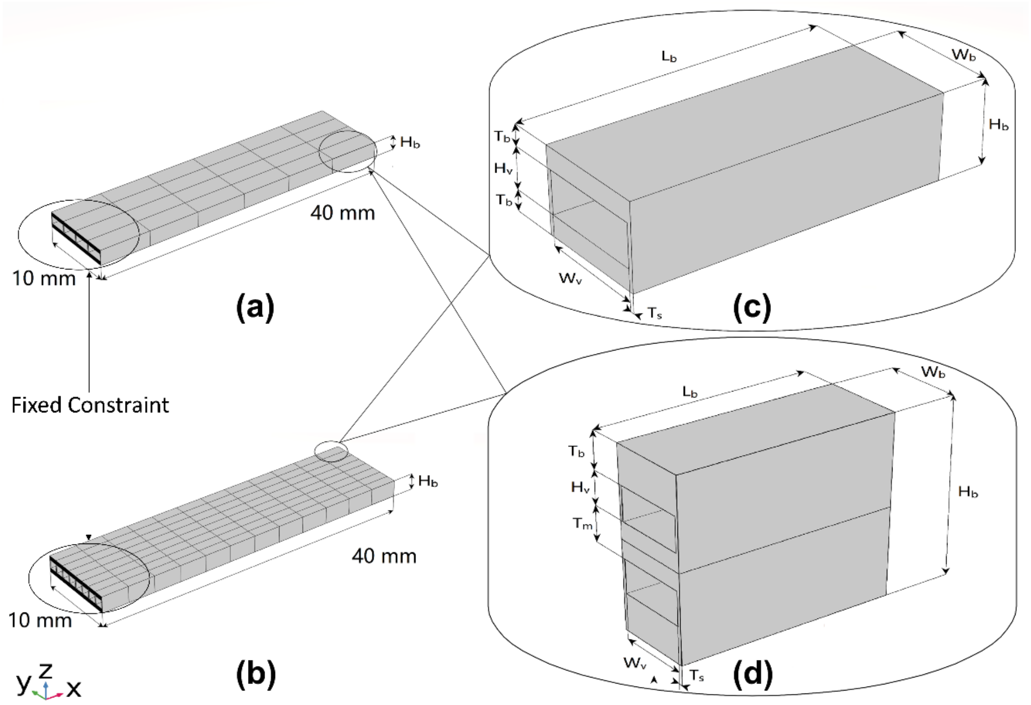

Figure 4.3. The cantilever beam domain is discretised into (a) 24 voxels and (b) 96 voxels, showing the details of the (c) type A or (d) type B structure. In these particular examples, the height H_b is 2 mm for the type A voxel and 4 mm for the type B. The void height H_v is 1 mm for both; and the cross-web thickness T_m for type B is also 1 mm.

There are bounds to the voxel height and its wall thickness due to various practical considerations. During the evolutionary design search, the voxel geometrical parameter values were constrained to the ranges defined in Table 4.2, and the voxelated beam structures corresponding to these high and low bounds are illustrated in Figure 4.4. The resulting ranges of beam's natural frequencies, as calculated by the finite element eigenvalue analysis, are listed in Table 4.3. It is pertinent to point out that the target frequencies defined in Table 4.1 fall within these natural frequency ranges.

Table 4.2. The bounds on the voxel geometric parameters for the design domain

	24 voxel test case			96 voxel test case		
Geometric parameter (See Figure 4.1)	**Type A voxel low bound**	**Type B voxel low bound**	**Type A and B voxel high bound**	**Type A voxel low bound**	**Type B voxel low bound**	**Type A and B voxel high bound**
L_b	6.66	6.66	6.66	3.33	3.33	3.33
W_b	2.5	2.5	2.5	1.25	1.25	1.25
H_b	0.5	0.5	20	0.5	0.5	20
T_b	0.1	0.1	N/A	0.1	0.1	N/A
H_v	0.3	0.1	N/A	0.3	0.1	N/A
T_s	0.1	0.1	N/A	0.1	0.1	N/A
W_v	2.3	2.3	N/A	1.05	1.05	N/A
T_m	N/A	0.1	N/A	N/A	0.1	N/A

Table 4.3. The ranges of beam's natural frequencies that result from the ranges of voxel geometrical parameters are listed in Table 4.2

	24 voxel beam		96 voxel beam		24 and 96 voxel beam
Natural frequency	**Type A voxel low bound (Hz)**	**Type B voxel low bound (Hz)**	**Type A voxel low bound (Hz)**	**Type B voxel low bound (Hz)**	**Type A and B voxel high bound (Hz)**
1st	3.85	3.44	3.29	3.93	59.08
2nd	23.889	21.29	20.55	24.46	103.55
3rd	28.49	25.6	24.12	29.29	173.39
4th	57.45	57.34	57.09	57.01	293.26
5th	66.372	58.76	57.49	68.28	376.24
6th	85.474	76.57	74.25	89.57	384.87

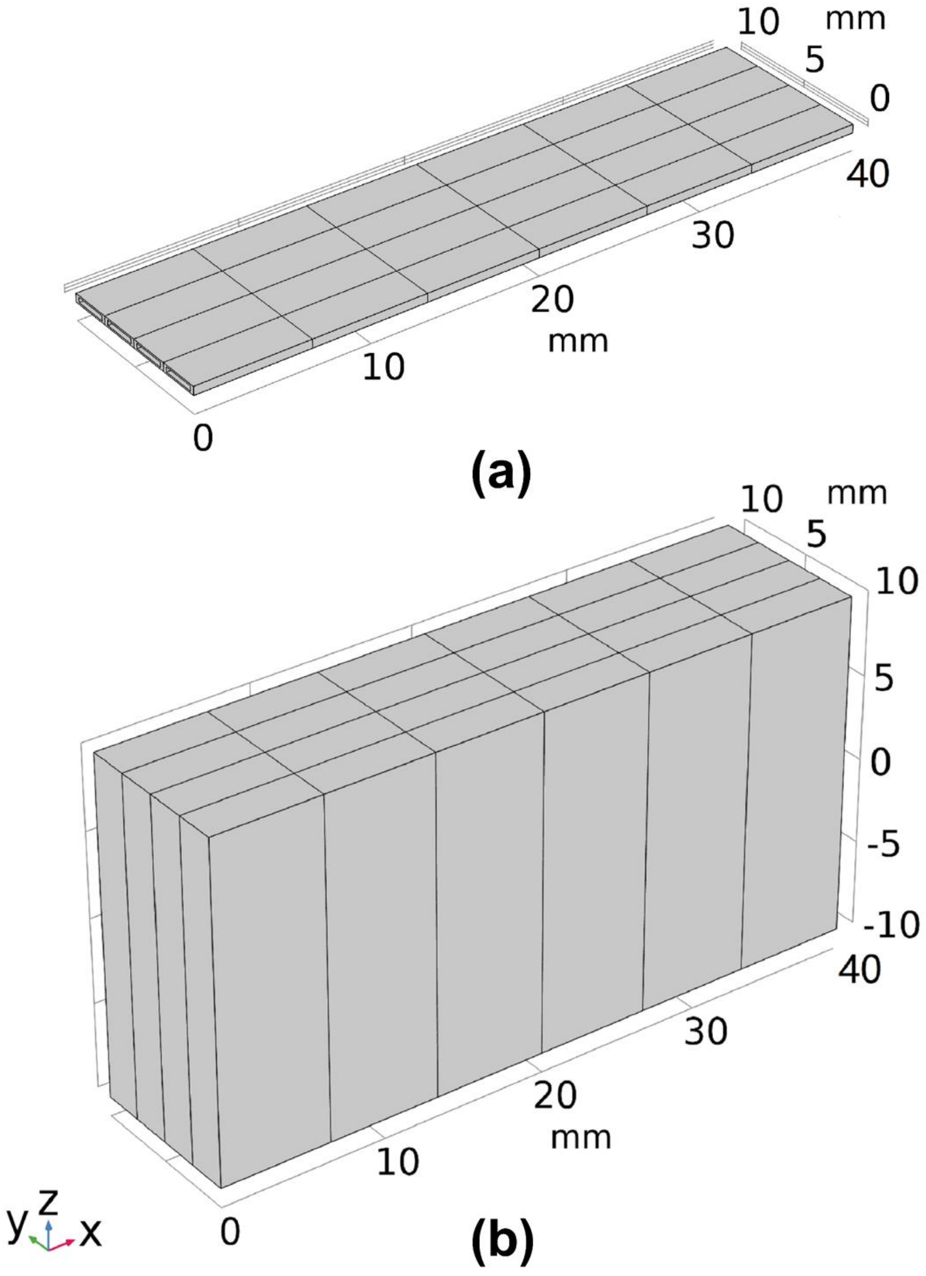

Figure 4.4. The 24-voxel type A structure corresponds to (a) low bound and (b) high bound of the natural frequencies.

4.4.2. Material properties

A linear elastic material is assumed, whose properties are representative of a relatively soft polymer. This is to facilitate the comparison with the results of the multi-material solution per Section 4.3.2. In order to compare with the recorded result, stiffer materials also lead to very thin voxel walls and extremely fine meshing for finite element analysis. This was found to cause numerical challenges and greatly increased computation times. As the main objective is to evaluate the effectiveness of structured material voxels as a means of tailoring the natural frequencies of the problem domain, the material property values are set to Young's modulus = 4 MPa, Poisson's ratio = 0.4, and density = 1145 kg/m^3.

4.4.3. Initial configuration

The evolutionary process has to start from some initial configuration. The initial dimensions of each of the structural voxels that make up the beam are randomly selected within a certain range for each evolution run. For type A voxels, the initial height H_b of each voxel is randomly set to a value between 40 to 60 % of the range from the lowest to the highest height bounds. The void height H_v is also randomly selected to be between 40% and 60% of the overall height H_b of the voxel. For type B voxels, the voxel height H_b of each voxel shares the same setting as the type A voxels. The initial height H_v of each of the two voids is randomly selected to be between 20% and 30% of the overall height of the voxel H_b and the thickness T_m of the middle cross web is also randomly selected to be between 40% to 60% of H_b. Typical initial configurations for structured beams with 24 voxels of type A and B are shown in Figure

4.5.

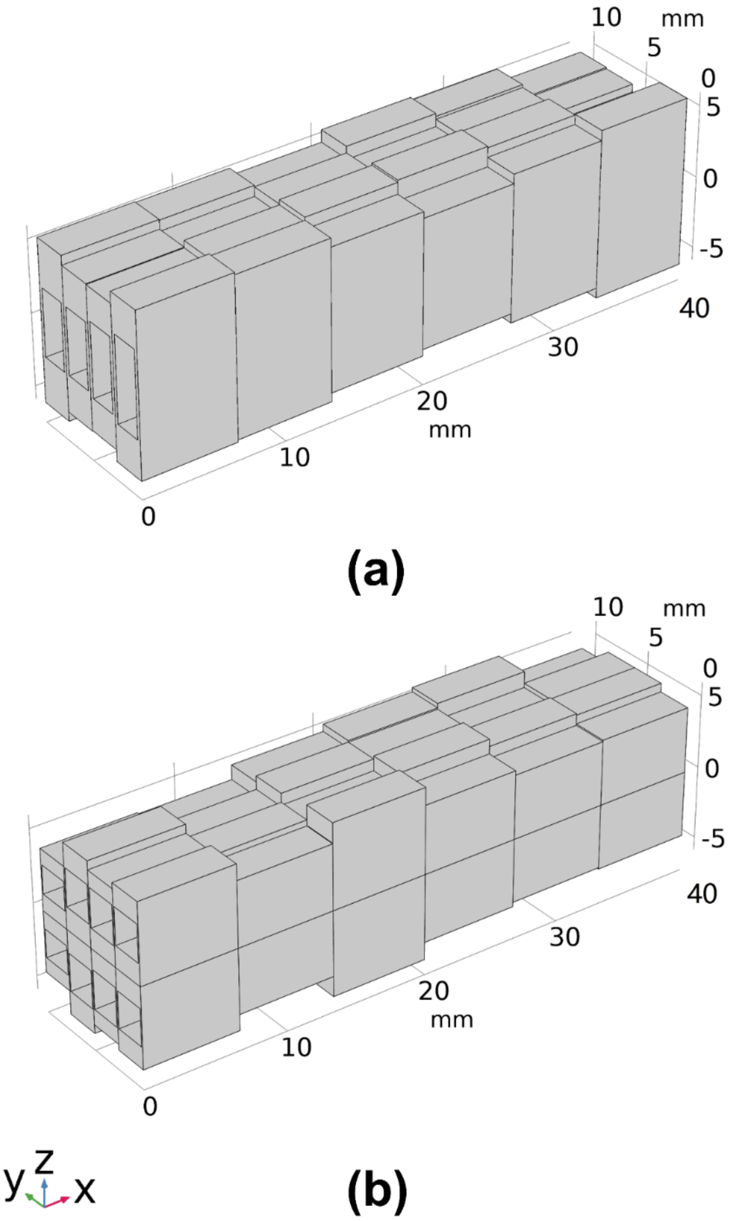

Figure 4.5. Examples of initial randomly generated configurations of beams with 24 voxels of (a) type A and (b) type B.

4.5. Structural optimisation results and discussion

4.5.1. Void structures and beam mode shapes

A typical distribution of the type A voxel shapes evolved using the CMA-ES algorithm for Target Set 2 is illustrated in Figure 4.6. It may be observed that the height of the individual voxels varies widely, resulting in what started as a uniform rectangular beam becoming a much more complex structure. The distribution of the voxel sizes is also unsymmetrical. While such a multi-directional form is novel as an engineering solution, complexity like this is quite common in many naturally evolved structures. Engineering design has traditionally avoided consideration of such complex forms because of manufacturing difficulties. However, these are yielding advancements in digital manufacturing. In particular, different additive manufacturing processes can realise such structures in different materials, provided proper build orientations and slicing strategies are employed.

The mode shapes corresponding to the first six natural frequencies are shown in Figure 4.7. It can be seen that the first three are global beam modes, namely in-plane bending, out-of-plane bending and torsion (1st to 3rd eigenfrequencies). However, the next three (4th to 6th eigenfrequencies) are highly localised modes, spanning mainly one or two voxels, not the desired global modes. Therefore, only half of the beam's natural frequencies have actually been matched to the targets. In particular, the fifth eigenmode mode, shown in Figure 4.7 (e), is confined to one wall of a single voxel. This is because the design algorithm is attempting to adjust the dimensions of each and every voxel in order to comply with all the six target frequencies, while the eigenvalue solver does not discriminate between local and global modes. As a result, a single voxel had a large void volume, resulting in thin walls and excessive flexibility.

The design scheme has not found appropriate combinations of voxel geometries to satisfy all the frequency settings globally within the stiffness and mass combinations possible with the type A voxel structure.

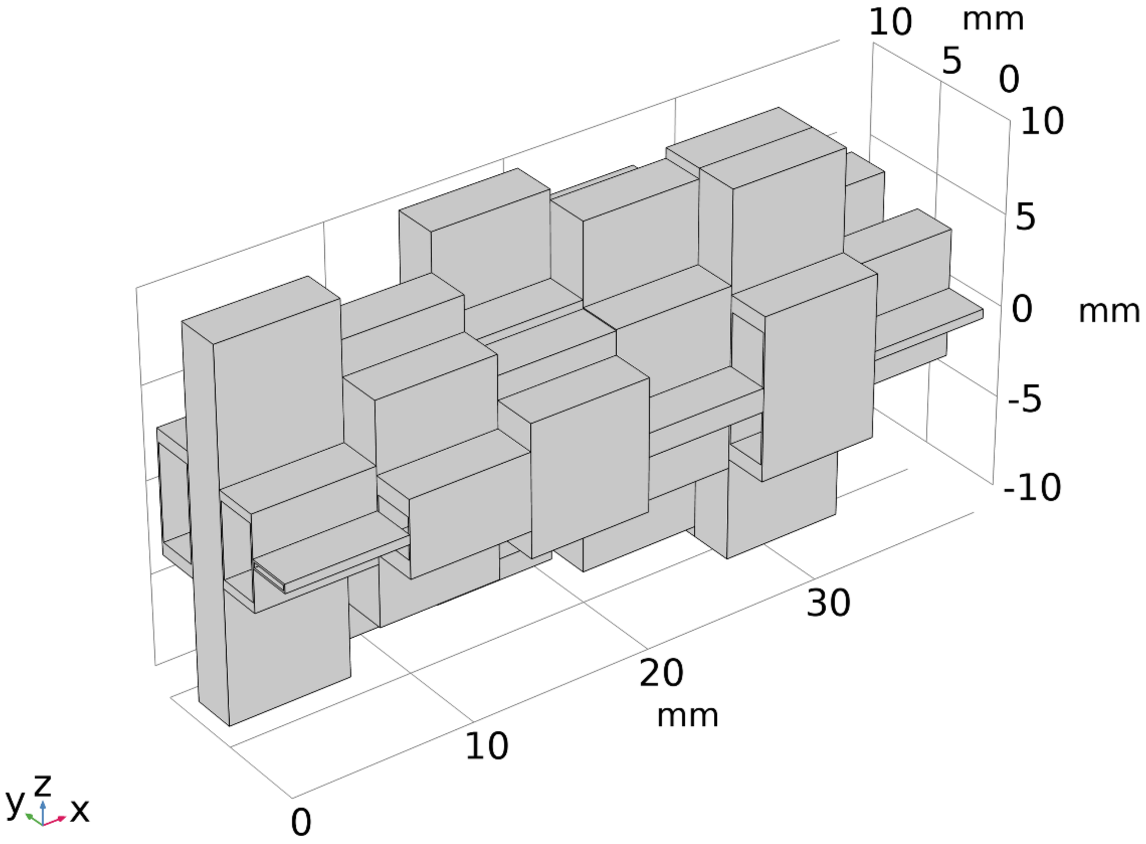

Figure 4.6. An example of a beam structure evolved for Target Set 2 using CMA-ES with 24 type A voxels.

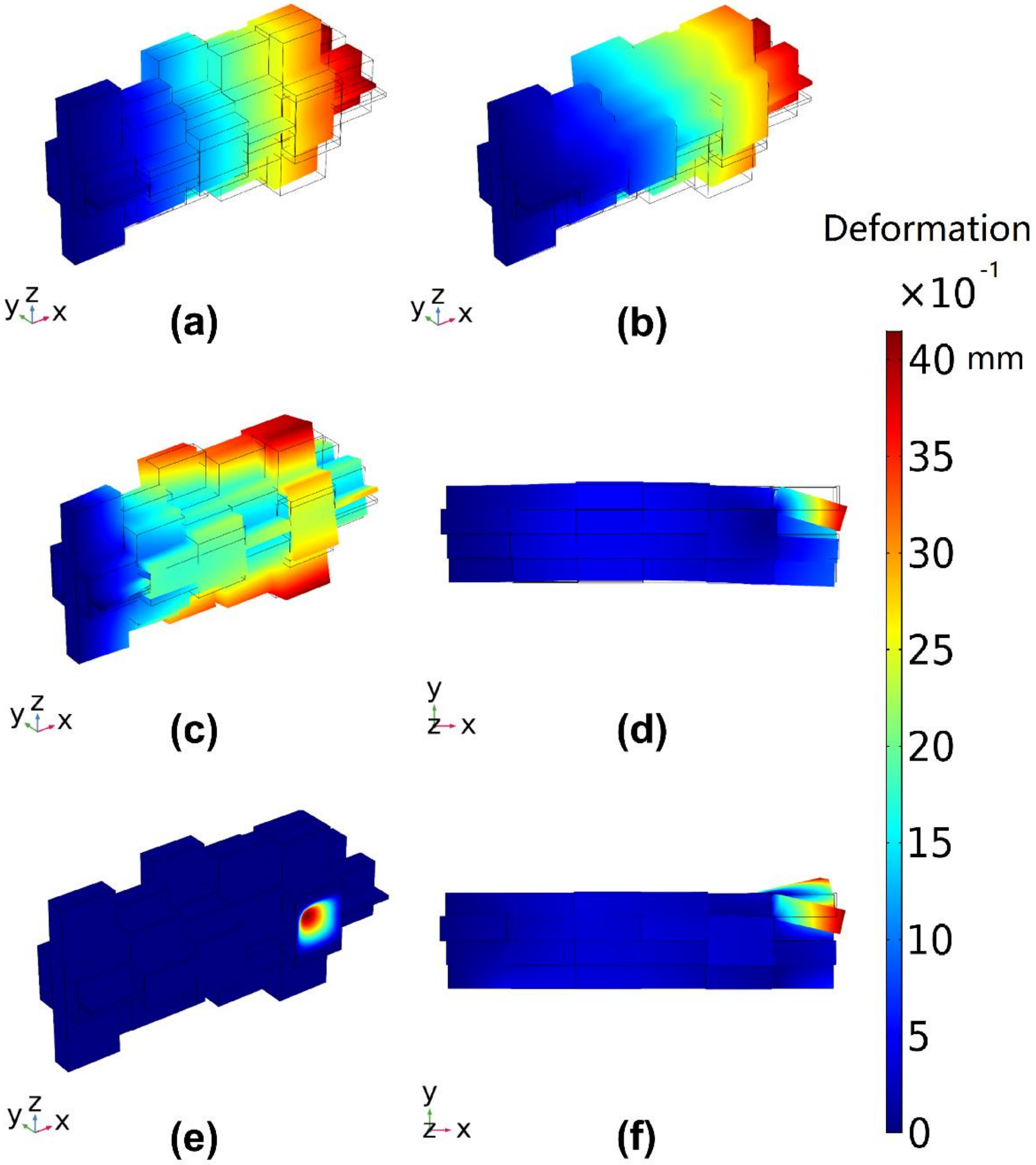

Figure 4.7. The mode shapes of the first six natural frequencies for the beam are illustrated in Figure 4.6. The total displacements plotted in (a) to (f) represent the 1st to 6th eigenmodes.

The double-void type B voxel structure was tested as a solution with the aim of eliminating local modes in the frequency range of interest, thus avoiding the increased computational burden of calculating additional eigenfrequencies and attempting to mathematically discriminate between local and global modes. A typical distribution of the type B voxel shapes evolved by CMA-ES for Target Set 2 is illustrated in Figure 4.8. Once again, the height of the individual voxels varies widely, resulting in a structure as complex as that obtained with type A voxels and yet significantly different. The resulting deformation mode shapes for the first six natural frequencies are presented in Figure 4.9. It is evident that all six eigenmodes are the desired global modes. Further validation was undertaken by repeating the evolutionary process five times each with the type A and B voxels, with standard variations in initial configurations. The results are summarised as box plots in Figure 4.10. It is clear that the type B voxel structure allows a much better convergence and fitness, with the median of the mean square error is approximately halved and the range of variation reduced by over 40% relative to the beam with type A voxels.

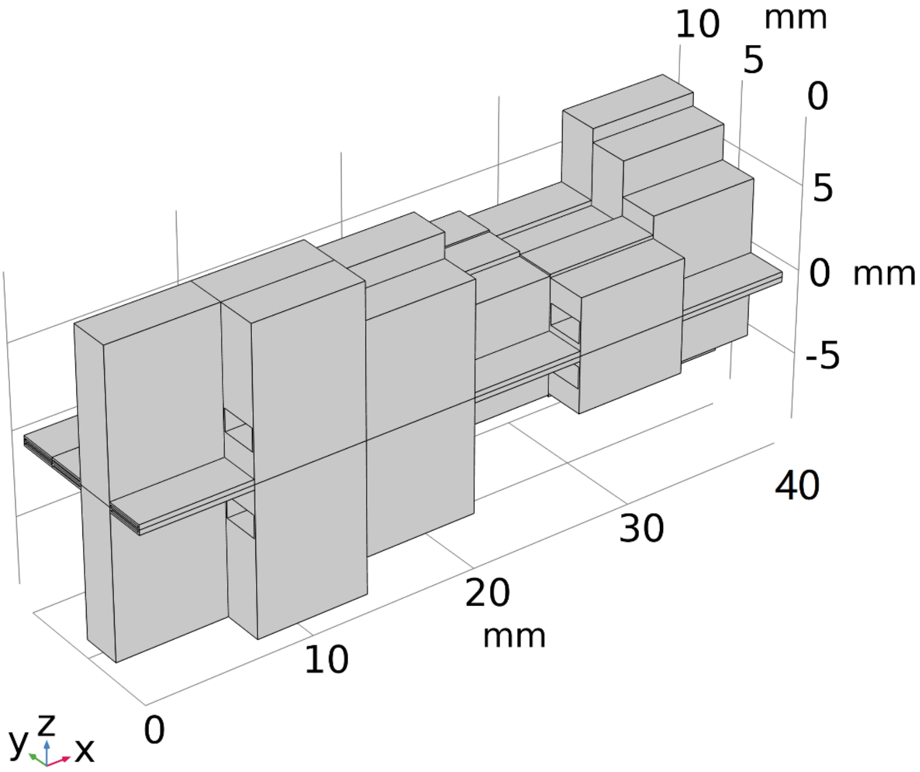

Figure 4.8. An example of a beam structure evolved for Target Set 2 with 24 type B voxels.

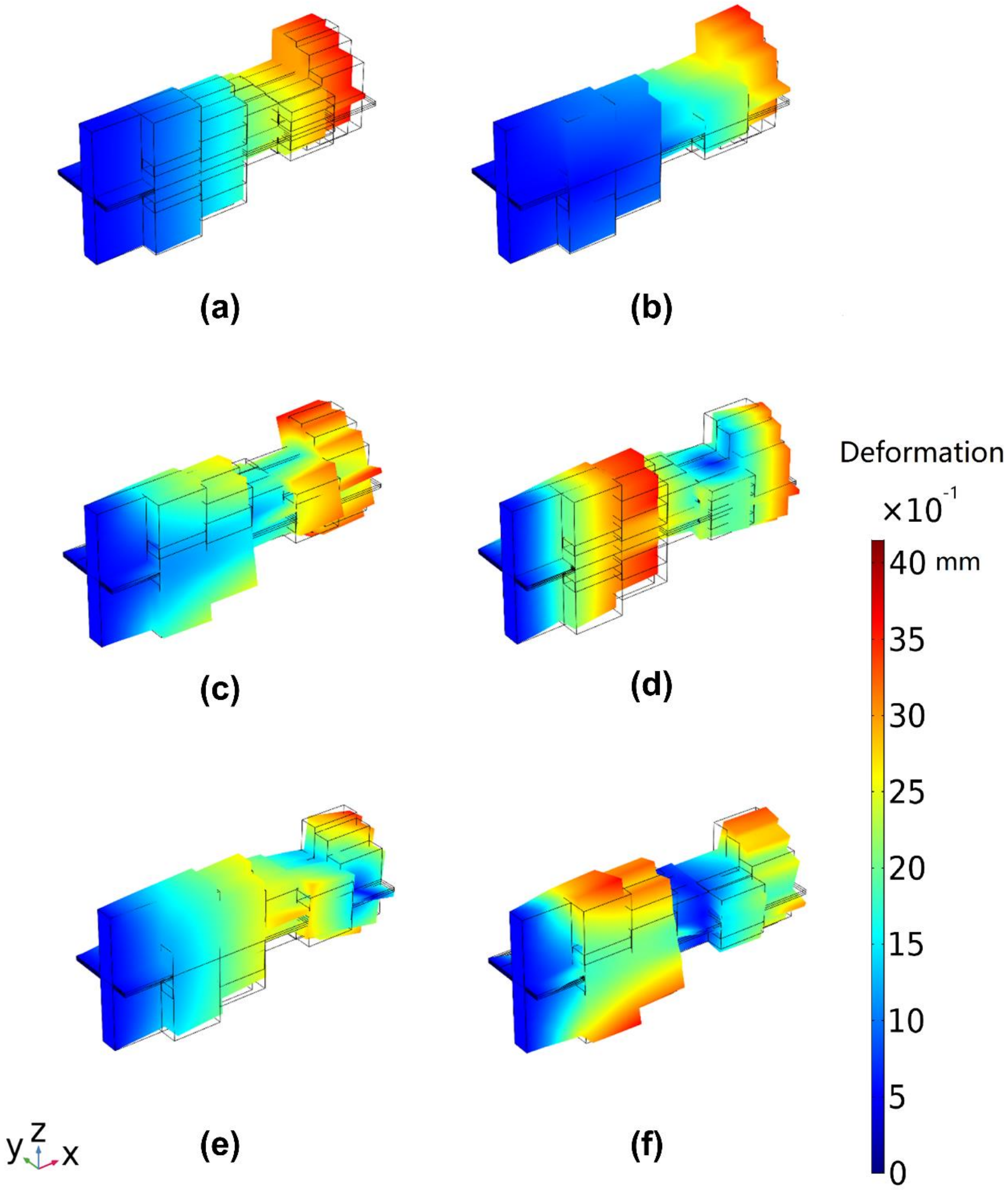

Figure 4.9. The mode shapes of the first six natural frequencies for the beam are illustrated in Figure 4.8. The total displacements plotted in (a) to (f) represent the 1st to 6th eigenmodes.

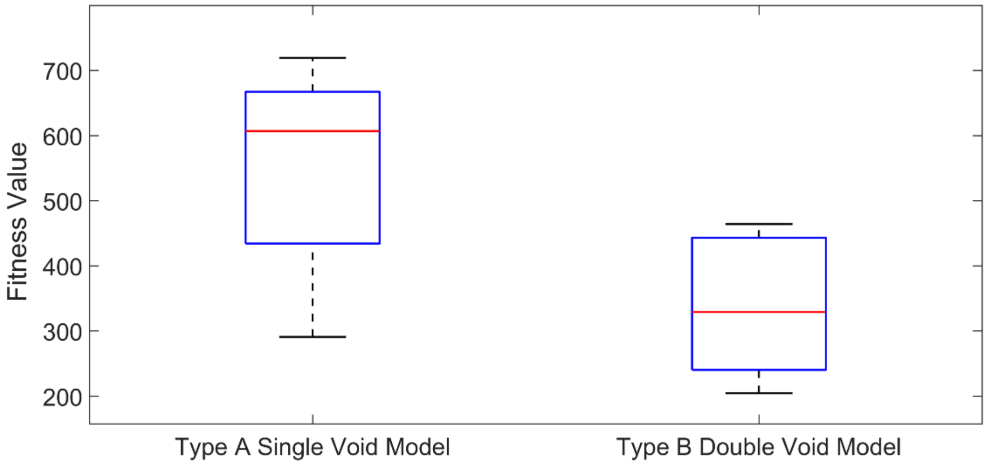

Figure 4.10. Comparison of fitness values obtained by CMA-ES, using single and double void voxel structures for Target Set 2. Five independent trials are conducted for each case. The solid lines indicate the median fitness values, and the boxes represent the 25th and 75th percentiles.

4.5.2. Tuning the algorithm

The standard CMA-ES algorithm is used in this work. The step size control and covariance update parameters are set as default values based on which the step size is not fixed at any given value but keeps updating each iteration based on the errors(N. Hansen et al., 2003; N. Hansen & Ostermeier, 2001; S. M. K. Heris, 2015). Its performance is dependent on the size of the population in relation to the number of design degrees of freedom, which itself is proportional to the number of voxels multiplied by the number of geometric parameters in each voxel. A small number of initial numerical experiments were conducted to identify the influence of the population size, overriding the algorithm's default population size setting, and using the target frequency set that produced the largest errors. As documented in the previous section, the type B voxel produced better fitness and eliminated local eigenmodes. Therefore, the model with 24 type B voxels was tested with a population size of 100, while the 96-voxel case was tested with both 100 and 200 population sizes.

The results for Target Set 2 are summarised in Figure 4.11. It may be clearly seen that there is no improvement in fitness as the population size is doubled, and in fact, there is a degradation in the fitness of the solutions as the number of voxels is increased from 24 to 96 voxels, with a constant population size of 100. However, a considerable increase in solution time needed to obtain the first six eigenfrequencies through finite element analysis was observed. Quadrupling the number of voxels increased computing time for each evaluation from 82 seconds to 187 seconds, and doubling the population size doubled computational requirements, which led to serious computational constraints. To avoid these computational difficulties, the 24-voxel model with a population size of 100 is used in what follows.

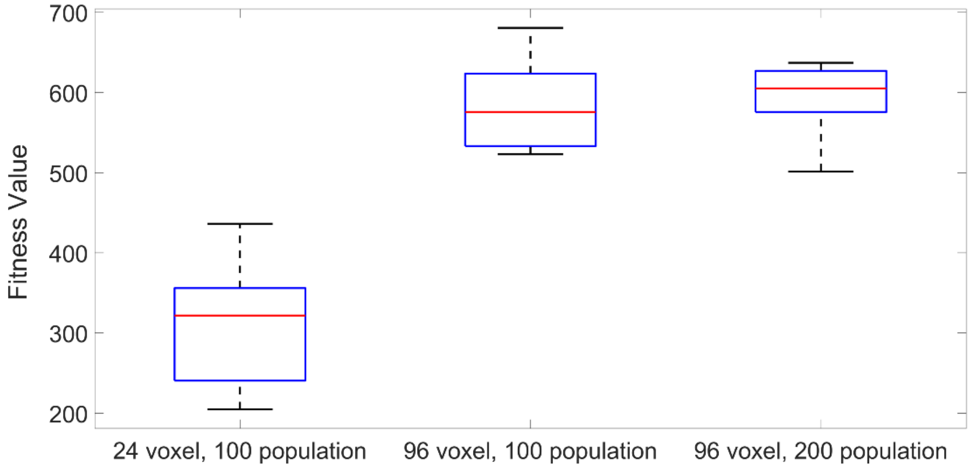

Figure 4.11. The effects of voxel number and population size on the fitness value for Target Set 2 with type B voxels. The solid red lines indicate the median fitness value, and the boxes represent the 25th and 75th percentiles.

4.5.3. Results based on the standard cantilever beam with double void voxels

As detailed in the previous sections, preliminary trials with the voxelated cantilever domain demonstrated the advantages of the double-void voxel geometry and that the number of voxels and the population size had little or no significant impact. Consequently, the cantilever beam domain was discretised into 24 double-void, type B voxels. Ten independent evolutionary runs were carried out for each of the three frequency target sets to gather data on the performance and variability of the proposed generative design approach.

The principal performance measure is how closely a beam design's eigenfrequencies match the targets. The differences between the eigenfrequencies computed by finite element analysis for the fittest solution produced by each trial run and the corresponding target frequencies averaged over these ten trials for each of the three target sets are plotted against the model number in Figure 4.12. Overall, a very good match has been achieved between the voxelated beam's eigenfrequencies and the targets. However, it is clear that certain target frequencies were a challenge to the algorithm. The maximum absolute error is 12 Hz at the fundamental frequency in Target Set 2, which results in a large percentage error. All other frequencies experienced errors of less than 8%, most of them significantly smaller. For Target Sets 1 and 3, the absolute errors are in the range of 2 - 4 Hz.

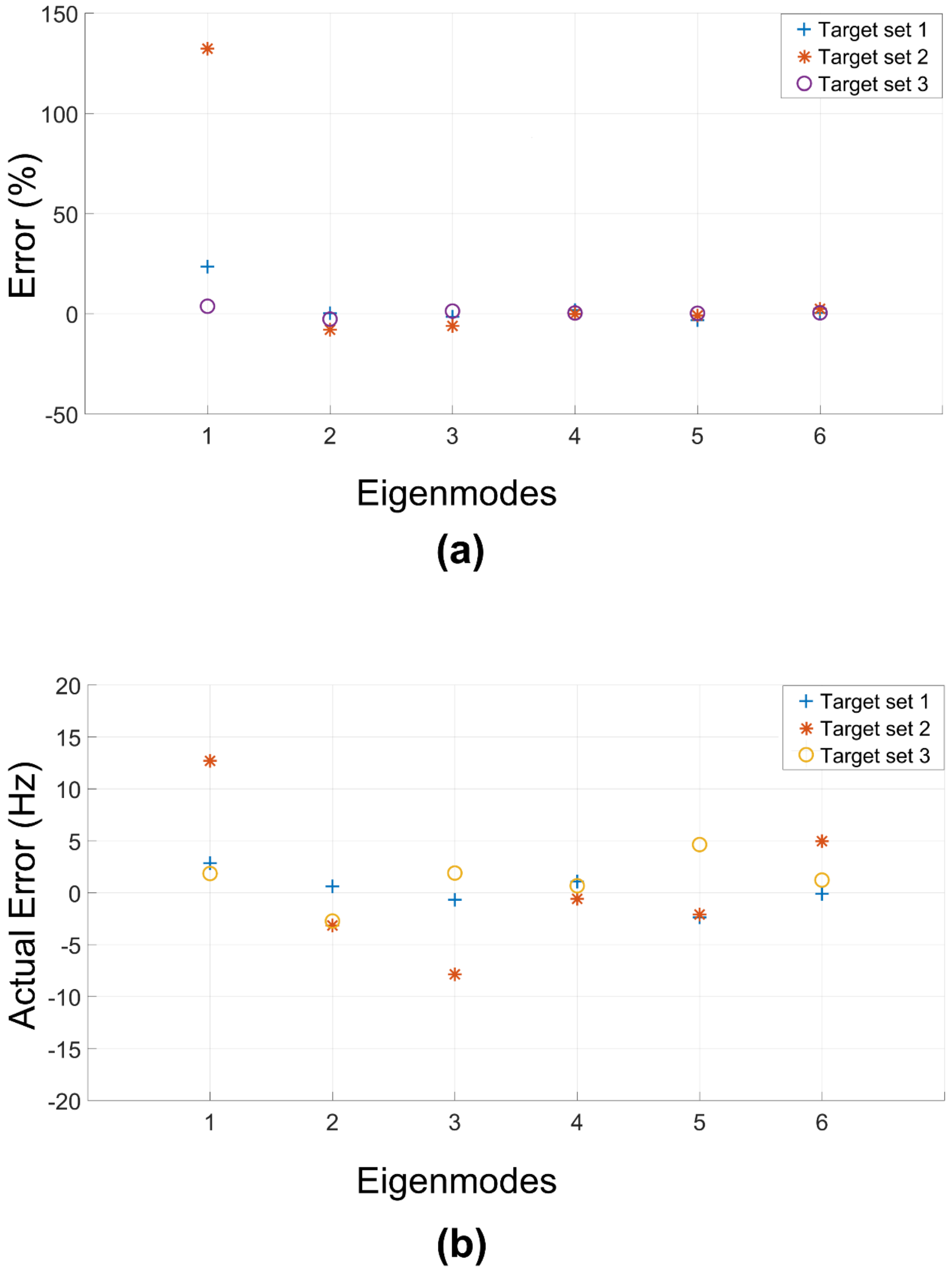

Figure 4.12. The mean of the difference between the first six beam eigenfrequencies and the corresponding target frequencies for each of the three Target Sets are expressed as (a) percentage and (b) actual frequency difference. Each data point corresponds to the mean value of 10 independent trials.

The variability of the error across ten trials of each target set is captured in Figure 4.13. The results are generally satisfactory, as the scatter from the mean of the actual error is 2 or 3 Hz for the first or fundamental frequency in all three target sets and overall, approximately 5 Hz or less in Target Set 1 and 3, with the notable exception of the 6th frequency. When expressed as percentages, the scatter of the error from the mean is within 10% except for the first fundamental frequency in Target Set 1 and 2. Though the actual error variations were the smallest for this first frequency, the percentage errors became the largest due to the target frequency being low at 10 Hz.

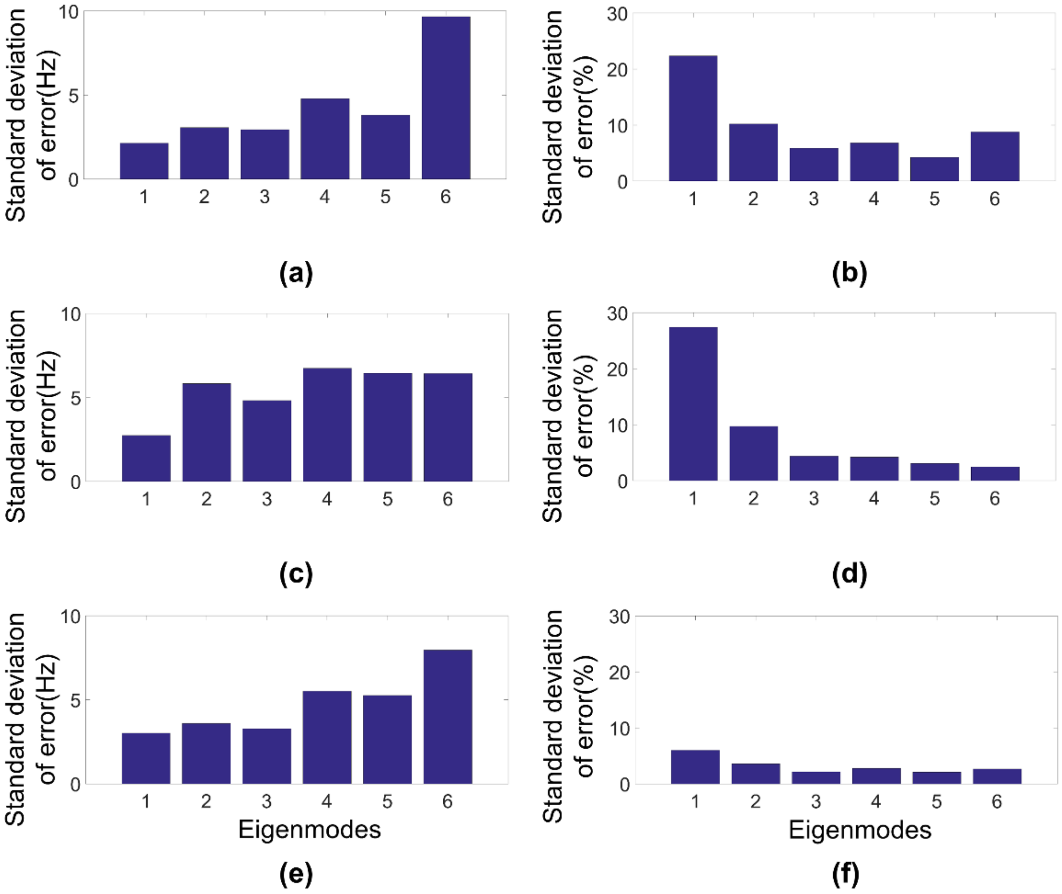

Figure 4.13. The standard deviation of the error across 10 runs in actual value (left) and percentage (right) for Target Set 1 to 3: (a) and (b) for Target Set 1; (c) and (d) for Target Set 2; (e) and (f) for Target Set 3.

As noted above, Target Set 2 produced the largest mean errors and the highest standard deviation. It may be deduced from this that the current voxel numbers and structural settings cannot provide enough degrees of freedom to achieve target frequency sets that have a low fundamental frequency and a comparatively larger frequency spacing, such as Target Set 2, which starts at 10 Hz and has a frequency spacing of 50 Hz. A similar issue was also observed with the multi-material solutions to this design problem (W. Yang et al., 2020). Given the lack of improvement with large increases in the number of voxels and population size, as summarised in Figure 4.11, it can be concluded that the issue is not simply the number of degrees of freedom or the width of the search but rather the limitations of the voxels themselves and their resulting properties.

It must be noted that each of the beam's natural frequencies is associated with a mode shape or pattern of deformation, typically involving bending or torsion around various axes. For the voxelated beam, the range of possible deformed shapes is constrained by the range of stiffnesses that are available from the individual voxels. Whether the voxel is a uniform solid as in the multi-material beams previously studied or a single-void or double-void structure, its bending, torsional and dilatational stiffnesses are interconnected. That is, the ratios between these stiffnesses are limited to a range determined by the structure or topology of the voxel and the allowed maxima and minima of its dimensions.

4.5.4. Comparing single structured material and multi-material beams.

Yang et al. (W. Yang et al., 2020) showed that binary GA provided better target frequency matching performance than the NEAT and CPPN-NEAT algorithms. Therefore, the single structured material (SSM) results from the previous sections are compared to the multi-material (MM) beam configurations evaluated using GA for the same three target sets. The MM beam was discretised into 400 voxels, and GA parameters such as mutation probability, percentage and crossover percentage used are detailed in (W. Yang et al., 2020). A population size of 100 was common to all. With the MM approach, the computational expenses are directly proportional to the number of voxels. The finite element solution times for computing the first six eigenvalues are 2, 4, 6, and 11 seconds respectively, with 400, 1600, 3200, and 6400 voxels models(W. Yang et al., 2020). However, with the SSM approach, the time taken by the finite element solution is also highly related to the complexity of the voxel structure. The computational time can vary from 18 seconds to 51 seconds, depending on the number of edges and surfaces in the geometry (on standard Intel i7 8700k processor).

Figure 4.14 summarises the results of this comparison in terms of solution fitness values, lower fitness being better. For Target Set 1, SSM and MM produced similar median fitness values from the ten trials, but SSM results had lower variance. For Target Set 3, SSM generated better frequency matching in terms of both absolute fitness value and variance. For Target Set 2 MM provided significantly better results. However, SSM still produced results that were comparable to MM results for other target sets, with average errors of less than 10 Hz for each of the six frequencies. It was observed that the CMAES algorithm used in conjunction with the SSM solution works the best when the target frequency sets are all either close to the lower or upper bounds or at the mid ranges of the six frequency responses listed in Table 4.3. The reason for the wider errors with the SSM approach for the middle frequency target set is that the first target frequency is close to the low bound while the rest of the target frequencies are closer to the mid-value of the range of frequencies possible with the geometrical variations of the voxels. Despite these variations, it is notable that SSM is able to produce similar and sometimes better performance in tailoring the frequency response spectra with only 6% of the number of voxels in MM, although since there are three design variables per double void voxel as illustrated in Figure 4.3, the total number of design degrees of freedom in SSM is 18%, but still less than one-fifth, of that used in MM. An important practical consideration is that SSM provides a much more feasible route for implementation given the more advanced state of art of single-material additive manufacturing processes, which are now routinely used in production. In particular, processes such as selective laser and electron beam melting can produce such structures with real engineering material systems such as steel, titanium or aluminium alloys.

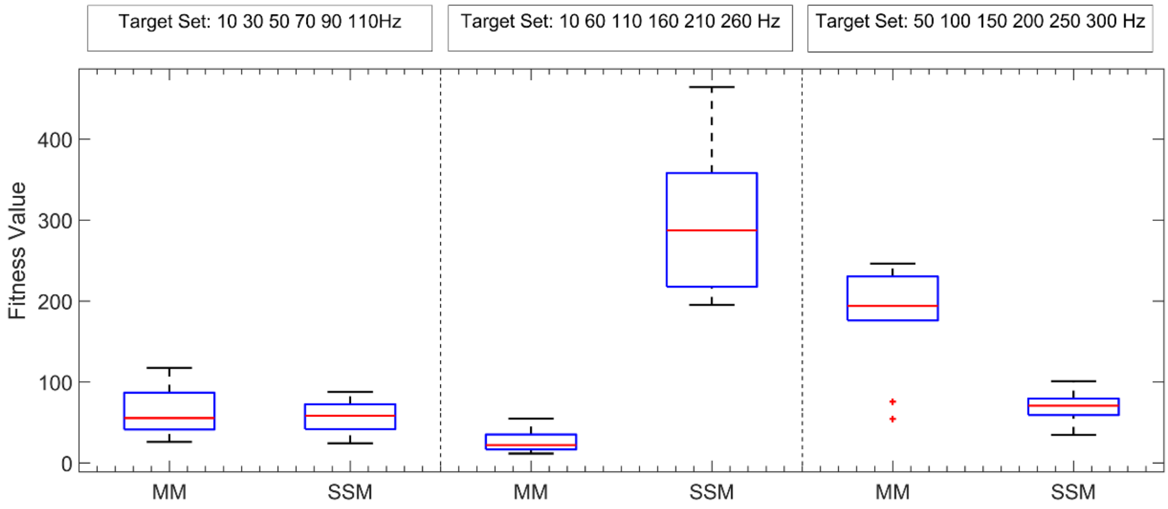

Figure.4.14. Comparison of fitness values for multiple-material (MM) and single structured material (SSM) solutions for target frequency sets Target Set 1-3. Each box plot represents the results of 10 trials for each target set. The lower the fitness value, the closer the eigenvalues were to the target frequencies. The solid red lines indicate the median fitness value, the top and bottom of the boxes represent the 25th and 75th percentiles, and cross marks indicate the outliers that are 1.5 times larger than the interquartile range.

4.5.5. Results based on an irregular beam with forced voids

To further validate the ability of the proposed CMA-ES algorithm for frequency optimisation, two different irregular geometries are tested. The beam case is designed to validate the performance of the optimisation scheme with irregular design regions such as forced voids. The target is to achieve the same frequency Target Sets (TS) 1 to 3, as listed in Table 4.1, for the beam geometries as depicted in Figure 4.15. The beam geometry has 24 voxels in total, but with the voids created at different locations, the two irregular beam structures result, referred to as A and B, as shown in Figure 4.15 (a) and (b), respectively.

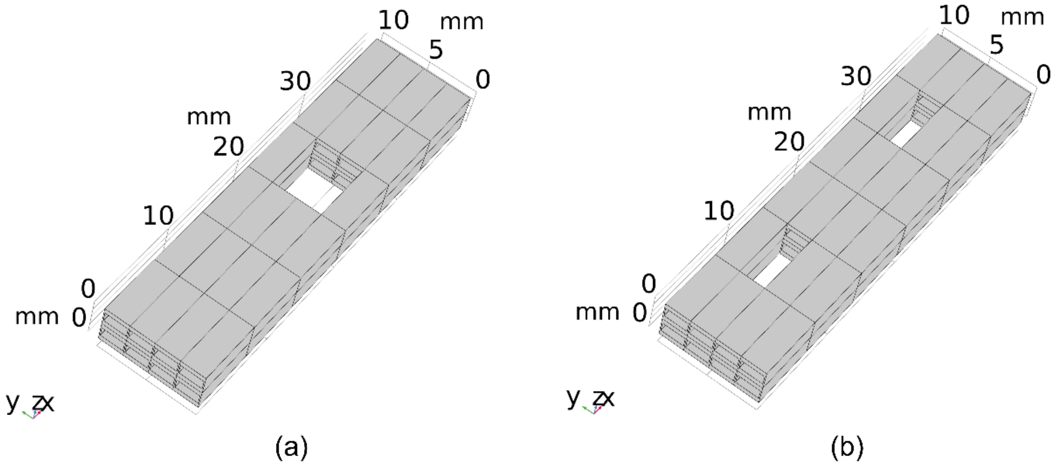

Figure 4.15. Cantilever beam with forced voids (a) geometry A and (b) geometry B

For the same Target Sets (TS) 1 to 3, as listed in Table 4.1, the two irregular beam geometries converged on the solutions with the error patterns as depicted in Figure 4.16 (a) and (b). Evidently, the eigenfrequencies of the two beams with the void structures with optimised voxel geometries have shown satisfactory matches with the target sets. Considering the frequency for TS 1 and TS 2 being low at 10 Hz, the percentage errors for the first or fundamental eigenfrequencies are relatively high, which is in similar lines to the previous cases. The TS 2 case remains challenging for the optimisation with these two beam geometries as the actual average error in the 1st eigenfrequency is 16 Hz for irregular geometry A and 14 Hz for irregular geometry B. The error levels are below 5% with all the other frequencies, and the actual error for most of them is less than 10 Hz. Figure 4.17 summarises the results comparing the fitness values of optimising the all the three beam geometries evaluated. The lower the fitness value indicates, the lower error. For TS 1, irregular geometry A and B obtained slightly lower errors. For TS 2 and TS 3, no significant difference can be observed. Overall, the results indicate that the proposed method can efficiently alter the eigenfrequency properties of irregular beam geometries also matching with the selected targets within reasonable error limits.

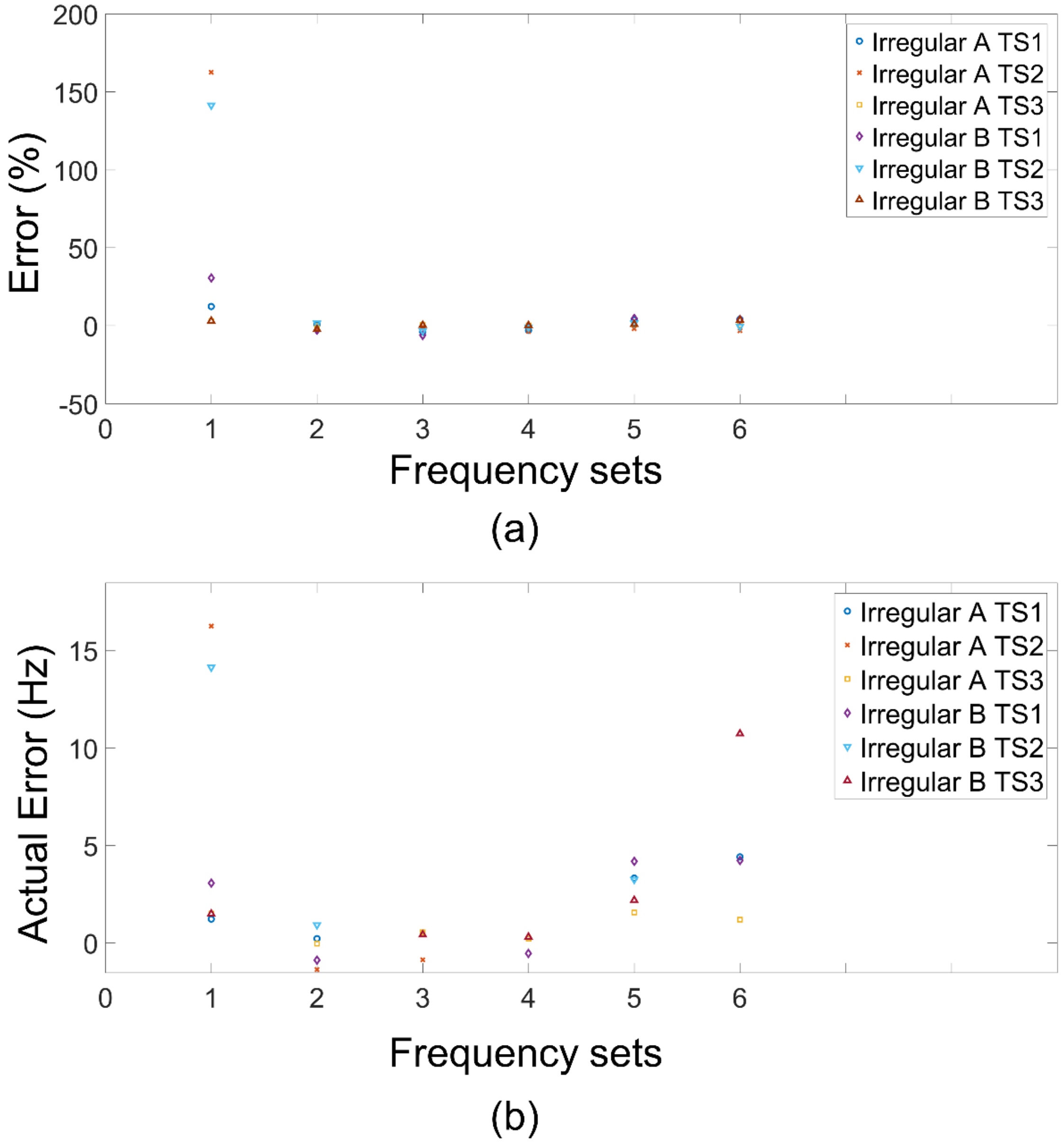

Figure 4.16. The mean of the difference between the first six beam eigenfrequencies and the corresponding target frequencies with the irregular geometry A and B for the three Target Sets (TS), illustrated as (a) a percentage and (b) actual frequency difference. Each data point corresponds to the mean value of 5 independent trials.

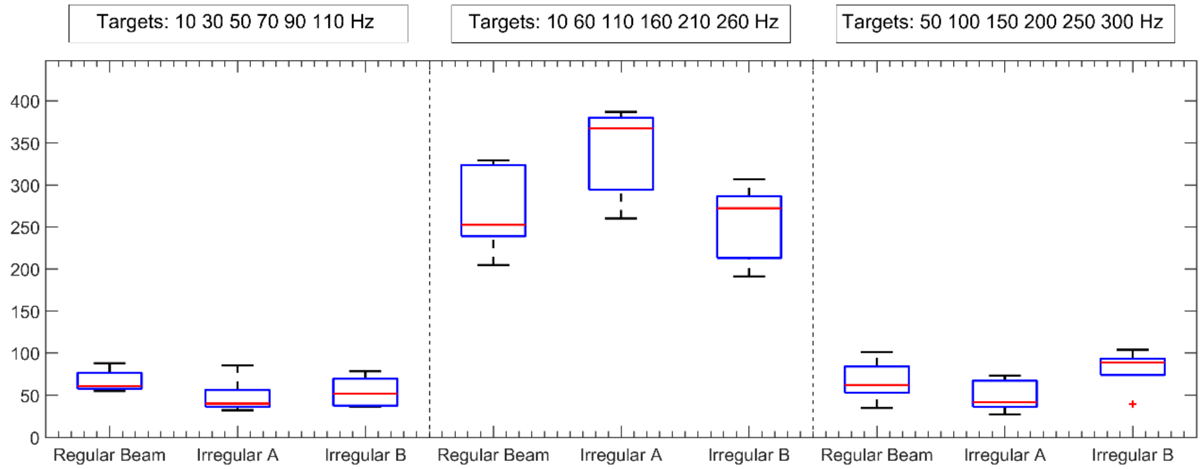

Figure 4.17. Comparison of fitness values for regular geometry and the irregular geometry A and B of the beam for target frequency sets TS 1-3. Each box plot represents the results of 5 trials for each target set. The lower the fitness value, the closer the eigenvalues were to the target frequencies. The solid red lines indicate the median fitness value, the top and bottom of the boxes represent the 25th and 75th percentiles, and cross marks indicate the outliers that are 1.5 times larger than the interquartile range

4.5.6. Regular and irregular beam geometries with pre-loading

To verify the performance and flexibility of the proposed method, the pre-stressed states of the three beam geometries are modelled. In order for easy fabrication in the future, the standard laser sintering material option nylon PA1101 as used on the EOS Formiga series commercial printers is selected as the test material. The material property values are set to : Young's modulus = 1600 MPa, Poisson's ratio = 0.4, and density = 990 kg/m^3 (EOS, 2021). As shown in Figure 4.18, a 20 N load is applied on the end surface of the beam structure along the X-axis. The same geometry boundaries used in the cases discussed above are used. Considering the nylon's material properties, a different target frequency set is used for the optimisation scheme. Based on initial simulation results, the optimisation target is set at the mid-level between the low bound and high bound frequency limits, as listed in Table 4.4. The results of the analysis based on pre-loaded beam cases, as illustrated in Figure 4.19, clearly show the numerical results of the frequencies matching with the target frequencies at satisfactory levels. Overall, the percentage errors for all six target frequency modes are less than 6%, and significantly smaller error levels are obtained in many cases. This final test clearly elucidates that the CMA-ES optimisation scheme can also handle pre-loaded beam cases with varying geometry and material considerations for target frequency responses.

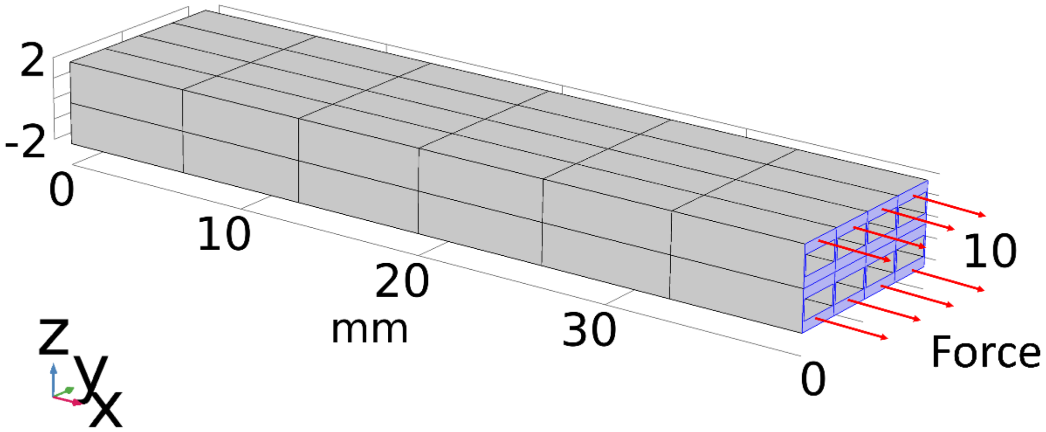

Figure 4.18. The pre-loaded condition in the regular beam geometry for the eigenfrequency optimisation.

Table 4.4. The target set was used in the three beam geometries with pre-loading.

The target frequency set	Regular beam structure (Hz)	Irregular beam structure A (Hz)	Irregular beam structure B (Hz)
1st	905.9	906.2	911.8
2nd	1538.2	1564.8	1564
3rd	2564.1	2452.9	2429.5
4th	3988.5	4093.6	3624.6
5th	5190.4	5020.3	5064.6
6th	5608.5	5439	5545.1

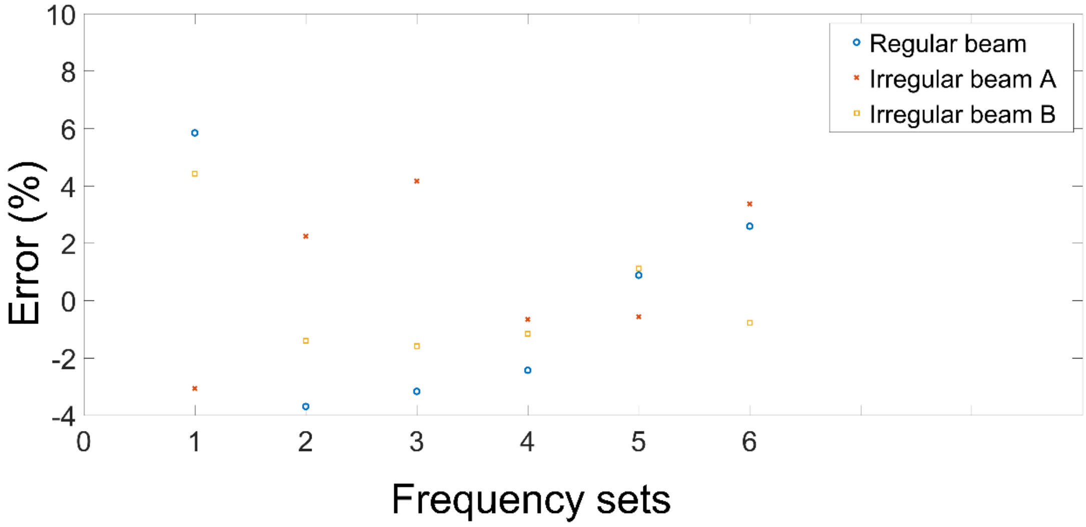

Figure 4.19. The mean of the percentage difference between the first six beam eigenfrequencies and the corresponding target frequencies of the three-beam geometries with pre-loading. Each data point corresponds to the mean value of 5 independent trials.

4.6. Additive manufacturability of the SSM beams

The powder bed fusion-based additive manufacturing methods are well suited for the direct production of the complex beam structures optimised in this study based on the

CMAES algorithms. In particular, selective laser sintering can directly be applied to the CAD files resulting from the optimisation schemes without any further modifications. The eos FORMIGA P100 system available at the additive manufacturing centre of the Auckland University of Technology was successfully used to produce one of the optimised structural beams by importing the optimised geometry from the COMSOL Multiphysics platform and converting the same into the .stl format. Nylon PA1101 was the powder material used.

While these polymer-based solutions are a good means of physically realising the geometrically optimised beams shapes, the practical implementation of these structures would need the use of better material systems. The powder metal-based selective laser melting process is the option to evaluate the suitability of the geometries to be directly produced from the digital CAD data. The main problem with building such structures with real engineering metals is the need to insert support structures under overhanging features and the consequent difficulties in removing the same at the end. If the part geometry can be reproduced without the use of any support structures in the internal cavities that are difficult to access for post-printing trimming operations, the part will qualify for production by metal printing methods.

The feasibility of building the general form of the optimised beam structures using the Renishaw AM400 selective laser melting system available at the additive manufacturing research centre of the Auckland University of Technology is evaluated. The key aspect of importance is to verify if there is any particular build orientation in which support structures at all internal cavities could be avoided. For this, the .stl format file of one of the representative beam geometries is imported into the QuantAM software, which is the user interface for the Renishaw AM400 system. After a few trials, the build orientation with the key surfaces of the beam oriented at 450 to the baseplate, as depicted in Figure 4.20, is found to eliminate the need for any internal support structures. Fig 4.20 (a) to (d) are screenshots of the simulation of the laser scanning at 25%, 50%, 75% and 100% of the printing process. It may be observed that the internal support structures could be completely avoided, while the remaining external support structures can easily be removed during the post-printing trimming stages. A video recording of the animation sequence of the layer by laser processing and the raster path dynamics is included as part of the supplementary data. These software-based evaluations clearly demonstrate that the complex beam configurations resulting from the optimised voxel geometries are amenable for manufacturing by the metal powder bed fusion technologies. The actual printing of the structures and developing experimental methodologies to verify the predictions of the current simulation studies are the future course of this work.

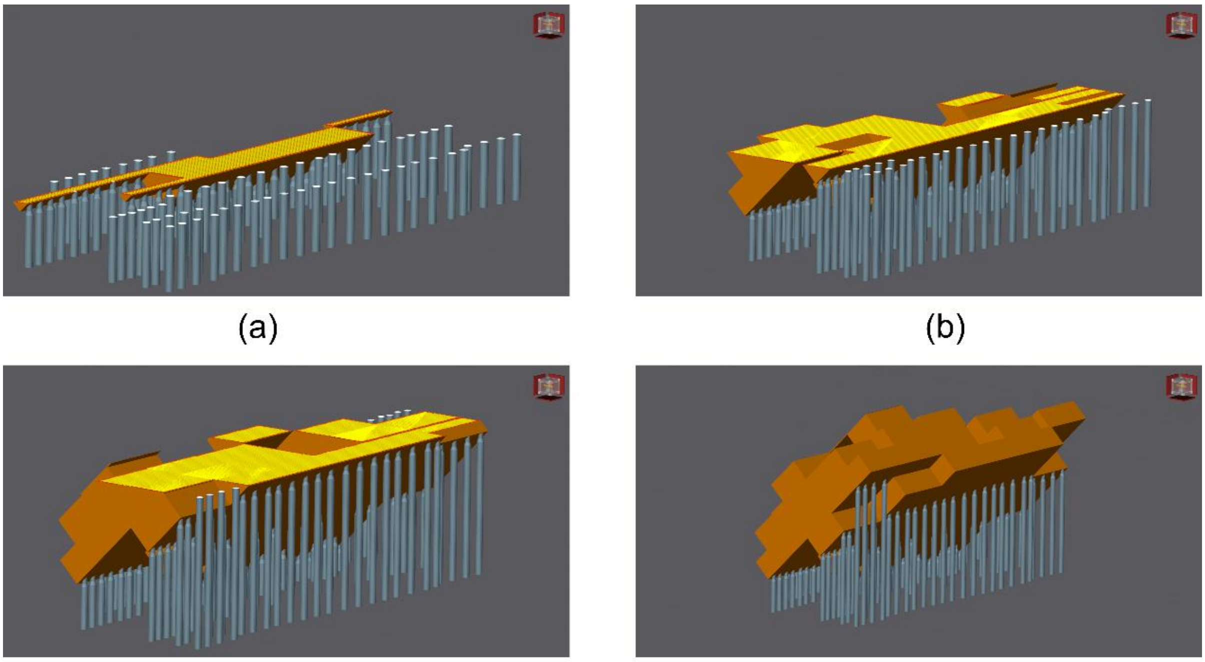
(a) (b) (c) (d)

Figure 4.20. Selective laser melting simulation of the optimised beam structure at 45^0 orientation to the base plate, demonstrating the feasibility of printing the optimised beam geometries by selective laser melting. Images are slice and raster path depictions at (a) 25%, (b) 50%, (c) 75%, and (d) 100% processing stages based on the build simulations using the QuantAM software, which is the user interface for the Renishaw AM400 selective laser melting system.

4.7. Summary of Chapter 4

An evolutionary design approach based on a single structured material solution is proposed and tested by tailoring the structural eigenfrequency responses of a cantilever beam. A set of numerical experiments were conducted to evaluate the performance of the SSM-based solution in matching the first six natural frequency responses of the beam against designated target frequency sets. Results indicated that the single structured material (SSM) approach using the classic CMA-ES algorithm is able to match three different sets of evenly spaced target frequencies with modest errors, often less than 5%. The mean of the actual error is 5 Hz or less at most frequencies. The SSM solutions were on par with or, in some cases, better than the more cumbersome multi-material solutions obtained using genetic algorithms. The SSM solutions are also more amenable to implementation in real engineering materials using existing additive manufacturing processes. Further studies also demonstrated that the proposed optimisation scheme could cope with pre-loaded cases and different material settings while maintaining the error within a reasonable range. Problems were encountered with the target set characterised by a low fundamental frequency and relatively larger frequency spacing (TS2) as the errors of convergence were relatively large. Further and more detailed exploration of the relationships between the errors, frequency distribution, and the nature of the design degrees of freedom is warranted, together with the integration of parallel computing schemes to expedite the evaluation of the fitness functions.

Chapter 5

Topology optimisation for controlled structural deflections

5.1. Cellular structures for controlled beam deflections

Closely controlling the mechanical behaviour and characterization of the deflection of a beam structure is a well-known and widely studied engineering problem. The progress in additive manufacturing methods and the possibilities to closely control the material property variations with the controlled placement of materials further widen the opportunities to achieve given beam deflection criteria. However, the multi-material additive manufacturing (MMAM) solutions suffer from the lack of real engineering material options, and the quality and performance of the printed parts are usually unsuitable for producing functional parts. The novel cellular structure solution, as evaluated in the previous chapter, is again proposed here to optimise geometries of the individual cells of the single material structured beam to obtain deflection profiles closely matched with pre-set conditions under different loading conditions.

The cellular geometry of the structured beam is continually altered for searching and converging on the optimal structure of the cells by the covariance matrix adaptation evolution strategy (CMA-ES) algorithm in an iterative manner. The beam with the optimised cellular structure is able to match specific deflection sets with modest errors.

Furthermore, the optimised beam can be fabricated with multiple additive manufacturing technologies currently available, such as fused deposition modelling (FDM) and powder-bed based selective laser sintering (SLS) or melting (SLM) processes with real engineering polymer or metal material options.

5.2. Compliant mechanisms and deflection of beams

Beam mechanisms and beam theory have been widely used in systems using compliant mechanisms, such as soft robots (DeMario & Zhao, 2018; Fang et al., 2016; Jung, Choi, & Cho, 2017), leaf springs(Al-Obaidi, Ahmed, & Sukar, 2020; Shepherd & Rouse, 2017), and flexible hinges (Cao, Dolovich, & Zhang, 2015; Ling, Howell, Cao, & Chen, 2020; Z. Xie, Qiu, & Yang, 2020). Compliant mechanisms were first proposed by Her and Midha in the 1980s (Her & Midha, 1987). The theory refers to mechanical devices gaining their mobility through the elastic deformation of flexible parts (Howell, 2013). Compliant mechanisms use deflection of the beams to transfer force and motion without using movable parts. Compared to a rigid-body system, they can reduce friction and wear and do not require lubrication and assembly (Ling et al., 2020).

For example, in a soft robot, the precisely controlled elastic deflection in the compliant system is an important design factor for the accurate grip and gait simulation. It is widely used for robotic leg mechanisms (DeMario & Zhao, 2017, 2018; Fang et al., 2016; Jung et al., 2017) and grippers (Hao, Li, Nayak, & Caro, 2018; Petković, Pavlović, Shamshirband, & Anuar, 2013; Xu, 2015). A leaf spring uses elastic deflection to absorb and store the energy of impacts. It is more compact and lightweight compared to coil springs for providing the same stiffness and energy storage capability. Flexible hinges are also widely used as compliant mechanisms that gain mobility while eliminating the sliding friction of contact surfaces(Z. Xie et al., 2020).

For the effective application of the compliant mechanisms, it becomes necessary to closely control the mechanical behaviour of beam structures. The prediction and characterization of the deflection of beam mechanisms is a well-known and widely studied engineering problem. The investigation of the deflection curve for simply supported or a cantilever beam under different loading can track to Galileo since 1638 (Venetis & Sideridis, 2015). There are numerous methods for finding the deflection of beams, such as the double integration method, the moment area method, and the finite element method (Beer, Johnston, & DeWolf, 1999; Ling et al., 2020). Furthermore, to closely control the deformation behaviour of the beam, several methods have been proposed. For example, the solid isotropic material with the penalization (SIMP) method (Brackett et al., 2011) transforms a topology optimization problem into a problem of material density optimization and then identifies whether each element is solid or void in a fixed domain of finite elements (Deaton & Grandhi, 2014). SIMP has been applied to beam structural optimization problems such as stiffness to weight ratio (Kandemir et al., 2018; Krishna et al., 2017; Ole Sigmund, 2007).

The truss-based method, such as the ground structure method, can control the mechanical properties of the beam by reducing the truss number and optimizing the truss location (Bendsøe, Ben-Tal, & Zowe, 1994). Ground structure methods have been applied to optimal design for minimum compliance and weight (Wang & Tai, 2005) and weight minimization with stress and displacement limitations (Kawamura et al., 2002). The Particle Swarm Optimization (PSO) algorithm has also been proposed for desired beam deflection curve by optimizing the widths of each segment of the beam (F. Gao et al., 2020). The bi-directional evolutionary structural optimisation (BESO) method is also well studied for improving the mechanical properties of the beam, which allows the object to evolve to the optimal structure by gradually removing the redundant material and adding material to locations of high sensitivity (X. Huang et al., 2010). It is used for various targets such as stiffness to weight ratio optimisation (Pais et al., 2021; X. Y. Yang et al., 2005), beam geometry optimization under multiple load cases (Li et al., 2018), and multi-objective optimization for stiffness and fundamental natural frequencies (Teimouri & Asgari, 2019). The evolutionary algorithm, non-dominated sorting genetic algorithm II (NSGA-II), was used for optimising the beam geometry for desired deformation behaviour (Gadhvi, Savsani, & Patel, 2016).

Besides single material structural optimisation, several multi-material approaches are also proposed with the advent the multi-material additive manufacturing (MMAM) technology to improve the mechanical properties of beams. For example, gradual BESO, an enhanced version of BESO, is purposed for stiffness to weight ratio optimisation and is capable of handling more material and geometry cases (Ghabraie, 2015). The material distribution topology for desired deformation curve (Cheney et al., 2014; J. Hiller & H. Lipson, 2009) and the genetic algorithm (GA) is also adopted to optimise the distribution topology of soft and stiff materials for desired deformation curve responses (Cheney et al., 2014; J. Hiller & H. Lipson, 2009). However, as already stated, multi-material approaches usually suffer from the lack of real engineering material options. Current multi-material additive manufacturing systems can only offer digitally mixed acrylic polymer options consolidated with UV curing (Kumar & Kruth, 2010).

In the current approach, a novel alternative is presented to closely control the beam deflection curve under multiple load conditions. Instead of using solid voxels, a hollow structure with controlled dimensions is used for each voxel to alter its effective mechanical properties and mass. By using structured voxels, the mechanical property of the object is not only governed by the material properties and the overall geometry but can also be altered by the internal cellular structure of each voxel while preserving the original geometry. Such macro changes in the structures of voxels are possible to achieve in real engineering materials by additive manufacturing technologies that have become common in recent years. In this work, instead of controlling the beam deflection behaviour by multi-material distribution, the Covariance Matrix Adaptation Evolution Strategy (CMA-ES) is adapted to optimise the beam deflection behaviour to the desired profile by varying the structures of the voxels so that the overall optimised structure can be fabricated with a single material using an appropriate additive manufacturing technology.

CMA-ES was originally designed and developed for handling optimisation problems involving continuous variation of the critical parameters (N. Hansen & Ostermeier, 2001). It has been widely used in various studies in computer science and engineering, such as parameter tuning for neural networks and ranking support vector machines (Jin, 2005; Kern et al., 2006; Loshchilov & Hutter, 2016; Loshchilov et al., 2012). Truss layout optimisation for minimising the weight (Xiao et al., 2013), topology optimization for cloaking polarized light (Fujii et al., 2018), and optimising metallic shapes and dielectric properties for desired electromagnetic scattering and radiation characteristics (Gregory et al., 2011) are other examples of applications. However, there was no evidence that the generative design method CMA-ES was adopted for controlling beam deflection behaviour by structural optimization. The proposed approach fills this gap, demonstrating the ability to control the beam deflection behavior under multiple loading conditions by cellular structural optimisation using CMA-ES.

5.3. Analytical, numerical, and experimental methods

5.3.1. Generative design algorithm

Generative design represents the design discipline that applies the natural inspiration of variation and reproduction of all life. The “survival of the fittest” mechanism enforces the reproduction of each generation to move towards targets specified by the objective function in an iterative manner. Then the ‘fittest survivors’ can be selected from the final generation (Fischer & Herr, 2001).

The proposed approach is to vary the distribution of effective stiffnesses and density by altering the structure of the voxels while the base material and the overall geometry remain the same. With the advent of increased computational power and improved algorithms, generative design methods have been applied to finding solutions in numerous computer science and engineering applications (V. Singh & Gu, 2012;

Tyflopoulos, Tollnes, Steinert, & Olsen, 2018). For the current problem, the method is to locally alter the internal structure of the voxels to achieve the variation of the material property while keeping the overall geometry the same. The problem domain is divided into multiple brick-like hexahedral elements or voxels with the same length and width. The structural parameter of the voxels, such as the sizes, numbers and the location of the internal hollow structures, are represented as numerical parameter inputs for the optimization algorithm. The commercial finite element analysis software package, COMSOL Multiphysics, is used to evaluate deflection behaviour. The deflection behaviour can be closely governed by exploiting the variations in the geometries of structured voxels under multiple load conditions. A standard 3 point bending test is selected to verify and compare the actual deflection behaviour of the optimised structures.

5.3.2. Optimisation Algorithm and Functional evaluation

The covariance matrix adaptation evolution strategy (CMA-ES) algorithm is designed for handling continuous optimisation problems (N. Hansen & Ostermeier, 2001). Studies claim that CMA-ES gives superior performance amongst more than a hundred classical and modern optimization algorithms with different black-box functions (Loshchilov, Schoenauer, & Sèbag, 2013). It is widely applied for optimisation in various computer science and engineering studies. Hyperparameter tuning for neural networks (Jin, 2005; Loshchilov & Hutter, 2016), ranking support vector machines (Kern et al., 2006; Loshchilov et al., 2012), structural optimization for optimal truss layouts (Xiao et al., 2013) and thermal cloaking performance (Fujii & Akimoto, 2019), topology optimization for cloaking polarized light (Fujii et al., 2018), and identifying optimal metallic shapes and dielectric properties for desired electromagnetic scattering and radiation characteristics (Gregory et al., 2011) are notable examples.

In this work, the CMA-ES algorithm originally proposed by Hansen and Ostermeier (N. Hansen & Ostermeier, 2001) is adopted to solve the problem of optimizing the geometries of cellular structures targetting the convergence of the beam deflection to a pre-defined form. CMA-ES is an iterative algorithm; in each iteration, the offsprings or a number of candidate solutions for the next generation are sampled from a normal distribution of multiple variables with a step size of the current generation. The fitness of these solutions is evaluated, and the sampling distribution of the next generation is adjusted according to the fitness of each solution in the current generation(N. Hansen & Ostermeier, 2001). The major steps of the structural optimization scheme are summarized in the flowchart, as shown in Figure 5.1. The commercial finite element analysis software package COMSOL Multiphysics (Version 5.6, release date November 11, 2020, COMSOL Inc., Stockholm, Sweden) is used for evaluating the deflection behaviour. The standard quadratic solid elements are used for the finite element discretisation and analysis.

The objective function minimizes the fitness value that is defined as the weighted (w) mean square errors of the actual and the target deflection of each selected point (i) in the structure. The overall optimisation scheme is implemented in MATLAB (R2017B, release date September 14, 2017, MathWorks, Natick, Massachusetts, USA)

$$fitness = \sum_{i=1}^{N} w_i \left(deflection_i^{target} - deflection_i^{result}\right)^2 \quad (5.1)$$

$$w_i = l^2/d_i \quad (5.2)$$

Where $deflection_i^{target}$ and $deflection_i^{result}$ are the target and the deflection computed by the finite element analysis; N and i indicate the total number of the sampling point and the index of the deflection of the current sampling point. And the weight value is calculated by the length of the beam l and the distance between the points of load and the supporting points d.

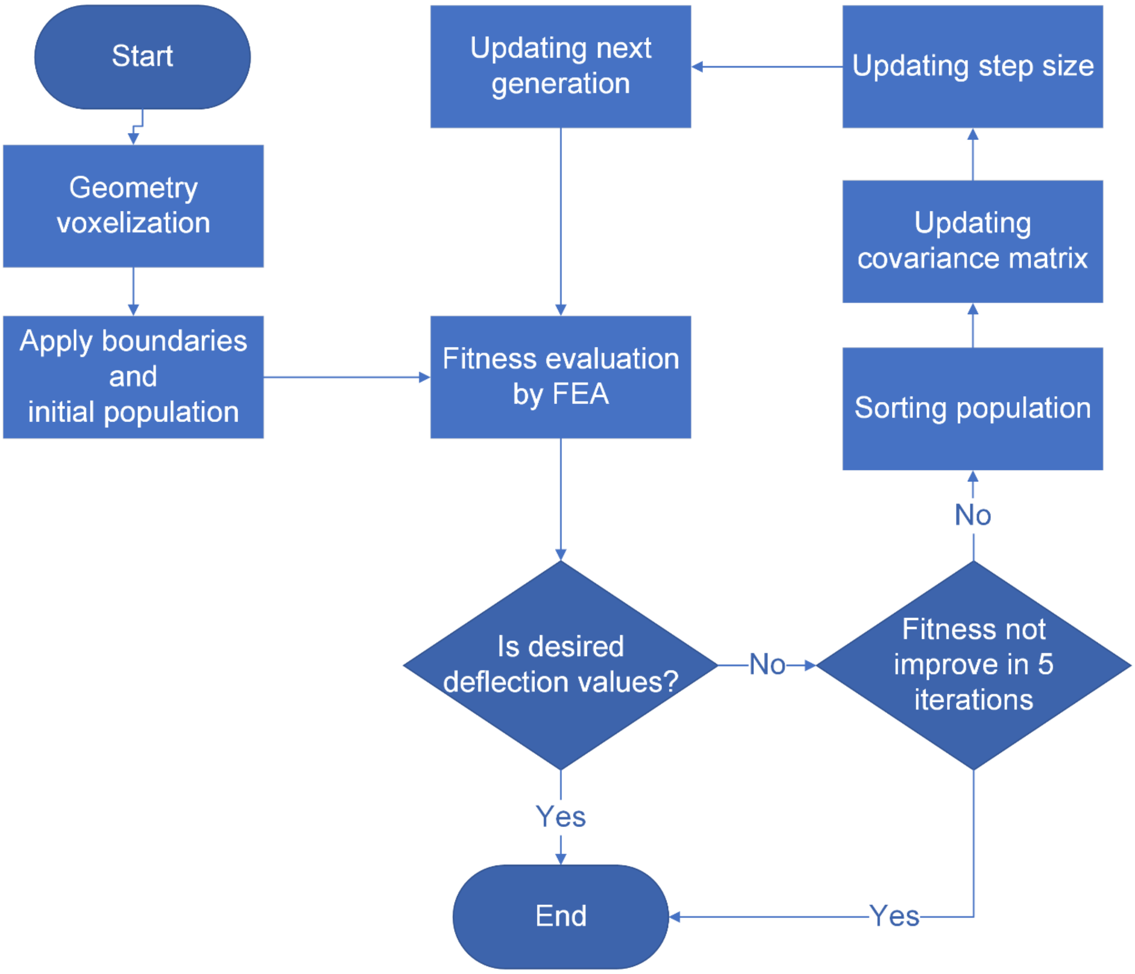

Figure 5.1. The flowchart of the overall optimisation scheme based on the implementation of the CMA-ES algorithm with Comsol Multiphysics solution for the beam deflection problem

5.4. The beam deflection problem

5.4.1. Voxelization and cellular geometry settings

Two setups of voxelisation were tested, which divided the beam structure into 20 and 40 voxels, respectively. The overall dimensions (L x B x H) for the beam structure remain the same at 200 mm x 30 mm x 10 mm for all voxelisation and cellular structure settings. The CAD models of the beam structures with different voxelisation subdivisions are shown in Figure 5.2. The CMA-ES optimisation algorithm will alter the height of the void, which changes the moment of inertia of each voxel and controls the overall deflection behaviour to match the desired deflection profile. Further, three voxel geometry settings are designed to comprehensively validate the performance of the proposed optimisation method, namely, symmetric and asymmetric single void and double void voxel geometry settings. CAD models of the three voxel geometry settings are depicted in Figure 5.3.

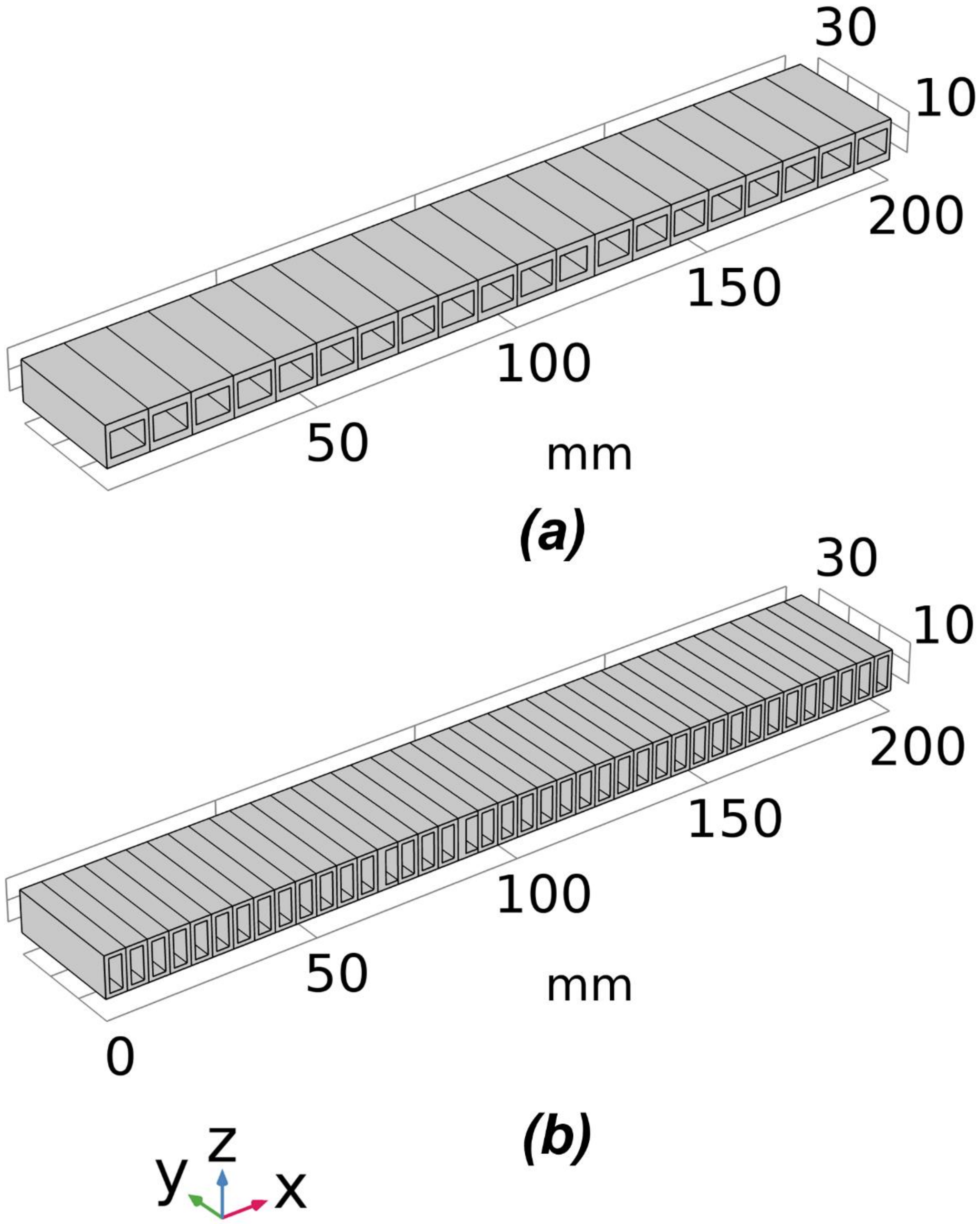

Figure 5.2 The cellular beam structures with 20 and 40 voxels. The length of voxels is 10 mm and 5 mm, respectively, for 20 voxels (a) and 40 voxels (b) models.

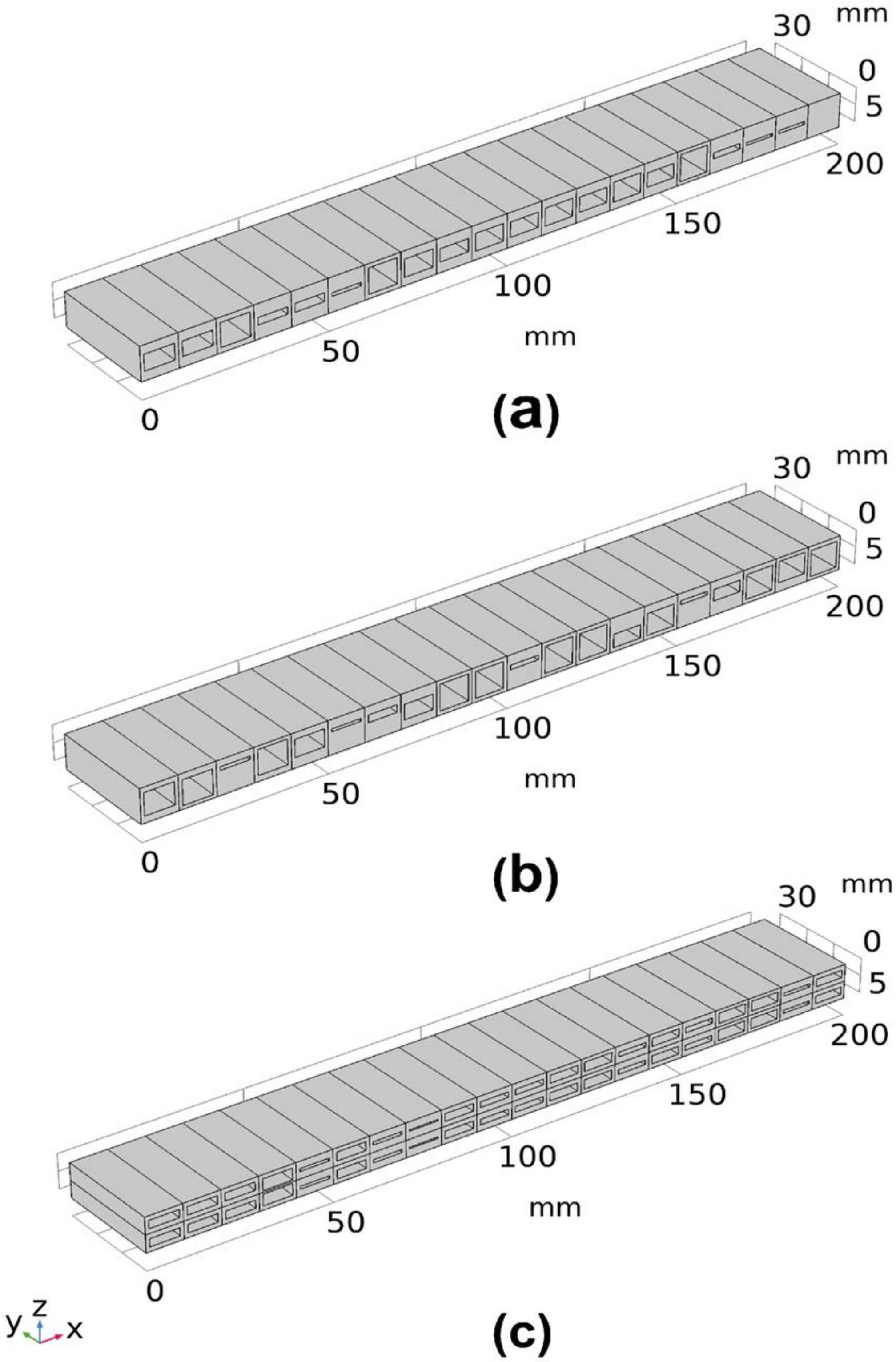

Figure 5.3. CAD models of the 20 voxel structures with the three different voxel cellular geometry settings. (a) single symmetric void, (b) single asymmetric void and (c) double void setting.

In order to maintain the overall dimensions of the beam structure, the height of the hollow structure of each voxel (H_v) is used as the optimisation parameter for both symmetric single void and double void setup. Additional optimisation parameter T_b is used to control the location of the void within the voxel. The detailed voxel geometry settings are depicted in Figure 5.4

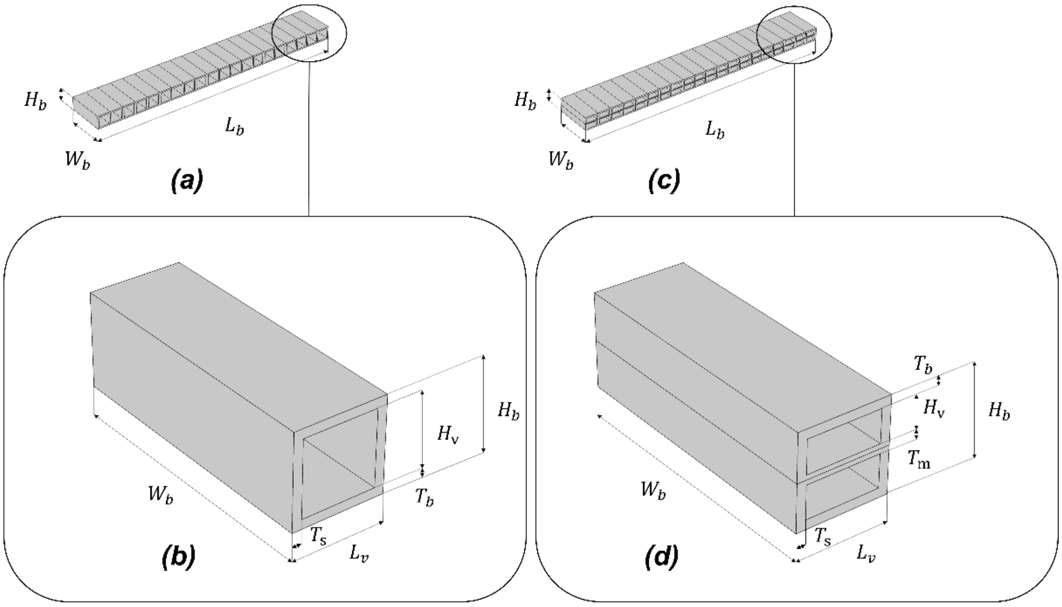

Figure 5.4. The beam domain example for 20 voxels model with single symmetric or asymmetric void setting (a) and double void setting (c). The details of voxel geometry settings are shown in (b) and (d), respectively. In these particular examples, the voxel height H_b is 10 mm, and the hollow structure height H_v is 8 mm for both examples.

5.4.2. Boundary settings for the cell geometry

The bounds of the optimisation parameter are related to various practical considerations, such as the accuracy and the building dimensional limits of the current available AM processes. Considering the fabrication quality and maintaining the overall dimensions, the height of the beam (H_b) is fixed to 10 mm, and the minimum thickness is limited to 1 mm. Therefore, for the minimum top and bottom thickness T_b of each voxel is 1 mm, the side thickness T_s of each voxel is also fixed to 1 mm. For double void voxel geometry setting, the minimum thickness of the middle layer T_m is also limited to 1 mm. With these as the limiting boundary values, the single void voxel structure (for both symmetric and asymmetric settings) can vary anywhere from a solid cell to a voxel with a hollow structure of 8mm height H_v.

The low bound provides the highest stiffness and the lowest deflection, and it can be considered as a solid beam. With the same overall dimensions, the low bound for all voxelization settings can be considered as the same solid beam as depicted in Figure 5.5 (a). Similarly, the high bound provides the lowest stiffness and the highest deflection. Therefore, the beam structure with the largest hollow geometry for the cells is considered as the high bound. The high bound for the symmetric and asymmetric single void 20 voxel model is shown in Figure 5.5 (b), and the high bound for the double void 20 voxel model is shown in Figure 5.5 (c). Due to the increased voxel numbers, the side layer structures of each voxel provide more internal support, which leads to higher stiffness and smaller deflection. The high bound for 40 voxels settings are shown in Figure 5.5 (d) and (e).

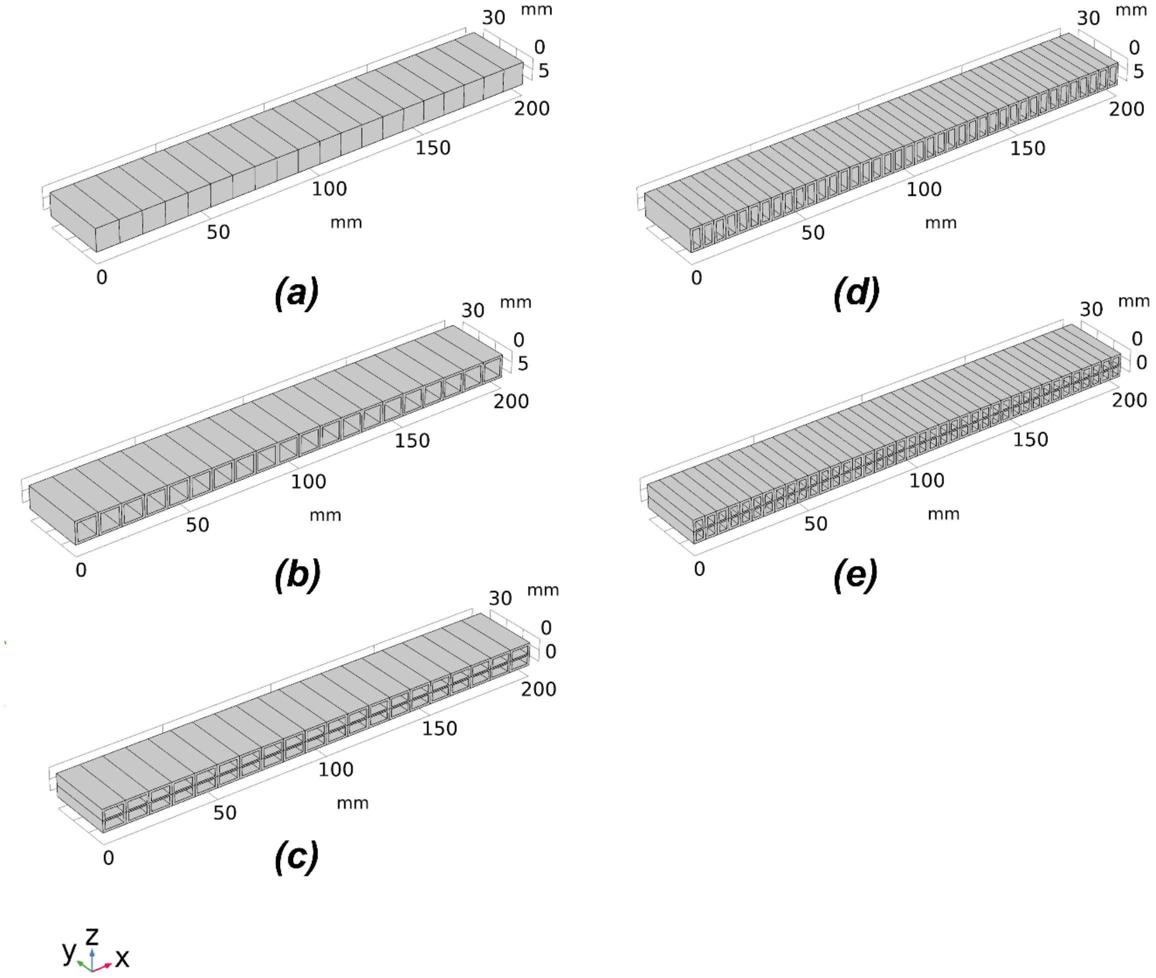

Figure 5.5. The low bound and high bound structural settings for the voxels for optimising the deflection behaviour of the beam. (a) the low bound structure for all voxelisation settings; (b) high bound structure for 20 voxels model with single symmetric or asymmetric voids; (c) high bound structure for 20 voxels model with the double voids; (d) high bound structure for 40 voxels model with single symmetric or asymmetric voids; (e) high bound structure for the 40 voxels model with the double voids.

5.4.3. Material properties

The standard fused deposition modelling material option based on polylactic acid (PLA) is selected as the test material. The material property values are set to : Young's modulus = 3600 MPa, Poisson’s ratio = 0.35, and density = 1240 kg/m3 (SD3D.COM, 2022). This choice is based on the fact that it is easy to demonstrate the physical printing of the structures and experimental validation of the analytical and numerical predictions.

5.4.4. Experimental conditions and initial and target sets

Experiments with multiple load settings are conducted to demonstrate the capability of the CMA-ES in structural optimization. As shown in Figure 5.6, the beam bending behaviour is evaluated in a standard 3 point bending setup. Three sampling points are considered located at the 1/4 1/2 and 3/4 distances along the length of the beam structure to test the efficiency of the proposed structural optimisation method to control the deflection behaviour of the entire beam. The beam deflection response is controlled during the structural optimisation to provide the exact desired deflections at three selected points with applied load at three different locations, as shown in Figure 5.6 for the three-point bending cases simulated in COMSOL Multiphysics. The load of 100 N distributed overran area is applied to the beam through a roller with a diameter of 6 mm. As shown in Figure 5.6, this load is applied at the 1/4th (load case 1 as shown in Figure 5.6 (a)), 1/2 (load case 2 as shown in Figure 5.6 (b)), and 3/4th (load case 3 as shown in Figure 5.6 (c)) distances along the length of the beam structure, in the three experimental conditions studied. The sampling points match with these load points, but each loading point gives a different set of deflections for three points of interest. Consequently, the deflections at three specific points under three loading conditions result in a challenging multi-objective optimisation problem. Notably, the multiple load cases are designed to test the capability of the proposed structural optimisation method to optimize a single structured beam to have the desired deflection behaviour under multiple different loading conditions.

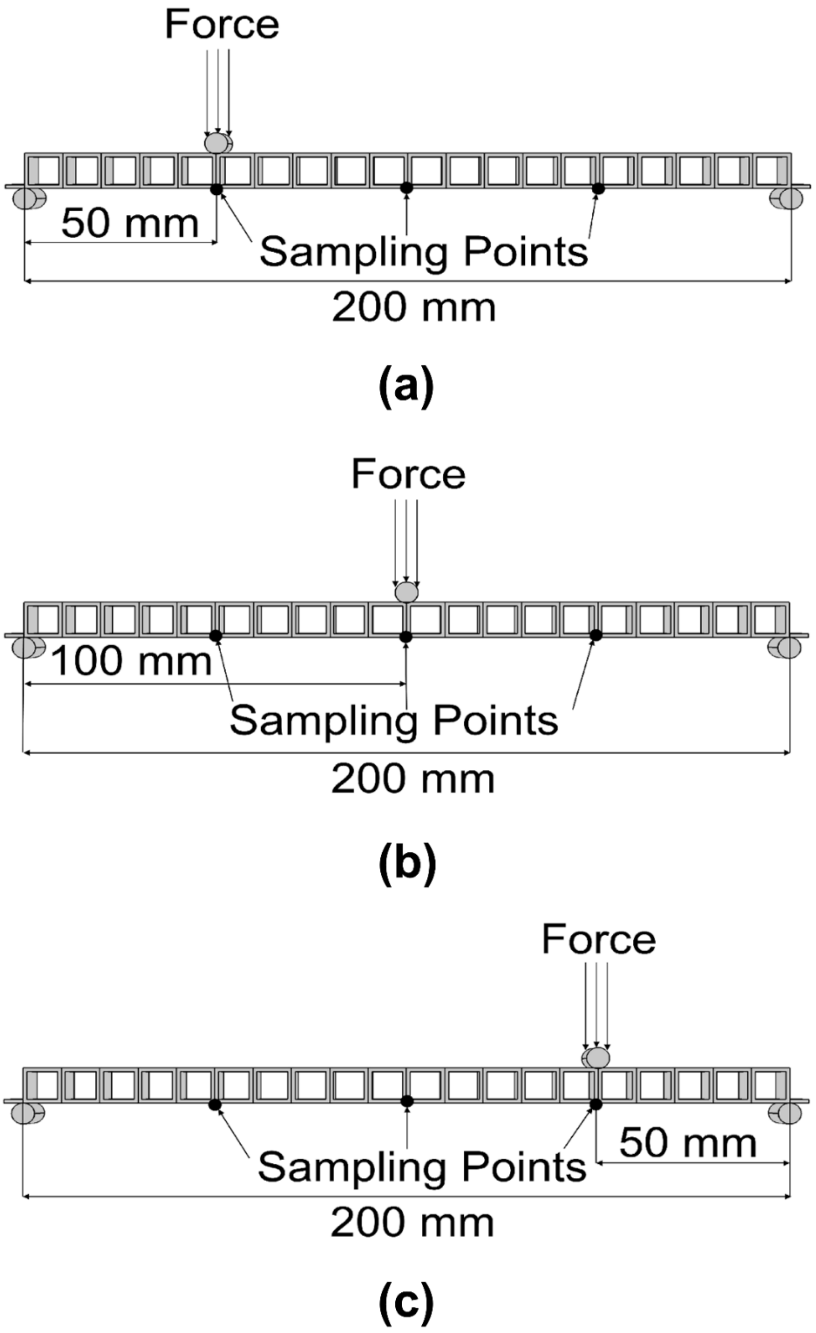

Figure 5.6. The 20 voxel beam which showing the three load and deflection sampling points at the 1/4th, ½, to 3/4th distances along the length of the beam structure.

The CMA-ES evolutionary process starts from an initial configuration, where the height of the hollow structure of each voxel (H_h) in the initial population is randomly generated, ranging from a full solid voxel to the one with a hollow structure within the boundary limits explained previously. In accordance with these limits, the parametric values of the voxel geometries are constrained to the values listed in Table 5.1 during the evolutionary search. The voxelised beam structures corresponding to these high and low bound limits are illustrated in Figure 5.5. The resulting ranges of deflection in multiple load cases and voxel geometry settings, as calculated by the finite element analysis, are listed in Table 5.2. The target sets (TS) tested for the 20 voxel single void structure model are listed in Table 5.3. The initial target sets for the desired beam deflection values are selected as the midpoint (TS1) between the low and high bound limit results and then varied around the midpoint. In TS2 and TS3, The desired beam deflection target sets are varied at +0.2 mm and -0.2 mm from the midpoint, respectively. And in TS4 and TS5, The desired beam deflection target sets are varied at +0.2 mm and -0.2 mm from the midpoint, respectively. For the 40 voxel and double void structured models, the high bound limit is different. Therefore, different target sets are used to verify and compare the performance, and the final target sets used for 40 voxel models are listed in Table 5.4. Similar to the single void structured model, TS6 is the midpoint between the results of the low and high bound limits. The target set for desired beam deflection is varied at +0.2 mm in TS7, which is the largest possible variation for the double void model.

Table 5.1. The limits of the voxel geometric parameters for the beam models

	20 voxel			40 voxel		
Geometric parameter (mm)	**high bound (single symmetric and asymmetric void)**	**high bound (double void)**	**low bound**	**high bound (single symmetric and asymmetric void)**	**high bound (double void)**	**low bound**
L_v	10	10	10	5	5	5
W_b	30	30	30	30	30	30
H_b	10	10	10	10	10	10
T_b	1	1	N/A	1	1	N/A
T_s	1	1	N/A	1	1	N/A
H_v	8	3.5	N/A	8	3.5	N/A
T_m	N/A	1	N/A	N/A	1	N/A

Table 5.2. The limiting ranges of beam deflections at the sampling points resulting from the voxel geometrical parameters as listed in Table 5.1

Unit: mm	20 voxels	20voxels	40 voxels	40 voxels	Low bound (All setup)
	Single void settings	Double void settings	Single void settings	Double void settings	
	High bound	High bound	High bound	High bound	
Loading 1 Sampling point 1 (L1S1)	-2.4774	-1.807	-1.437	-1.151	-0.469
Loading 1 Sampling point 2 (L1S2)	-2.241	-1.714	-1.515	-1.241	-0.514
Loading 1 Sampling point 3 (L1S3)	-1.172	-0.875	-0.809	-0.634	-0.242
Loading 2 Sampling point 1 (L2S1)	-2.235	-1.708	-1.509	-1.235	-0.511
Loading 2 Sampling point 2 (L2S2)	-3.812	-2.888	-2.421	-1.987	-0.831
Loading 2 Sampling point 3 (L2S3)	-2.235	-1.708	-1.509	-1.235	-0.511
Loading 3 Sampling point 1 (L3S1)	-1.172	-0.875	-0.809	-0.634	-0.242
Loading 3 Sampling point 2 (L3S2)	-2.241	-1.714	-1.515	-1.241	-0.514
Loading 3 Sampling point 3 (L3S3)	-2.474	-1.807	-1.437	-1.151	-0.469

Table 5.3. The target deflection sets for 20 voxel single void structured beam

Unit (mm)	L1S1	L1S2	L1S3	L2S1	L2S2	L2S3	L3S1	L3S2	L3S3
Low bound	-0.468	-0.514	-0.242	-0.511	-0.831	-0.511	-0.242	-0.514	-0.468
High bound	-2.474	-2.241	-1.172	-2.235	-3.812	-2.235	-1.117	-2.241	-2.474
Midpoint (TS1)	-1.471	-1.377	-0.707	-1.373	-2.321	-1.373	-0.707	-1.377	-1.471
Midpoint +0.2(TS2)	-1.271	-1.177	-0.507	-1.173	-2.121	-1.173	-0.507	-1.177	-1.271
Midpoint -0.2(TS3)	-1.671	-1.577	-0.907	-1.573	-2.521	-1.573	-0.907	-1.577	-1.671
Midpoint +0.4(TS4)	-1.071	-0.977	-0.307	-0.973	-1.921	-0.973	-0.307	-0.977	-1.072
Midpoint -0.4(TS5)	-1.871	-1.777	-1.107	-1.773	-2.721	-1.773	-1.107	-1.777	-1.871

Table 5.4. The target deflection sets for 40 voxel beam

Unit (mm)	L1S1	L1S2	L1S3	L2S1	L2S2	L2S3	L3S1	L3S2	L3S3
Low bound	-0.468	-0.514	-0.242	-0.511	-0.831	-0.511	-0.2420	-0.514	-0.4680
High bound	-1.4368	-1.5153	-0.809	-1.509	-2.421	-1.509	-0.809	-1.5153	-1.4368
Midpoint (TS6)	-0.953	-1.015	-0.526	-1.01	-1.626	-1.01	-0.526	-1.015	-0.953
Midpoint +0.2 (TS7)	-0.753	-0.815	-0.326	-0.81	-1.426	-0.81	-0.326	-0.815	-0.753

5.5. Results of the structured beam deflections and discussion

5.5.1. Tuning the algorithm

The standard CMA-ES algorithm is used in this work. The step size control and covariance update parameters are set as default values and will update in each iteration based on the obtained fitness value. The optimization performance is highly dependent on the population size and iteration number, which govern the range of the search domain. The voxel number is also a vital parameter, which is proportional to the number of degrees of freedom. However, large population size, iteration number, and voxel number can lead to excessive computational times.

A small number of initial numerical experiments were conducted to identify the influence of each parameter. The 20 voxel model with a single symmetric voxel setting and the target set TS4 are used in the initial tests for identifying the most efficient population size for the optimisation. TS4 contains the highest variance between each sampling point, which is the most challenging target set for the optimisation scheme. The results of five independent trials are summarized in Figure 5.7. The lower the fitness value, the better the results. It is clearly evident that when the population size is doubled to 50, the optimisation method can provide a closer match and at an approximately 50% lower fitness value compared with the trials with a population size of 25. With a further increase in the population size to 100, both the variance and fitness value further decreased by approximately around 10%. However, with increasing population size, the computational time also increases proportionately, leading to heavy computational constraints. To avoid excessive computational times and associated time constraints, the population size is fixed at 50 in all the rest of the tests presented next.

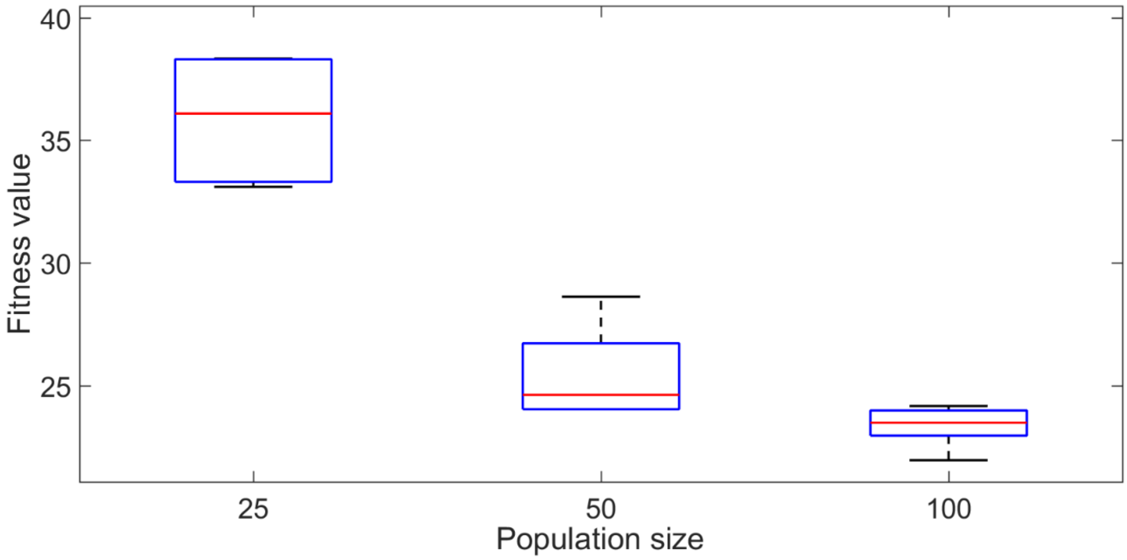

Figure 5.7. The effect of population size on the fitness value for TS4 using the 20 voxel single symmetric model. The solid red lines indicate the median fitness value, and the boxes represent the 25th and 75th percentiles.

In terms of the voxel numbers, both the 20 voxel and 40 voxel models are tested. The midpoint (TS1 and TS6) and the target set with the highest achievable variance from the midpoint (TS4 and TS7) are selected respectively for the 20 and 40 voxel models. The results of five independent trials are illustrated in Figure 5.8. Once again, based on the premise that the lower the fitness value, the better, it is clear that the 40 voxel model can provide a superior result compared to the 20 voxel model in both variance and fitness values. However, as depicted in Figure 5.9, the mean of the difference between the actual deflection and the corresponding target deflection at the nine sampling points is less than 0.1 mm in most cases. It indicates that both 20 voxel and 40 voxel models can provide satisfactory results in matching the target deflection sets.

Computationally, the 40 voxel model is significantly more expensive compared to the 20 voxel model in terms of both time and other constraints. The fitness function computation time for a single evaluation is increased from 9 seconds to 33 seconds on a standard Intel i7 9700k processor when moving from 20 to 40 voxel cases. As a balance between the computational costs and the performance of the optimisation scheme, the 20 voxel model is used with a population size of 50 as the standard setting in the CMA-ES optimisation in all the experiments following.

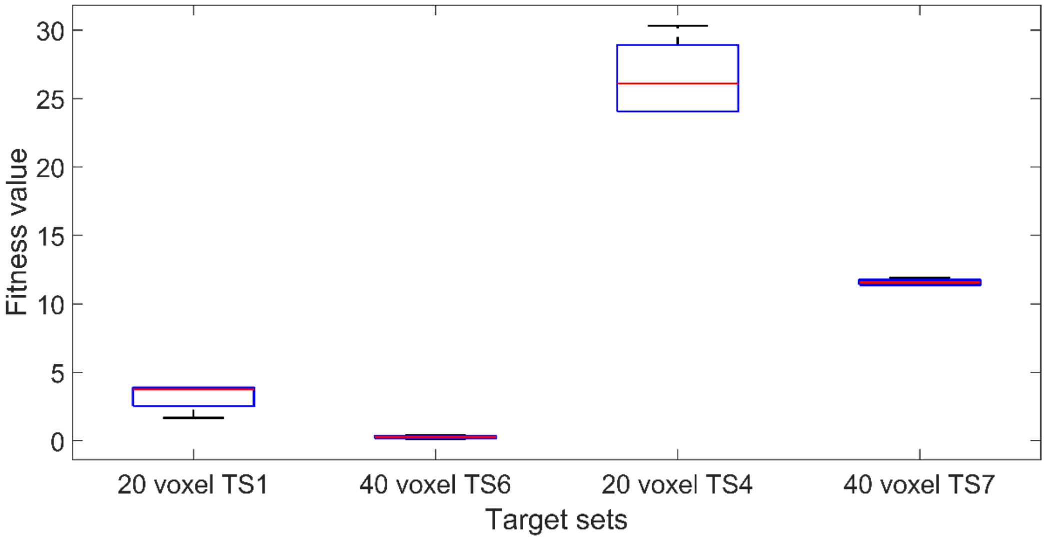

Figure 5.8. The effects of voxel number on the fitness value. The solid red lines indicate the median fitness value, and the boxes represent the 25th and 75th percentiles.

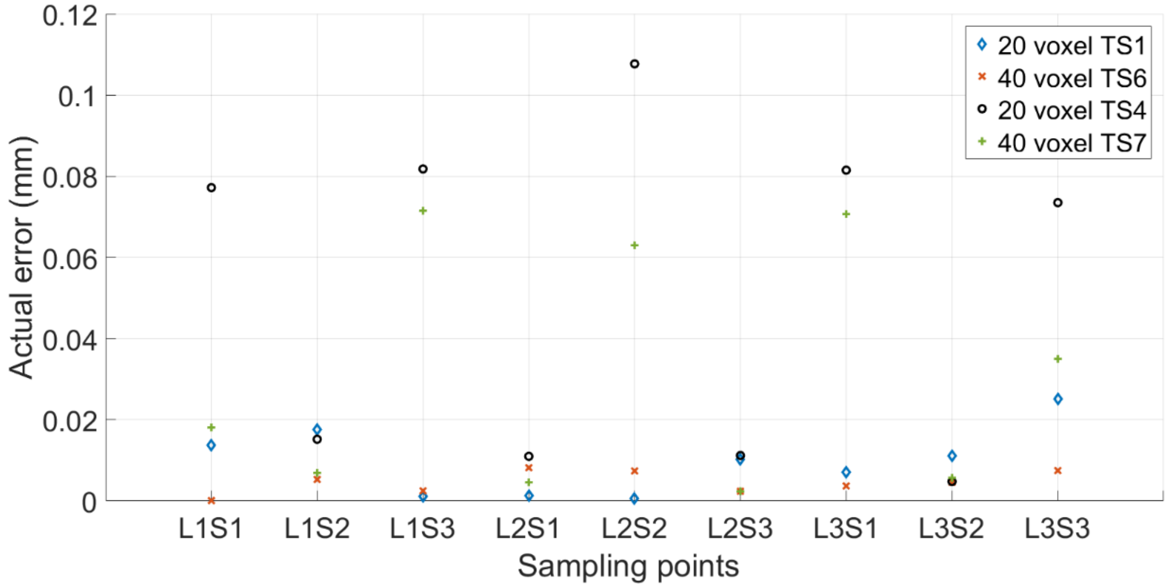

Figure 5.9. The mean of the difference between the actual deflection and the corresponding target deflection in the nine sampling points

5.5.2. Results based on the beam with standard single symmetric void voxels

As discussed in the previous sections, a population size of 50 is used in all the following test cases analysed. The deflection target sets TS1 to TS5 are used for the standard single symmetric void beam model. The structural form of the optimised beam for TS1 is illustrated in Figure 5.10 (a) and the deflection patterns with the three loading cases in Figures (b) to (d). The fitness values obtained with the different target sets as compiled in Figure 5.11 indicate that the result for TS1 attained the lowest fitness value. The target sets TS4 and TS5 ended up with the highest fitness values, indicating the highest error levels. Referring back to the listings of the deflection ranges in Table 5.3, TS4 and TS5 have the largest variation from the midpoint between the low and high bound limits and the deflection targets with sampling points L1S3 and L3S1 for TS4 and TS5 are close to the low and high bound limits respectively, while the deflections at the other sampling points still remain relatively close to the midpoint. For example, to match with the target deflections corresponding to the settings of L1S3 and L3S1 cases in TS4, the optimisation scheme needs to create the largest void dimensions for obtaining the lowest overall stiffness of the structure while the stiffness matrix of the beam structure also has to maintain higher stiffness for matching the target deflection at other sampling points. This conflict between the demanding conditions at the opposite ends at different sampling points is the main reason for the higher error in the trials TS4 and TS5. It is pertinent to point out that the sampling points L1S3 and L3S1 in TS4 and TS5 are the major sources of error in Figure 5.12 (a), adding strength to the above arguments. The optimised beam provided the deflections to closely match the pre-set conditions with an error of less than 10% in all other sampling points and a much lower error in many cases.

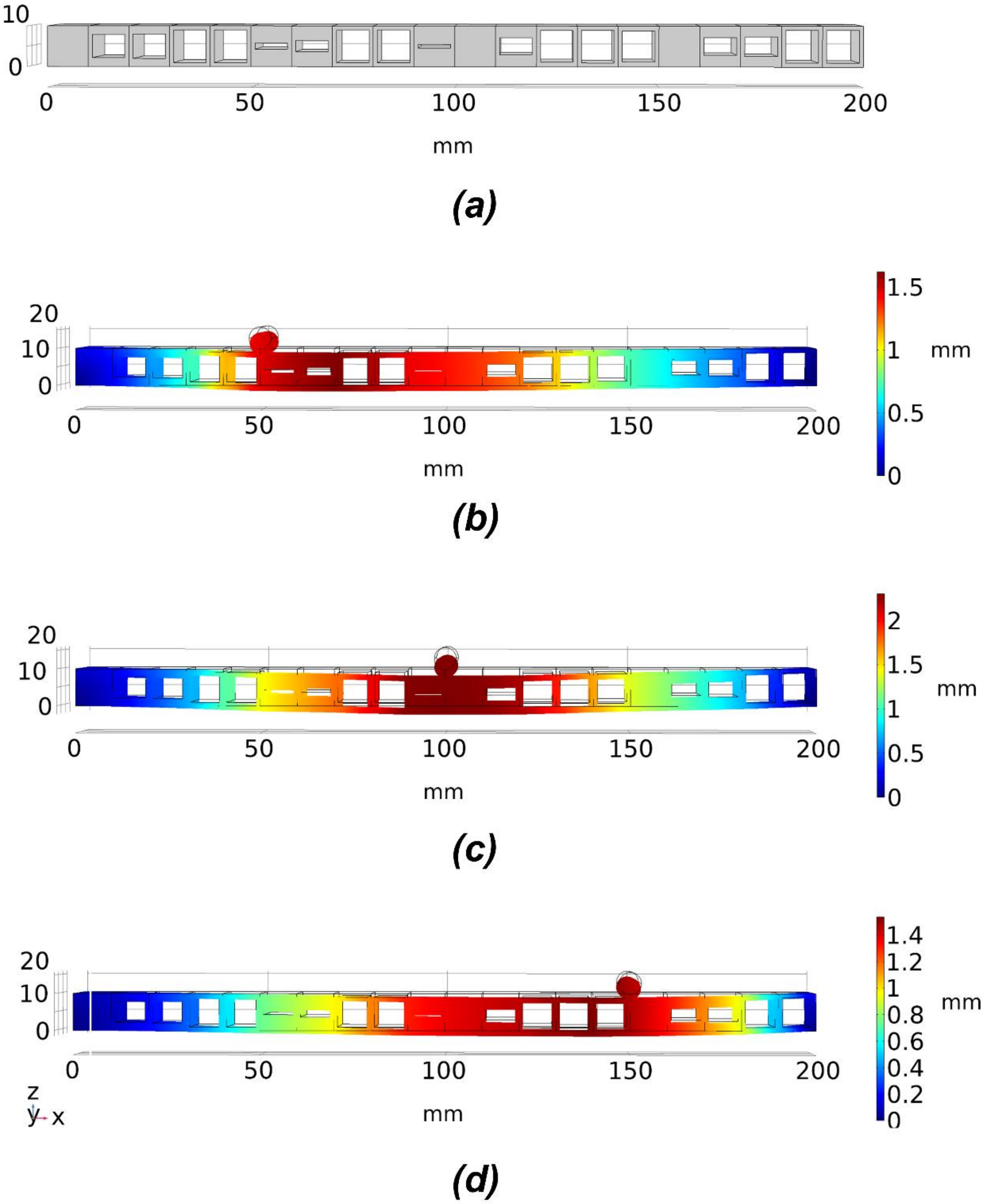

Figure 5.10. The optimised beam structure for TS1. (a) the geometry of the optimised beam model and (b) to (d) deflection patterns under loading conditions 1-3.

TS4 and TS5 both have the same variation (0.4mm) from the midpoint between the low and high bound. However, as shown in Figure 5.12 (a), it can be seen that the proposed optimisation scheme obtained better performance in TS5. The main reason is that TS4 has a smaller deflection value compared with TS5, which represents a higher error in percentage. From Figure 5.12(b), it can be seen that the optimised beam obtained a similar error for matching the conditions of TS4 and TS5. Overall, as shown in Figure 5.12 (b), the proposed optimisation scheme provided satisfactory accuracy levels in matching the deflection profiles with any case of the target sets within a maximum deviation of 0.1 mm.

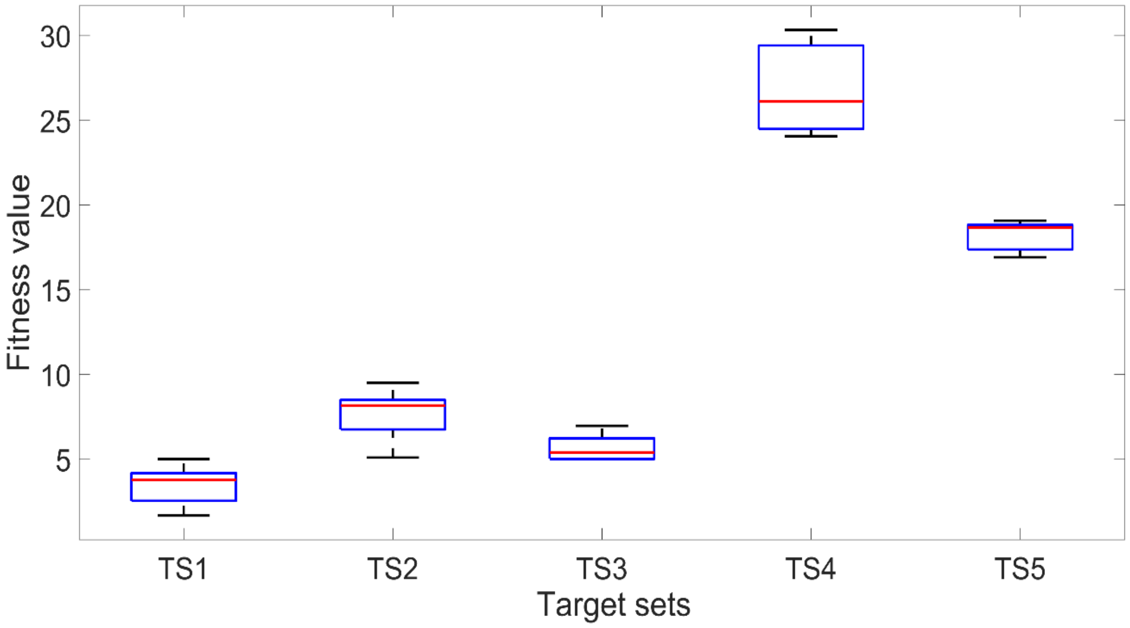

Figure 5.11. Comparison of fitness values with the 20 voxel single symmetric void model for target deflection sets TS 1-5. Each box plot represents the results of 5 trials for each target set. The lower the fitness value, the closer the obtained deflection sets to the target deflection sets. The solid red lines indicate the median fitness value, the top and bottom of the boxes represent the 25th and 75th percentiles.

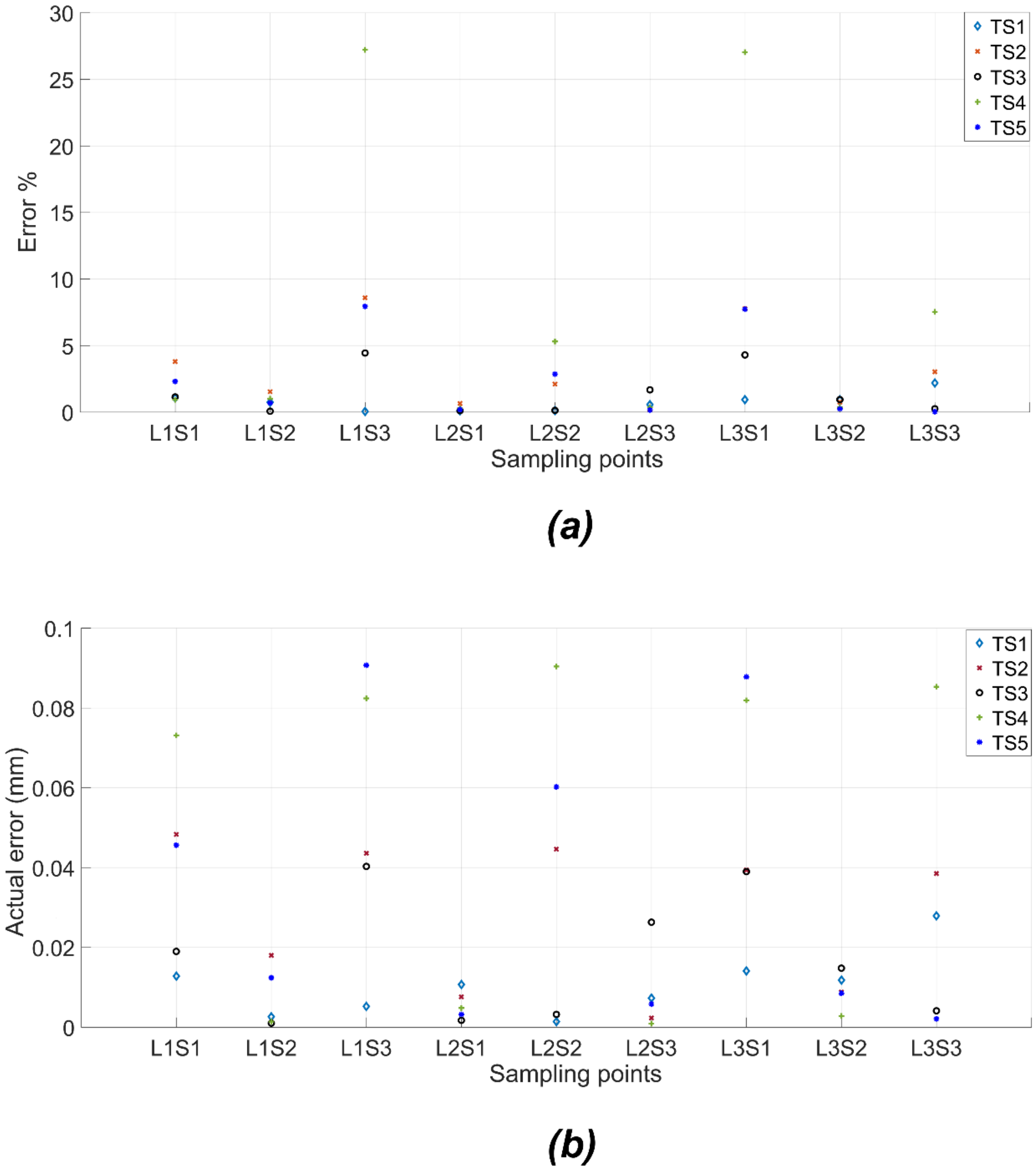

Figure 5.12. The mean of the difference between the deflection in nine sampling points and the corresponding target deflections for TS1 to TS5 in 20 voxel symmetric single void models is expressed as (a) percentage and (b) actual deflection difference. Each data point corresponds to the mean value of 5 independent trials.

5.5.3. Results based on the beam with double and asymmetric void voxels

The next step is to evaluate the ability of the proposed CMA-ES algorithm to optimise the beam deflection patterns based on the two cellular structure variants as described in Section 5.4.1. The more complex double void cellular structures with a middle layer in the voxels and the asymmetric void structures offer opportunities for wider property variations, giving better possibilities for the search algorithms to explore and find the optimum solutions. The single material printed structural option has relatively limited capability in terms of the range of property variation within the continuum. Any additional degree of freedom to expand the limits of material property variations will further help the search algorithms to converge on optimal solutions in more demanding situations.

For the double void model, the thickness of the middle layer T_m serves as an extra parameter in the optimisation scheme, which provides an additional degree of freedom and better control in the design domain while also adding more complexity and a further dimension in the search domain of the proposed optimisation scheme. As a result of the extra middle layer in the cellular structure, the high bound limit of the achievable deflection is different. As listed in Table 5.5, different target sets, TS8 and TS9, are used. TS8 corresponds to the midpoint between the low and high bound limits of the achievable deflections, while TS9 is the target set with +0.2 mm variation from the midpoint, which is the highest achievable variation for the double void voxel model. An example of the optimised 20 voxel double void beam structure is depicted in Figure 5.13. The resulting beam structure is made up of double void voxels with varying internal dimensions for the voids that are symmetric about the central web.

Table 5.5. The target deflection sets for double void 20 voxel beam

Unit (mm)	**L1S1**	**L1S2**	**L1S3**	**L2S1**	**L2S2**	**L2S3**	**L3S1**	**L3S2**	**L3S3**
Low bound	-0.468	-0.514	-0.242	-0.511	-0.831	-0.511	-0.2420	-0.514	-0.4680
High bound	-1.807	-1.714	-0.875	-1.708	-2.888	-1.708	-0.875	-1.714	-1.807
Midpoint (TS8)	-1.141	-1.118	-0.5615	-1.114	-1.865	-1.114	-0.561	-1.118	-1.141
Midpoint +0.2 (TS9)	-0.941	-0.918	-0.362	-0.914	-1.665	-0.914	-0.3615	-0.918	-0.9411

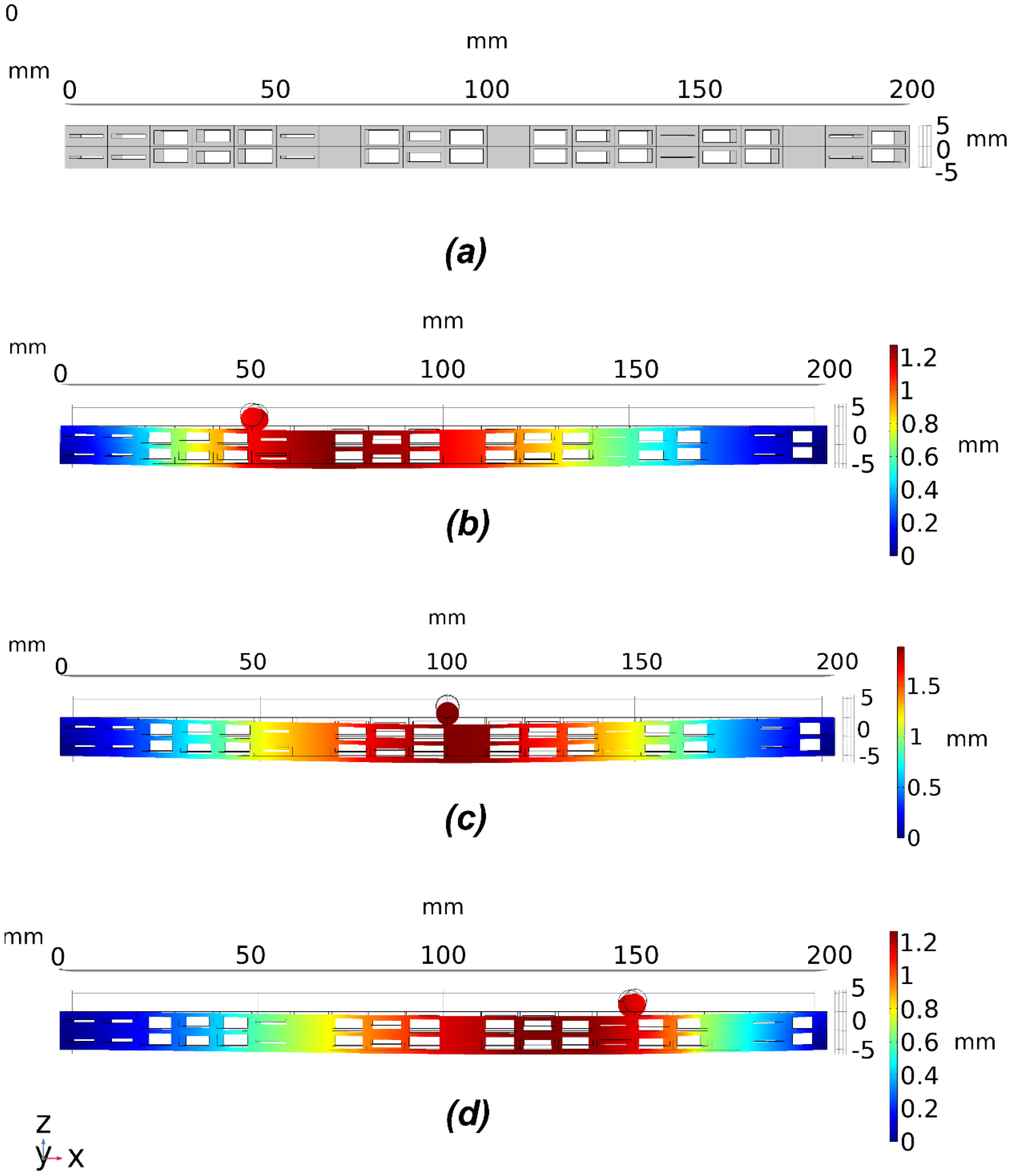

Figure 5.13. An example of the optimised 20 voxel double void beam model for the target set TS8. (a) the geometry of the optimised beam model and (b) to (d) are deflection plots under loading conditions 1 to 3, respectively.

As shown in Figure 5.14, the fitness values for target sets TS8 and TS9 are approximately 1 and 4, respectively. The fitness value is essentially a weighted mean square error. Compared with the single symmetric void model, the double void voxel model obtained better performance with the same number of voxels. Evidently, with the additional manipulation of the thickness of the middle layer in the double void cellular structure, the optimisation scheme had better control over the overall stiffness matrix, which in turn governs the deflection profile of the beam. Moreover, the additional middle layer leads to a smaller range of the possible search space, which may also lead to a relatively better coverge in the double void model. The percentage and actual deviations between the target and achieved values resulting from the FE simulations of the optimised beam structures are presented in Figure 5.15 (a) and (b), respectively. The results in Figure 15 (a) and (b) clearly indicate the better performance of the CMA-ES optimisation scheme in converging on the most optimum structural geometry of the cellular beam, effectively utilising the added degree of freedom from the double void geometry. The optimised cellular beam structures achieved deflection patterns close to the values of the desired deflection target sets TS8 and TS9. At all the sampling points, the percentage and actual deviations between the predicted and desired deflection levels (errors) are less than 6% and 0.06 mm, respectively.

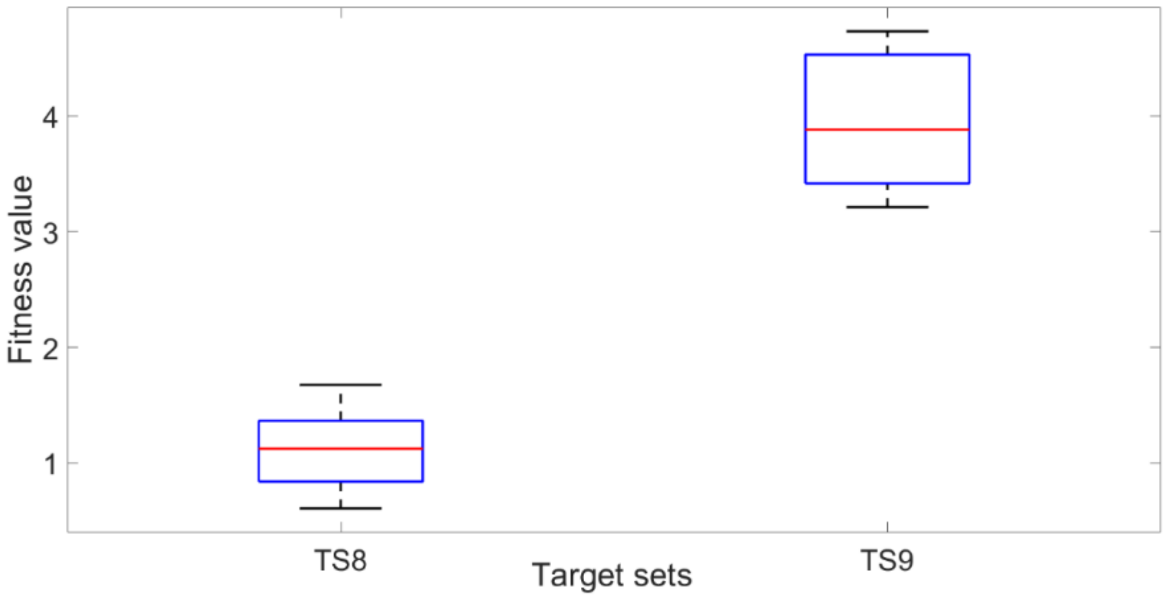

Figure 5.14. Comparison of fitness values for 20 voxel double void model for target deflection sets TS8 and TS9. Each box plot represents the results of 5 trials for each target set. The lower the fitness value, the closer the obtained deflection sets were to the target deflection set. The solid red lines indicate the median fitness value, the top and bottom of the boxes represent the 25th and 75th percentiles.

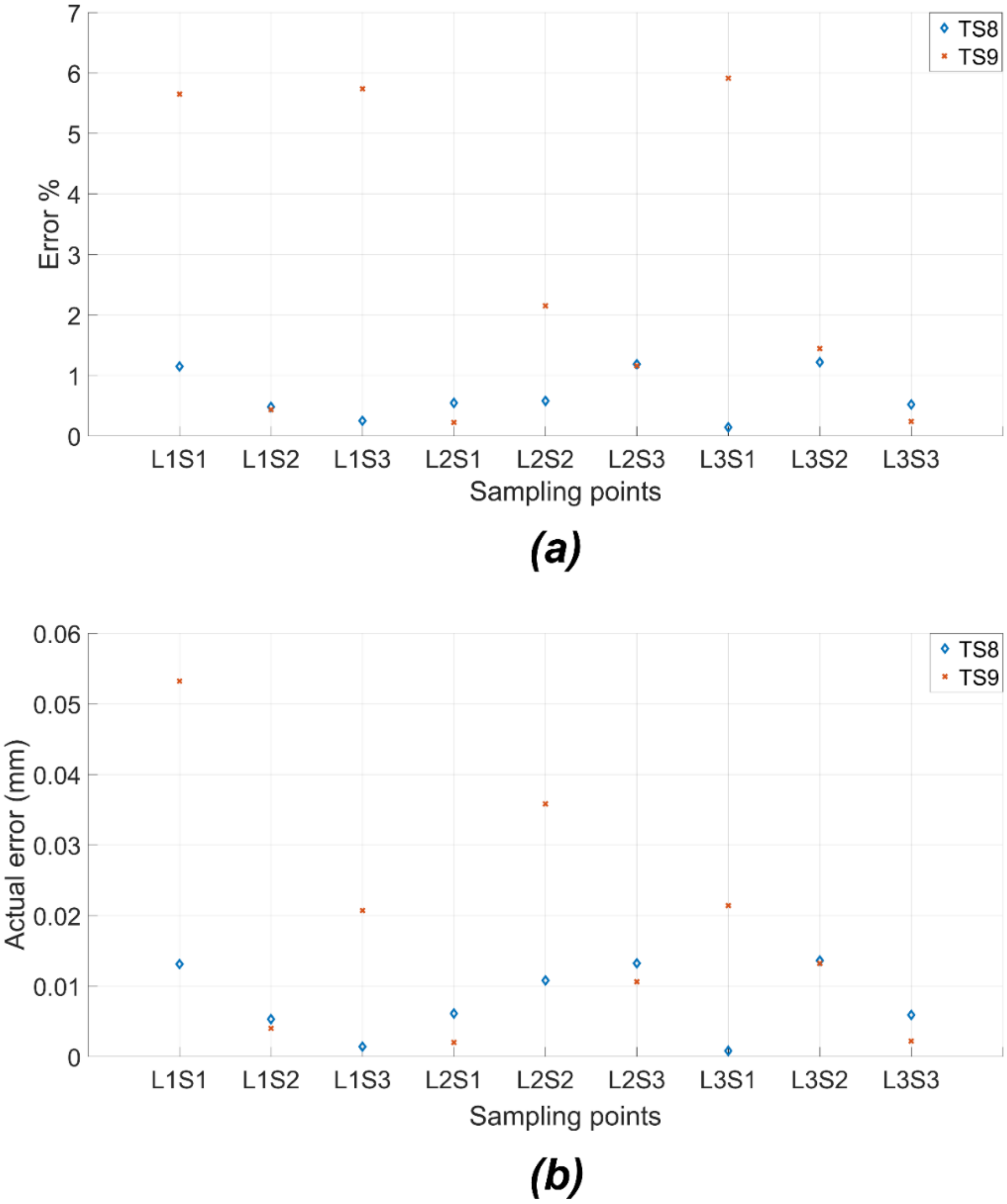

Figure 5.15. The mean of the difference between the deflection in nine sampling points and the corresponding target deflections for TS8 and TS9 in 20 voxel double void models is expressed as (a) percentage and (b) actual deflection difference. Each data point corresponds to the mean value of 5 independent trials.

For the asymmetric single void model, the void structure can be asymmetrically located in each voxel within the boundary rather than centred around the middle line. Referring back to Figure. 5.4 again, in this case, the thickness of the bottom web, T_b can be used as an additional parameter to control the location of the void within the voxel, which will double the geometric parameters for optimisation compared to the single void symmetric cellular structure. This additional parameter T_b is again expected to allow the optimisation scheme to gain better control over the deflection behaviour of the beam model while also increasing the complexity and the dimensions of the searching problem. The asymmetric single void model shares the same low and high bound limits for the deflections as the symmetric single void voxel model. Therefore, the same target deflection sets TS1 and TS4 as employed in section 5.5.2 are used. An example of the optimised cellular geometry of the beam with the asymmetric single void structure is depicted in Figure 5.16 (a) and the deflection profiles in Figure 5.16 (b) to (d) as obtained with the three loading cases. The variation of the geometry of the cells based on asymmetric positioning of the voids as obtained by the optimisation scheme is clearly reflected in Figure 5.16 (a).

As illustrated in Figure 5.17 and Figure 5.18, the optimisation with the asymmetric single void model obtained similar trends in results as the standard symmetric single void model. The maximum deviation between predicted and target results is less than 10% or 0.08 mm in most of the cases. Though the optimisation scheme was effective in handling the additional degrees of freedom, there is no specific improvement in the convergent results based on the asymmetric model compared to the symmetric single void model. The main reason for this is the fact that there is no substantial variation in the property ranges that can actually be obtained by shifting from the symmetric to the asymmetric variations in the single void cellular geometries.

The results for sampling points L1S3 and L3L1 still suffered from larger errors. Similar to the results based on the standard symmetric single void model, the targets for sampling points L1S3 and L3L1 are close to the high bound deflection limits, while the targets for the other sampling points still remain relatively close to the midpoint between the low and high bound limits. To match with the target values of the sampling points L1S3 and L3L1, the optimisation scheme is required to use more void structures that provide higher deflection, while fewer void structures for lower deflection are required in nearby voxels to match the targets in other sampling points. Evidently, even with the additional control over the beam structure, the conflicts between the target deflection profiles of different sampling points play significant roles in the performance of the optimisation scheme.

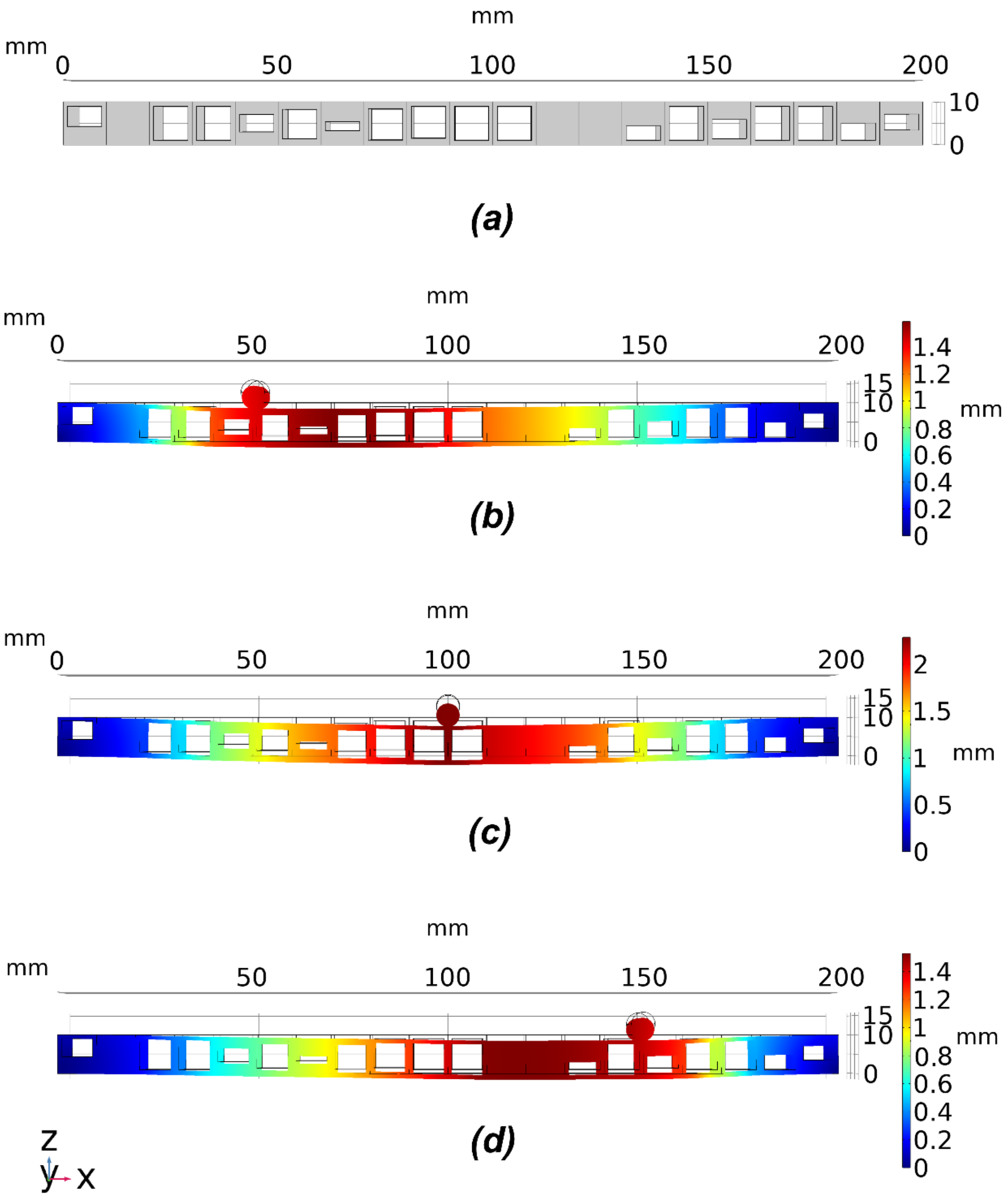

Figure 5.16. An example of the optimised 20 voxel asymmetric single void beam model for target set TS1. (a) the geometry of the optimised beam model and (b) to (d) is the deflection under loading conditions 1-3.

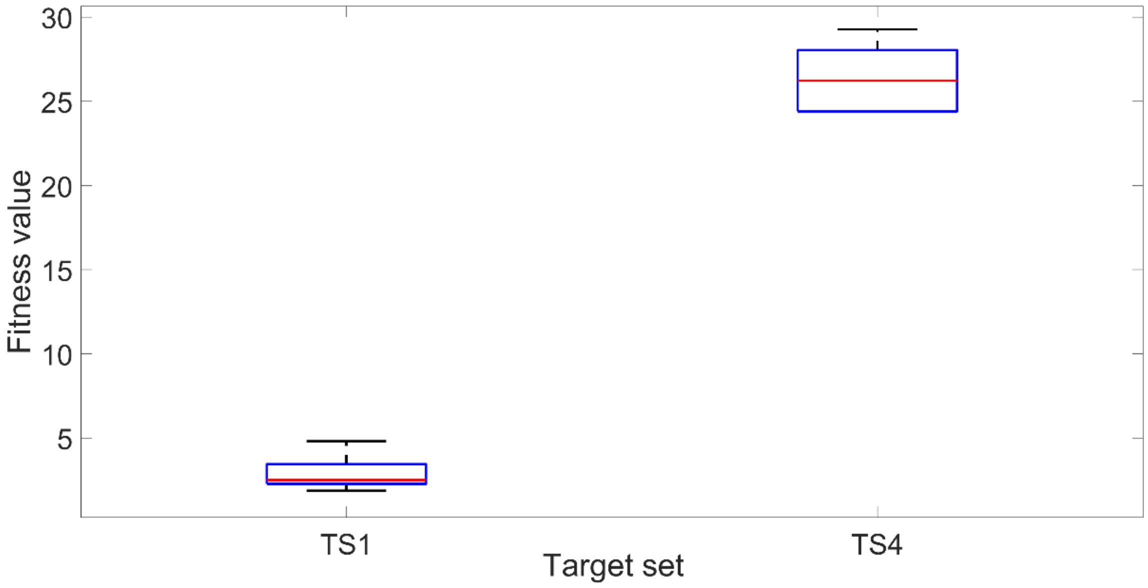

Figure 5.17. Comparison of fitness values for 20 voxel asymmetric single void beam model for target deflection sets TS1 and TS4. Each box plot represents the results of 5 trials for each target set. The lower the fitness value, the closer the obtained deflection sets were to the target deflection set. The solid red lines indicate the median fitness value, the top and bottom of the boxes represent the 25th and 75th percentiles.

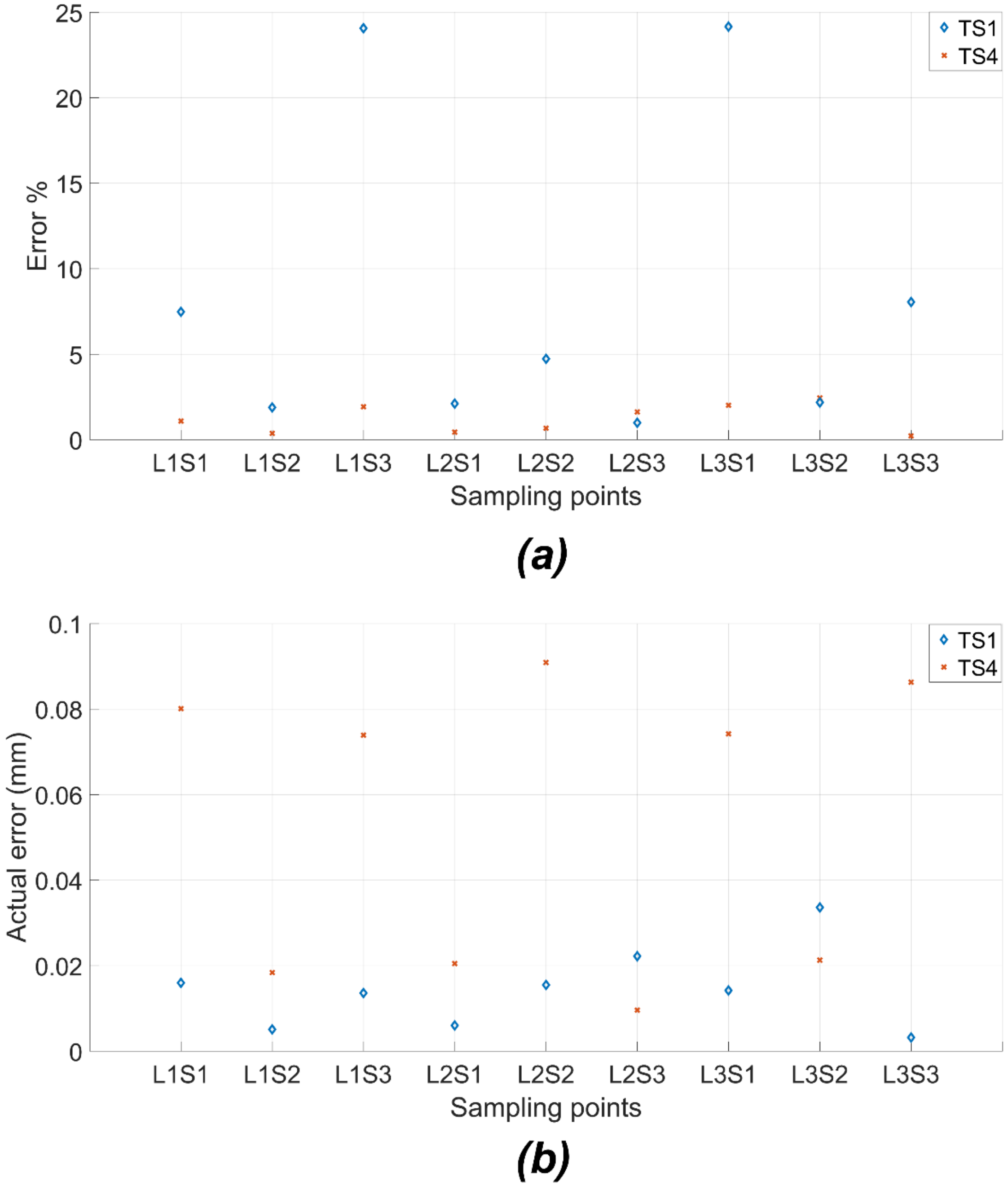

Figure 5.18. The mean of the differences between the deflection at nine sampling points and the corresponding target deflections for TS1 and TS4 in 20 voxel asymmetric single void beam model is expressed as (a) percentage and (b) actual difference in the deflection. Each data point corresponds to the mean value of 5 independent trials.

5.5.4. Additive manufacturing of optimised beam structures and three-point bending tests

The standard symmetric single void specimens are used in the experimental verification. All the specimens are printed using the CreatBot 3D printer (Model F430) using PLA filaments as the raw material. The parameters used in the FDM process are listed in Table 5.6. The printed samples are shown in Figure 5.19 and the beam loading setup is shown in Figure 5.20 and the result used in the verification is the average of three independent trails. Based on the three-point bending experiment results on the beams with solid, 20%, 40%, 60%, and 80% voids, the incremental void case, and the optimised 20 voxel single symmetric void beam for TSE1- TSE3, as shown in Figure 19 (a) to (f). The Young’s modulus is calibrated to 1600 Mpa for matching the actual experimental results performed on the FDM printed specimens. With different material properties, different target sets are used in the optimisation scheme for experimental verification, as listed in Table 5.7. The printed specimens optimised for TSE1 to TSE3 are shown in Figure 5.19 (g) to (j), respectively.

Table 5.6. The target deflection sets for symmetric single void 20 voxel beam with calibrated material properties

Unit (mm)	**L1S1**	**L1S2**	**L1S3**	**L2S1**	**L2S2**	**L2S3**	**L3S1**	**L3S2**	**L3S3**
Low bound	-1.06	-1.16	-0.54	-1.15	-1.869	-1.15	-0.54	-1.16	-1.06
High bound	-5.57	-5.04	-2.64	-5.03	-8.58	-5.03	-2.64	-5.04	-5.57
Midpoint	-3.31	-3.09	-1.59	3.08	-5.22	-3.09	-1.59	-3.09	-3.31

(TSE1)									
Midpoint+0.2mm (TSE2)	-3.11	-2.89	-1.39	-2.88	-5.02	-2.89	-1.39	-2.89	-3.11
Midpoint-0.2mm (TSE3)	-3.51	-3.29	-1.79	-3.28	-5.42	-3.29	-1.79	-3.29	-3.51

Table 5.7. The printing parameters used in the FDM process based on PLA filaments

Nozzle temperature (°C)	**Bed temperature (°C)**	**Printing speed (mm/s)**	**Layer Height (mm)**	**Nozzle diameter (mm)**	**Infill density (%)**
210	60	55	0.2mm	0.4	100

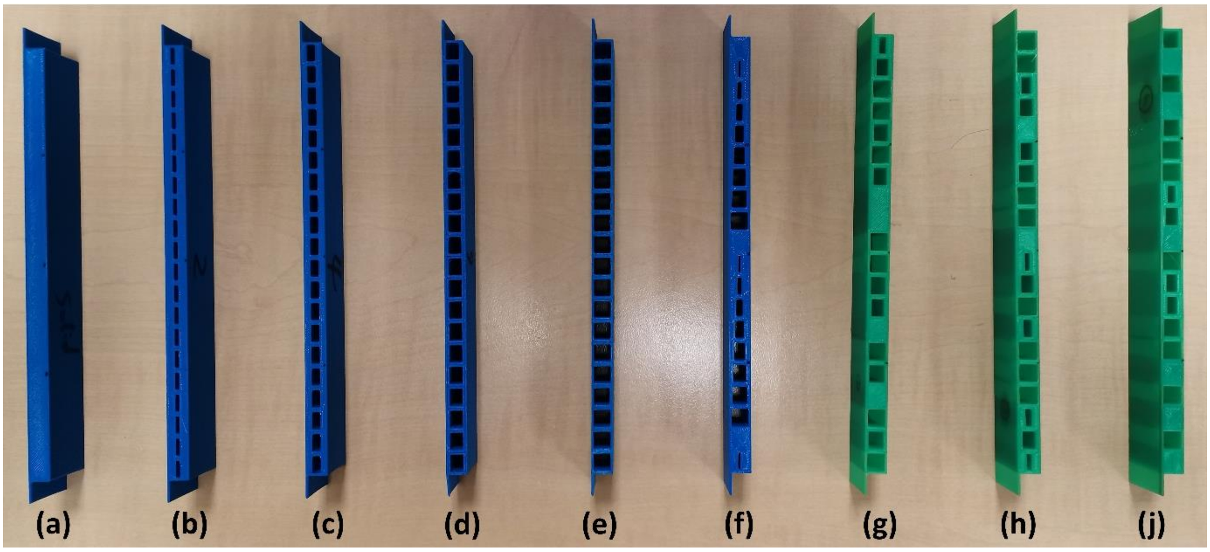

Figure 5.19. 3D printed samples (a) low bound 20 voxels single void beam; (b)-(e) 20 voxels single void beam with 20% 40% 60% and 80% void respectively; (f) 20 voxels single void beam with incremental void sizes; (g)-(j) optimised 20 voxels single symmetric void beam for TSE1-TSE3.

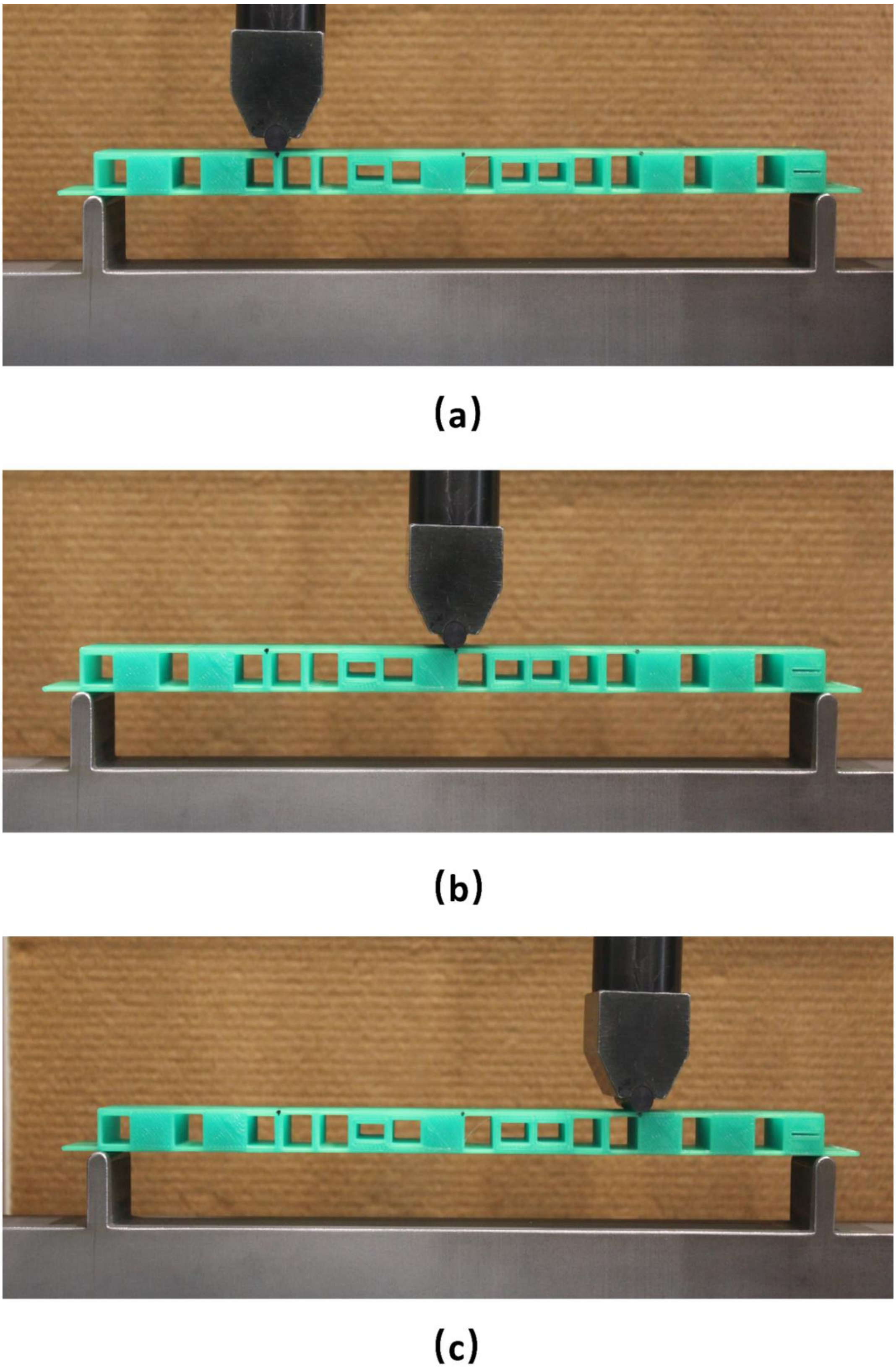

Figure 5.20. The loading setup in the three-point bending test; (a) to (c) indicate loading points 1 to 3

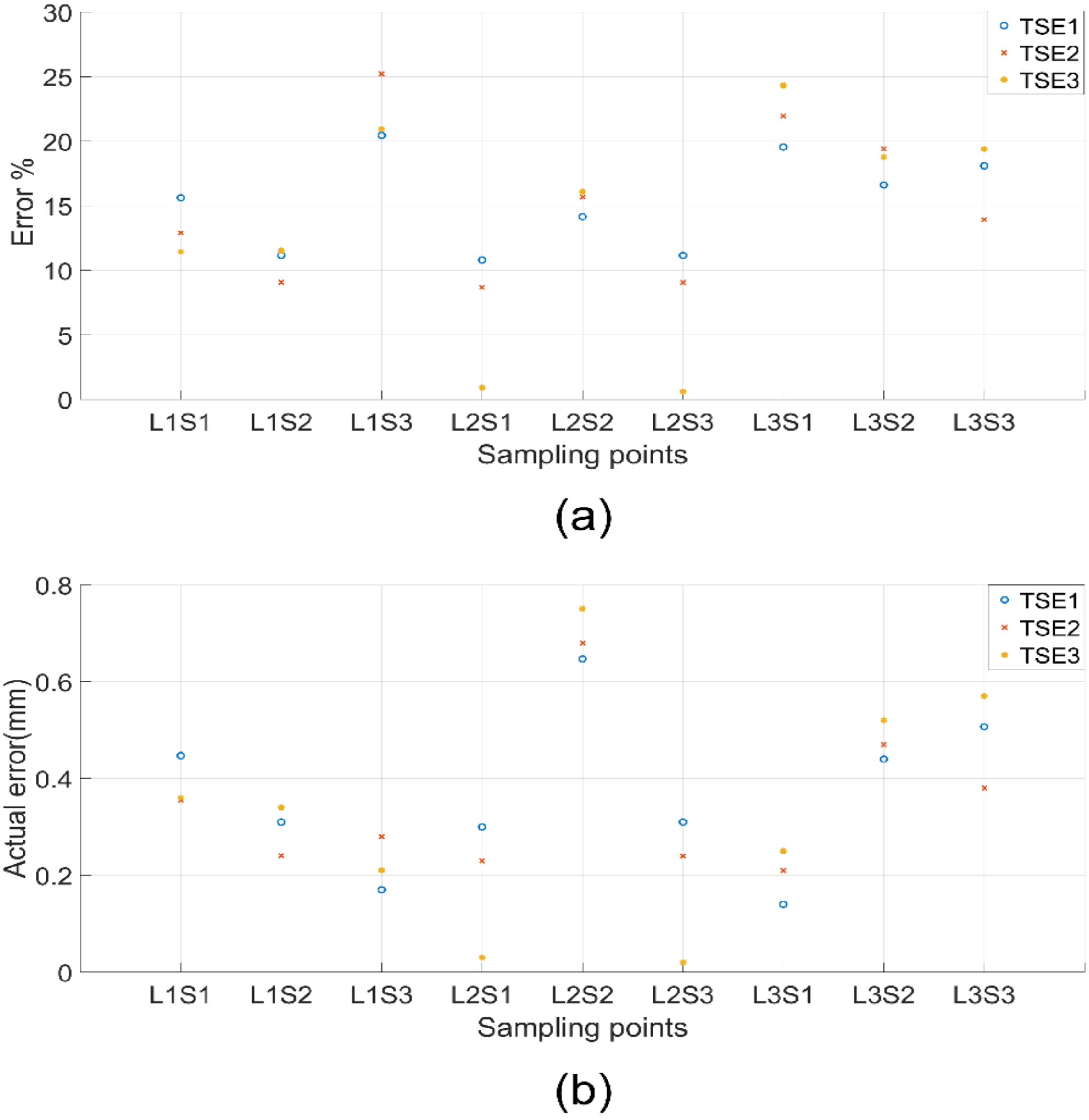

Figure 5.21. The percentage error (a) and the actual error (b) between the target set TSE1-TSE3 and the three-point bending test result of the printed specimen.

Figure 5.21 represents the deflection difference between the printed specimens optimised for TSE1 to TSE3 and the target sets. The overall results from the three-point bending tests confirm the proposed optimisation scheme can effectively alter the deflection profile to match with the selected target deflection sets. As shown in Figure 21, in most of the cases, the error is less than 20% and 0.6 mm. It is noticeable that the percentage error on L1S3 and L3S1 is relatively high. The main reason for this is that the deflection value in these sampling points are low (less than 2 mm). The large error may be caused by the FDM printing quality and the measurement error during the three-point bending test. Considering that the deflection value is small, the FDM printing quality and the possible experimentl errors, the overall result of the experimental verification is satisfactory.

5.6. Summary of Chapter 5

Functionally graded material property responses were achieved by means of computationally altered geometrical forms of voxelised cellular structural forms. The optimisation of geometries of individual cells and the overall responses of the structural continuum were evaluated considering the controlled deflection responses of a simply supported beam with a point load. Three load cases with three specific locations of importance each for deflection responses were considered in combinations to evaluate the effectiveness of the generative search algorithm to converge on the optimised cellular structure of the beam. The classical CMA-ES algorithm is used for the multi-objective optimisation together with the Comsol Multiphysics based finite element evaluations for exploring the generative design space.

Different sets of numerical experiments were conducted to evaluate the performance of the proposed cellular optimisation scheme to match the beam deflection responses at critical points with the designated target deflection sets. Three specific cellular geometries, single void symmetric, double void and single void asymmetric cellular forms, were used to achieve different levels of control over the range of variation of the properties within the continuum of a single material based beam structure. The scheme of controlled property variation achieved by varying the cellular geometries based on the optimisation using the CMA-ES algorithm together with the finite element evaluation worked well in achieving the overall objectives to control the deflection profiles of the single point load simply supported beams. The double void geometry was by far the best possible option to achieve an optimised beam structure with less than 5% maximum deviations between the predicted and target deflections at critical points.

The optimised structures were printed successfully using a relatively simple FDM system CreatBot Model F430 using PLA in filament form. Experimental verification of the results was only attempted in one case due to COVID restrictions, but there are many scopes to undertake a complete set of experimental validation trials in the future. The optimisation results are satisfactory, but the trends indicate that the more the voxels, the better the convergence on the target responses. Considering this, it is desirable to undertake evaluation using 40 and more voxels, but at the cost of excessively higher computations time and costs. Future research could also consider analysis with a finer voxelised structure based on better computational efficiency through the use of the most advanced technologies such as compute unified device architecture (CUDA) parallel computing (Nvida.com, 2022).

Chapter 6

Conclusion

6.1. Objectives and achievements

Controlled property variation through functional grading of materials has been studied comprehensively. Numerous experimental studies were conducted examining the possibility of varying the mechanical properties and obtaining the desired material performance attributes and behaviours in the fabricated objects. The research presented in this thesis further expands the understanding of the possibilities with functional grading of materials, dwelling deeper into the generative design methods needed to understand the multi-dimensional scenarios arising out of the possibility of seamlessly controlling the materiality in any fabricated part. Centred around the renewed functional material grading possibilities due to the advent of additive technologies, the overall objective is to explore the computational methods that can be used to realise the unlimited design opportunities possible through controlled material topologies.

Different approaches are used to evaluate the possibilities for accurately controlling the properties and behaviours of the design domain. Firstly, controlling the natural frequency responses by multi-material topology optimisation is investigated. A generative design method based on the binary GA is proposed and used to identify the optimal material distribution of a multi-material cantilever beam structure for the desired eigenfrequency responses. The GA optimisation scheme iteratively performs crossover and mutation on the genome representation and creates offspring for the next iterations. By evolving the offspring based on the fitness value, the GA optimisation schemes gradually evolved the genome representation or the material topology to the combination with better fitness value, which leads to the identification of the optimal material topology for the desired natural frequency responses. The GA based material optimisation schemes worked well, and the results are also compared with alternative optimisation algorithms NEAT and CPPN-NEAT, which demonstrated superior accuracy for matching multiple selected eigenfrequency sets. Multiple target sets with the first six evenly spaced eigenfrequencies could be evaluated and achieved based on the performance of the proposed optimisation schemes.

Based on the same optimisation scheme using GA, the topology optimisation problem for the maximisation of the toughness is also resolved. The results indicated that the proposed GA optimisation scheme is able to efficiently optimise the material dispersions for maximising both stress and strain by converging on the optimal distribution of selected soft and stiff materials. The optimised specimen showed a significant increment in toughness compared to specimens of uniform or randomly generated material distributions. It is also notable that the GA topological optimisation scheme used in toughness optimisation only had minimum changes in the fitness evaluation compared to the version used for frequency optimisation, which demonstrated the versatility of the proposed GA optimisation scheme. These studies focus on the optimisation of materiality for pre-set frequency responses and maximisation of toughness answered the overarching research question by demonstrating that the multi-material solution is able to achieve closely controlled material property variations within given product domains to match with the selected property responses.

Next, functional grading based on cellular structures with homogeneous materials is used to control the effective stiffness matrix and mass of each voxel in the discretised cantilever beam model, leading to the control over the overall eigenfrequency responses. The same target sets with the first six evenly spaced eigenfrequencies are used in evaluating the performance of the proposed cellular structure optimisation scheme. The CMA-ES optimisation scheme is used to search for the optimal cellular structure combination. Case studies for pre-loaded cases and different material settings are also investigated. Compared to the GA based multi-material solutions, the results showed that the CMA-ES scheme based on structural optimisation could provide equal or better performance in matching with the selected evenly spaced target frequency sets. The proposed homogeneous material solution demonstrated that the controlled variation of the macro geometries of each voxel in the problem domain could lead to the control over the material properties within specific pre-set ranges based on the structure printed using a single material. The frequency responses of the problem domain could be tailored to a set of selected natural frequencies for the first six degrees of freedom in both free and forced vibration cases.

The structural manipulation of the voxelised beam method was used next for the optimisation of the beam deflection behaviour. The CMA-ES optimisation scheme is used to search for the optimal cellular structure combination for the controlled deflection behaviour. By optimising the internal hollow structures, the deflection behaviour could be closely governed to match with the selected deflection profiles under multiple load conditions. Three load cases with three specific locations were considered in combinations to evaluate the effectiveness of the generative search algorithm to converge on the optimised cellular structure of the beam. The results showed that the beam with optimised cellular structure obtained deflection profiles closely matching the pre-set values under multiple load conditions. The optimised structures were printed successfully using a relatively simple FDM system CreatBot Model F430 using PLA in filament form.

Overall, the objective of closely controlling the properties and behaviours in the fabricated objects by using the multiple-material topology optimisation and the structural optimisation with uniform material approaches was achieved. The results showed satisfactory accuracy and efficiency levels in controlling the frequency responses and deflection profiles to match with multiple selected target sets under different conditions. The case study on improving the toughness property also demonstrated the versatility of the multi-material topology optimisation scheme. The outcomes of the research clearly indicated that the multi-material topology and the structural optimisation methods have the potential to control the materiality and return functional responses of printed objects.

6.2. Discussion and comparison of critical results

6.2.1. The multi-material solution for natural frequency responses

In the multi-material topological optimisation solution applied to control the natural frequency responses as elaborated in Chapter 3, seventeen target sets with the first six evenly spaced natural frequencies are used to examine the performance of the proposed GA optimisation scheme as listed in Table 3.1. Of all the cases, the target set starting with 10Hz first natural frequency and frequency gap of 50Hz obtained the best result. All of the first six eigenvalues are very close to the target frequency values, with the error levels at less than 1%.

The target set with 150Hz first natural frequency and frequency gap of 100Hz, which uses a higher frequency target with larger frequency gaps, obtained the worst result. As shown in Figure 3.7 (b) and Figure 3.8, the major source of error is the first natural frequency in the target set 3. It is because the target of the first frequency of target set 3 (150Hz) is close to the first natural frequency of the fully stiff material (183.64Hz), while for the 2nd to 6th natural frequencies, the target set (250Hz-650Hz) is far from the fully stiff material model (1134.6Hz-3557.4Hz). Due to this, the GA optimisation scheme tends to evolve the material distribution to match the 2nd to 6th eigenvalues during the optimisation, rendering a large error in the first natural frequency target in the target set 3. Overall, the multi-material solution with the GA optimisation scheme provided a close match for all 17 tested target sets, with an average error of less than 8%. Moreover, as documented previously in Section 3.5.4, three target sets are tested in the alternative methods NEAT and CPPN-NEAT. The GA optimisation scheme generated better or similar results in both average and absolute error for the three selected target sets. From the results examined, it is evident that the multi-material topological optimisation solution with the proposed GA optimisation scheme can accurately control the first six natural frequencies to match a wide range of specific evenly spaced target frequency sets with the errors at moderate levels.

6.2.2. Structured voxels for natural frequency responses

As per the schemes presented in Chapter 4, the cellular structural design based on a uniform material is used to control the frequency responses of an object. The beam example is used again as the design domain to control the frequency responses. Instead of optimising the soft and hard materials distribution, the optimisation of the cellular structure of the voxelised model is used to control the stiffness matrix and mass, which leads to the control of the overall frequency responses. The CMA-ES algorithm is used to handle the design variables, which are continually searching for the optimal structure of each voxel to match the desired frequency responses.

As listed in Table 4.1, three target sets are used. The overall results on the standard cantilever beam are satisfactory, except for the first natural frequency in target set 2, which results in a large error percentage. All other frequencies experienced errors at less than 8%. Target set 2 starts at 10 Hz, and the frequency gap is 50 Hz, which has a low first natural frequency and a relatively large frequency spacing. The large error in target set 2 may refer to the relatively small voxel numbers and structural limitations that cannot provide enough degrees of freedom to achieve the first natural frequency target of a set with a large frequency spacing. Next, in the proposed CMA-ES algorithm for frequency optimisation, two irregular geometries with irregular design regions, such as forced voids, are examined.

As evaluated in section 4.5.5, the optimised cellular structured irregular geometries have shown satisfactorily matching results with the target sets. For target set 1, the two irregular geometries obtained slightly lower errors. For target set 2 and target set 3, no significant differences can be observed. Similar to the standard regular geometry, the target set 2 still remains challenging in both irregular models. Moreover, as documented in Section 4.5.6, the pre-loading conditions and different material settings have been tested in regular and irregular models to further verify the performance and flexibility of the proposed method. Because of the varied testing conditions, as listed in Table 4.4, different target sets are used. Overall, the results are satisfactory for both regular and irregular beams under pre-loading conditions, as the maximum percentage error for all six target frequency modes is less than 6%, and significantly smaller error levels are obtained in many cases. This final test clearly proved that the CMA-ES optimisation scheme is able to efficiently handle pre-loaded beam cases with different geometries and material settings in matching with target frequency responses.

6.2.3. Multi-material vs structured voxel-based solutions for natural frequency responses

Based on the numerical experiments and results, both multi-material solutions and single material solutions are able to efficiently control the frequency responses of the design domain to match with the desired target frequency sets with satisfactory levels of accuracy. Multi-material solutions can expand the achievable frequency range without altering the geometry by using different materials. In comparison, the achievable frequency range for the single material cellular structural model is largely limited by the geometry. To match the natural frequency responses ranges as with the multi-material solutions, the structural variations require the need for varying thin layers in the geometry, which may go beyond the capabilities of even the additive manufacturing technologies.

However, in practice, MMAM solutions suffer from the lack of real engineering material options as the current systems are only able to offer digitally mixed acrylic polymer options consolidated by UV curing and the quality of the printed multi-material parts are usually unsuitable for producing functional parts. Whereas the specimens optimised by the uniform material solution can be fabricated using a well-tested single material additive manufacturing process, enabling a wide variety of material options from polymers to metal. Overall, both the multi-material topological optimisation and the cellular structural optimisation solution provided satisfactory results in matching the selected frequency sets, but both methods have their pros and cons when it comes to the final manufacturability of the structures of controlled materiality.

6.2.4. Multi-material optimisation for toughness

As detailed in section 3.6, the versatility of the GA based topology optimisation scheme was tested by successfully optimising the material distribution in a tensile test specimen for maximum toughness. The results showed that the GA based topological optimisation is capable of efficiently resolving the maximisation of other material property responses also. Compared with specimens of single or randomly generated material distributions, the specimens with the optimised material dispersion clearly demonstrated significantly higher stress and strain responses before fracture. Overall, the optimised model provided approximately four times and two times higher toughness values compared with all soft and hard material models, respectively. The versatility of the proposed multi-material optimisation scheme is demonstrated through handling different property optimisation tasks.

6.2.5. Single material structural optimisation for the desired beam deflection

A similar structural optimisation scheme is used to control the deflection profile of a beam with voxelised cellular structure, as detailed in Chapter 5. Instead of matching the target frequency sets, the CMA-ES scheme is tuned for matching the desired deflection profiles under different loading conditions by varying the structure of each voxel in the design domain. Two voxel settings, three cellular shapes and nine target sets are tested as listed in Table 5.3 to Table 5.5.

As discussed in section 5.5, the optimisation of the deflection profile of all three cellular structure variants provided close matches to the target deflection profiles. The maximum actual error is less than 0.1mm, considering all target sets and cellular structure settings, while much lower errors are obtained in many other cases. The optimised model received the highest fitness values for target sets TS4 and TS5, which attained the highest error levels. The majority of the errors are observed with the sampling points L1S3 and L3S1. For matching the target deflections corresponding to the sampling points L1S3 and L3S1 cases in TS4 and TS5, the optimisation scheme needs to create the largest void dimensions for obtaining the lowest overall stiffness of the structure, while the stiffness matrix of the beam structure is required to maintain higher stiffness for matching with the target deflection at other sampling points. This conflict between different sampling points is the main reason for the higher error in the trials TS4 and TS5. Moreover, the tests conducted on three different cellular structures with different design parameters indicated that the optimised beam is able to provide the deflections closely matching the selected deflection profiles with a maximum error of less than 10% and a much lower error in many cases. Evidently, the proposed CMA-ES cellular structure optimisation scheme can handle different cellular settings and efficiently identify the optimal cellular structures combinations for desired deflection profiles.

6.3. General conclusions

The multi-material functional grading method based on the binary GA identifying the optimal material distribution of a cantilever beam structure to achieve the material design for the desired natural frequency responses. This is tantamount to achieving the first research objective, proving that the design of a material dispersion arrangement with the controlled dispersion of two different materials selectively is able to confirm the responses of the component to a set of selected natural frequencies for the first six degrees of freedom. The extension of the method to improve the toughness performance by using the optimised material distribution demonstrated the potential use of the multi-material functional grading for optimising mechanical property responses also.

The second research objective that a single material cellular structure can be used to optimise the structural performance of a printed part conforming to a set of selected frequency responses was achieved through the optimisation of the voxelised beam structure using the CMA-ES algorithms. Further extension of this approach to the beam deflection problem is allowed to achieve the third research objective, proving that the optimisation of the cellular beam structures can lead to closely controlled beam deflection profiles. Overall, the optimisation schemes based on the use of genetic, CPPN, CPPN-NEAT, and CMA-ES algorithms integrated with the finite element analysis solutions by COMSOL Multiphysics allowed achieving all the objectives set for this research, and the results of the numerical experiments provided answers to the key research question raised.

6.4. Quantitative inferences and conclusions

The following key quantitative conclusions can be drawn from the results of the numerical experiments conducted in this research, pursuing the three key objectives set:

Multimaterial optimisation by GA, CPPN, and CPPN-NEAT for controlled natural frequencies

- Based on initial trials and fine-tuning, the parameter settings: population size 100, crossover percentage 0.6, mutation percentage 0.08, mutation rate 0.08 and the roulette wheel selection were identified to be the most effective for the optimisation scheme based on GA for controlled natural frequency responses.

- Seventeen target sets were tested by the multi-material optimisation solution for desired natural frequency responses. The average error in any of the target sets is below 8%.

- The multi-material optimisation solution based on GA was compared with the NEAT and CPPN-NEAT optimisation schemes for the optimisation of the natural frequency responses with three target sets. Compared with the NEAT, the GA optimisation scheme obtained 10% and 15% of the fitness values for the target set 1 and target set 2, while they are 30% and 20% of the fitness value for the target set 1 and target set 2 compared to CPPN-NEAT.

- In target set 3, the GA optimisation scheme obtained a similar performance as NEAT (p-value 0.058 in paired t-test) and better performance compared with CPPN-NEAT (p-value: 0.002 in paired t-test)

- The proposed multi-material optimisation solution is used in the optimisation to improve the toughness performance. The optimised dumbbell model obtained approximately four times more toughness value compared with the all soft material model and about two times more toughness value compared with the all stiff material model.

Single material structural optimisation by CMA-ES for pre-set frequency responses

- Three target sets of six evenly spaced target frequencies were tested in the standard regular beam using cellular structured optimisation. The average percentage error is less than 5% for the 2nd to the 6th target frequencies in all the target sets. And the mean of the actual error is less than 5 Hz in the 2nd to the 6th target frequencies for all target sets.

- Three target sets of evenly spaced six target frequencies were tested in two irregular beams using cellular structured optimisation. The average percentage error is less than 5% for the 2nd to the 6th target frequencies for all target sets.

- For target set TS 2 in the above case, the average actual error in the 1st target frequency is 16 Hz for irregular geometry A and 14 Hz for irregular geometry B. And the average actual error is less than 5 Hz in the 2nd to the 6th target frequencies for both irregular beams.

- One target set of evenly spaced target frequencies was tested in the standard regular beam and two irregular beams with pre-loading conditions using cellular structured optimisation. The average percentage error is less than 6% for all three geometries.

Single material structural optimisation by CMA-ES for controlled beam deflections

- Five target sets of selected deflection profiles were tested on the beam with standard single symmetric void voxels using cellular structured optimisation. For all five target sets, the average actual error in nine sampling points is less than 0.1mm. The average percentage error for sampling points L1S3 and L3S1 in the target set TS4 obtained higher errors which are approximately 28% for both. All other results obtained percentage errors less than 10%

- Two target sets of selected deflection profiles were tested on the beam with double void voxels using cellular structural optimisation. The mean percentage error was less than 6%, and the mean actual error was less than 0.06mm in any of the target sets.

- Two target sets of selected deflection profiles were tested on the beam with asymmetric single void voxels using cellular structured optimisation. The maximum difference between simulation results and target results is less than 10% or 0.08 mm in most cases. The result in sampling points L1S3 and L3S1 in the target set TS4 still received a higher error, around 24% for both sampling points.

6.5. Future course

The main research objective of this thesis is to expand the current functional grading solutions to accurately match the pre-set material attributes through multi-material topology optimisation or structural optimisation with uniform material. The optimisation targets based on natural frequency, deflection profile and toughness have been tested numerically. The numerical analysis provided satisfactory results for the optimisation targets. However, due to the Covid-19 disruptions, the access to the experimental facilities was heavily restricted. The actual experiments could not be done to validate the simulation results. The properties of the materials used in the numerical analysis were not verified in the printed model, which may have led to the differences between the numerical and the actual results.

For these results to be more accurate, detailed experimental plans involving the establishment of the mechanical properties of the base materials and evaluation of the structures printed as per the optimised geometries need to be undertaken. By establishing the true properties, as well as the systematic comparison of the numerical and experimental results, will allow to further fine-tune the optimisation schemes for more realistic and reliable predictions. Further, all the optimisation schemes were performed on the standard desktop computers, with limited computational power compared with high-performance computing servers. Techniques such as parallel computing and graphic card acceleration were restricted in the current desktop platforms available for use in the current numerical work. As a result, the numerical experiments are based on comparatively simple models considering the restrictions on the computational cost. With a high-performance computational platform, experiments on more complex geometries and larger voxel numbers can be undertaken. With a larger voxel number, the optimisation performance can be improved with increased degrees of freedom, especially for conflicting optimisation targets.

Considering these limitations, the future work in this research can consider first establishing the true properties of the constituent materials. Detailed experimental plans need to be developed for printing the optimised structures using different materials options and advanced printing technologies such as selective laser sintering and melting or electron beam melting. Appropriate methodologies and test setups need to be developed to experimentally establish the frequency responses of optimised beam structures. With the accessibility to the experimental facilities restoring to normalcy, the parameters of the computational model can be calibrated based on the actual data from the experiments, which will allow to further improve the optimisation performance and adapt the numerical model for better alignment with the physical results. More complex geometrical forms can be considered, such as triple or quadruple void cells in the place of double void cellular structures for better convergence, based on a high-performance computing platform.

References

Abueidda, D. W., Almasri, M., Ammourah, R., Ravaioli, U., Jasiuk, I. M., & Sobh, N. A. (2019). Prediction and optimization of mechanical properties of composites using convolutional neural networks. *Composite structures, 227*, 111264. https://doi.org/https://doi.org/10.1016/j.compstruct.2019.111264

Ahmad, M., Saeed, M., Saleem, S., & Kamboh, A. M. (2016). Seizure detection using EEG: A survey of different techniques*IEEE.* Symposium conducted at the meeting of the 2016 International Conference on Emerging Technologies (ICET)

Al-Assaf, Y., & Kadi, H. E. (2007). Fatigue life prediction of composite materials using polynomial classifiers and recurrent neural networks. *Composite structures, 77*(4), 561-569. https://doi.org/https://doi.org/10.1016/j.compstruct.2005.08.012

Al-Obaidi, A. J., Ahmed, S. J., & Sukar, H. M. (2020). The effect of factors on the flexural of the composite leaf spring. *Materials today: proceedings, 20*, 566-571. https://doi.org/https://doi.org/10.1016/j.matpr.2019.09.190

Almeida, F. S., & Awruch, A. (2009). Design optimization of composite laminated structures using genetic algorithms and finite element analysis. *Composite structures, 88*(3), 443-454.

Almer, J. (2017). Engineering Materials. *Synchrotron Radiation News, 30*(3), 2-3. https://doi.org/10.1080/08940886.2017.1316123

ANSYS. (2019). *Structural analysis for every application and experience level* Retrieved 04/03, 2019, from https://www.ansys.com/products/structures

Ashby, M. F., & Bréchet, Y. J. M. (2003). Designing hybrid materials. *Acta Materialia, 51*(19), 5801-5821. https://doi.org/https://doi.org/10.1016/S1359-6454(03)00441-5

Ashby, M. F., & Jones, D. R. (2012). *Engineering materials 1: an introduction to properties, applications and design* (Vol. 1): Elsevier.

ASTM. (2022). Designation: D638 − 14 *Standard Test Method for Tensile Properties of Plastics*. US: ASTM International.

Beer, F., Johnston, E., & DeWolf, J. (1999). Mechanics of materials, 5th SI Edition. *Stress, 1*(10), 1.12.

Bendsøe, M. P. (1989). Optimal shape design as a material distribution problem. *Structural optimization, 1*(4), 193-202.

Bendsøe, M. P., Ben-Tal, A., & Zowe, J. (1994). Optimization methods for truss geometry and topology design. *Structural optimization, 7*(3), 141-159.

Betters, E. D., West, J., Noakes, M., Nycz, A., Smith, S., & Schmitz, T. L. (2020). Dynamic stiffness modification by internal features in additive manufacturing. *Precision Engineering, 66*, 125-134. https://doi.org/https://doi.org/10.1016/j.precisioneng.2020.04.024

Bickel, B., Bächer, M., Otaduy, M. A., Lee, H. R., Pfister, H., Gross, M., & Matusik, W. (2010). Design and fabrication of materials with desired deformation behavior*ACM.* Symposium conducted at the meeting of the ACM Transactions on Graphics (TOG)

Boschetto, A., & Bottini, L. (2014). Accuracy prediction in fused deposition modeling. *The international journal of advanced manufacturing technology, 73*(5-8), 913-928.

Brackett, D., Ashcroft, I., & Hague, R. (2011). Topology optimization for additive manufacturing*S.* Symposium conducted at the meeting of the Proceedings of the solid freeform fabrication symposium, Austin, TX

Buchanan, M. (2019). Going into resonance. *Nature Physics, 15*(3), 203-204. https://doi.org/10.1038/s41567-019-0458-z

Budinski, K. G., & Budinski, M. K. (2009). *Engineering materials* (Vol. 25)

Cao, L., Dolovich, A. T., & Zhang, W. (2015). Hybrid Compliant Mechanism Design Using a Mixed Mesh of Flexure Hinge Elements and Beam Elements Through Topology Optimization. *Journal of Mechanical Design, 137*(9). https://doi.org/10.1115/1.4030990

Cardenas, A. M., Rázuri, J. G., Sundgren, D., & Rahmani, R. (2013). Autonomous motion of mobile robot using fuzzy-neural networks*IEEE.* Symposium conducted at the meeting of the 2013 12th Mexican International Conference on Artificial Intelligence

Chapman, C. D., Saitou, K., & Jakiela, M. J. (1994). Genetic algorithms as an approach to configuration and topology design. *Journal of mechanical design, 116*(4), 1005-1012.

Chawla, K. K. (2013). *Ceramic matrix composites*: Springer Science & Business Media.

Cheney, N., Ritz, E., & Lipson, H. (2014). Automated vibrational design and natural frequency tuning of multi-material structures Symposium conducted at the meeting of the Proceedings of the 2014 Annual Conference on Genetic and Evolutionary Computation

Chipperfield, A., Fleming, P., Pohlheim, H., & Fonseca, C. (1994a). Genetic algorithm toolbox for use with MATLAB.

Chipperfield, A., Fleming, P., Pohlheim, H., & Fonseca, C. (1994b). *Genetic algorithm toolbox for use with MATLAB*. Retrieved 10/10, 2020, from http://citeseerx.ist.psu.edu/viewdoc/summary?doi=10.1.1.16.1178

Chu, S., Xiao, M., Gao, L., Li, H., Zhang, J., & Zhang, X. (2019). Topology optimization of multi-material structures with graded interfaces. *Computer methods in applied mechanics and engineering, 346*, 1096-1117. https://doi.org/https://doi.org/10.1016/j.cma.2018.09.040

COMSOL. (2017, 21/02/2017). *The Finite Element Method (FEM)*. Retrieved 17/03, 2022, from https://www.comsol.com/multiphysics/finite-element-method

COMSOL. (2019). *Finite Element Analysis (FEA) Software*. Retrieved 04/03, 2019, from https://www.comsol.com/multiphysics/fea-software

COMSOL. (2021). *Plasticity Model*. Retrieved 15/04, 2022, from https://doc.comsol.com/5.5/doc/com.comsol.help.sme/sme_ug_solid.07.15.html

Crowell, B. (2020). *Conceptual Physics* (1 ed.). California US: LibreText. Retrieved from https://phys.libretexts.org/Bookshelves/Conceptual_Physics/Book%3A_Conceptual_Physics_(Crowell)/04%3A_Conservation_of_Momentum/4.03%3A_Resonance

Ćurković, P. (2021). Optimization of Generatively Encoded Multi-Material Lattice Structures for Desired Deformation Behavior. *Symmetry, 13*(2), 293.

Da, D., & Qian, X. (2020). Fracture resistance design through biomimicry and topology optimization. *Extreme Mechanics Letters, 40*, 100890. https://doi.org/https://doi.org/10.1016/j.eml.2020.100890

Da, D., Yvonnet, J., Xia, L., & Li, G. (2018). Topology optimization of particle‐matrix composites for optimal fracture resistance taking into account interfacial damage. *International Journal for Numerical Methods in Engineering, 115*(5), 604-626.

de la Villa Jaén, A., García‐Santana, A., & Montoya‐Andrade, D. E. (2014). Maximizing output power of linear generators for wave energy conversion. *International Transactions on Electrical Energy Systems, 24*(6), 875-890.

Deaton, J. D., & Grandhi, R. V. (2014). A survey of structural and multidisciplinary continuum topology optimization: post 2000. *Structural and Multidisciplinary*

Optimization, 49(1), 1-38. Deaton2014. https://doi.org/10.1007/s00158-013-0956-z

Delfosse, D. (1998). Fundamentals of Functionally Graded Materials| S. Suresh and A. Mortensen IOM Communications Ltd, 1998 ISBN: 1-86125-063-0: Elsevier.

DeMario, A., & Zhao, J. (2017). A miniature, 3d-printed, walking robot with soft joints*American Society of Mechanical Engineers.* Symposium conducted at the meeting of the International Design Engineering Technical Conferences and Computers and Information in Engineering Conference

DeMario, A., & Zhao, J. (2018). Development and analysis of a three-dimensional printed miniature walking robot with soft joints and links. *Journal of Mechanisms and Robotics, 10*(4).

Do, D. T. T., Lee, D., & Lee, J. (2019). Material optimization of functionally graded plates using deep neural network and modified symbiotic organisms search for eigenvalue problems. *Composites Part B: Engineering, 159*, 300-326. https://doi.org/https://doi.org/10.1016/j.compositesb.2018.09.087

Du, J., & Olhoff, N. (2007). Topological design of freely vibrating continuum structures for maximum values of simple and multiple eigenfrequencies and frequency gaps. *Structural and Multidisciplinary Optimization, 34*(2), 91-110. Du2007. https://doi.org/10.1007/s00158-007-0101-y

EOS. (2021). *PA 1101 - Polyamide 11 White* Retrieved 09/09, 2021, from https://www.eos.info/en/additive-manufacturing/3d-printing-plastic/sls-polymer-materials/pa-11-nylon-abs-pa6

Evins, R., Vaidyanathan, R., & Burgess, S. (2014). Multi-material Compositional Pattern-Producing Networks for Form Optimisation*Springer Berlin Heidelberg.* Berlin, Heidelberg. Abstract retrieved from 10.1007/978-3-662-45523-4_16

Fang, T., Zhou, Y., Li, S., Xu, M., Liang, H., Li, W., & Zhang, S. (2016). Theoretical and experimental study on a compliant flipper-leg during terrestrial locomotion. *Bioinspiration & biomimetics, 11*(5), 056005.

Fischer, T., & Herr, C. M. (2001). Teaching generative design*Generative Design Lab, DiAP, Politechnico di Milano University.* Symposium conducted at the meeting of the The Proceedings of the Fourth International Conference on Generative Art 2001, Milan, Italy.

Fujii, G., & Akimoto, Y. (2019). Topology-optimized thermal carpet cloak expressed by an immersed-boundary level-set method via a covariance matrix adaptation evolution strategy. *International Journal of Heat and Mass Transfer, 137*, 1312-1322.

Fujii, G., Takahashi, M., & Akimoto, Y. (2018). CMA-ES-based structural topology optimization using a level set boundary expression—Application to optical and carpet cloaks. *Computer methods in applied mechanics and engineering, 332*, 624-643.

Fuller, C., Baker, W., & Pape, N. (1940). Crystalline behavior of linear polyamides. Effect of heat treatment. *Journal of the American Chemical Society, 62*(12), 3275-3281.

Gadhvi, B., Savsani, V., & Patel, V. (2016). Multi-objective optimization of vehicle passive suspension system using NSGA-II, SPEA2 and PESA-II. *Procedia Technology, 23*, 361-368.

Gao, F., Liu, G., & Liao, W.-H. (2020). Optimization Algorithm-Based Approach for Modelling Large Deflection of Cantilever Beam Subjected to Tip Load. *arXiv preprint arXiv:2010.16185*.

Gao, W., Zhang, Y., Ramanujan, D., Ramani, K., Chen, Y., Williams, C. B., . . . Zavattieri, P. D. (2015). The status, challenges, and future of additive manufacturing in engineering. *Computer-Aided Design, 69*, 65-89.

Ghabraie, K. (2015). An improved soft-kill BESO algorithm for optimal distribution of single or multiple material phases. *Structural and Multidisciplinary Optimization, 52*(4), 773-790. https://doi.org/10.1007/s00158-015-1268-2

Gholizadeh, S., & Barzegar, A. (2013). Shape optimization of structures for frequency constraints by sequential harmony search algorithm. *Engineering Optimization, 45*(6), 627-646.

Gibson, I., Rosen, D., & Stucker, B. (2015a). Directed Energy Deposition Processes [Gibson2015]. In *Additive Manufacturing Technologies: 3D Printing, Rapid Prototyping, and Direct Digital Manufacturing* (pp. 272-288). New York, NY: Springer New York. Retrieved from https://doi.org/10.1007/978-1-4939-2113-3_10. https://doi.org/10.1007/978-1-4939-2113-3_10

Gibson, I., Rosen, D., & Stucker, B. (2015b). Directed Energy Deposition Processes [Gibson2015]. In *Additive Manufacturing Technologies: 3D Printing, Rapid Prototyping, and Direct Digital Manufacturing* (pp. 245-268). New York, NY: Springer New York. Retrieved from https://doi.org/10.1007/978-1-4939-2113-3_10. https://doi.org/10.1007/978-1-4939-2113-3_10

Goldberg, D. E., & Holland, J. H. (1988). Genetic algorithms and machine learning. *Machine learning, 3*(2), 95-99.

Gopalakrishnan, K., Khaitan, S. K., Choudhary, A., & Agrawal, A. (2017). Deep Convolutional Neural Networks with transfer learning for computer vision-based data-driven pavement distress detection. *Construction and Building Materials, 157*, 322-330. https://doi.org/https://doi.org/10.1016/j.conbuildmat.2017.09.110

Gregory, M. D., Wang, X., & Werner, D. H. (2011). Flexible design of doubly periodic frequency selective surfaces with a prismatic mesh based FEBI simulation tool and CMA-ES*IEEE.* Symposium conducted at the meeting of the 2011 IEEE International Symposium on Antennas and Propagation (APSURSI)

Gu, G. X., Chen, C.-T., & Buehler, M. J. (2018). De novo composite design based on machine learning algorithm. *Extreme Mechanics Letters, 18*, 19-28. https://doi.org/https://doi.org/10.1016/j.eml.2017.10.001

Gu, G. X., Chen, C.-T., Richmond, D. J., & Buehler, M. J. (2018). Bioinspired hierarchical composite design using machine learning: simulation, additive manufacturing, and experiment. *Materials Horizons, 5*(5), 939-945.

Gu, G. X., Dimas, L., Qin, Z., & Buehler, M. J. (2016). Optimization of Composite Fracture Properties: Method, Validation, and Applications. *Journal of Applied Mechanics, 83*(7). https://doi.org/10.1115/1.4033381

Gurugubelli, S., & Kallepalli, D. (2014). Weight and deflection optimization of Cantilever Beam using a modified Non-Dominated sorting Genetic Algorithm. *IOSR Journal of Engineering, 4*(3), 19-23.

Hansen, M. (2003). Improved modal dynamics of wind turbines to avoid stall - induced vibrations. *Wind Energy: An International Journal for Progress and Applications in Wind Power Conversion Technology, 6*(2), 179-195.

Hansen, N., Müller, S. D., & Koumoutsakos, P. (2003). Reducing the time complexity of the derandomized evolution strategy with covariance matrix adaptation (CMA-ES). *Evolutionary computation, 11*(1), 1-18.

Hansen, N., & Ostermeier, A. (2001). Completely derandomized self-adaptation in evolution strategies. *Evolutionary computation, 9*(2), 159-195.

Hao, G., Li, H., Nayak, A., & Caro, S. (2018). Design of a compliant gripper with multimode jaws. *Journal of Mechanisms and Robotics, 10*(3), 031005.

Hašan, M., Fuchs, M., Matusik, W., Pfister, H., & Rusinkiewicz, S. (2010). Physical reproduction of materials with specified subsurface scattering*ACM.* Symposium conducted at the meeting of the ACM Transactions on Graphics (TOG)

Hepher, T. (2020). *Exclusive: Software under scrutiny in Airbus A220 engine failures*. Retrieved 03/03, 2021, from https://www.reuters.com/article/us-airbus-a220-exclusive-idUSKBN1X31ST

Her, I., & Midha, A. (1987). A compliance number concept for compliant mechanisms, and type synthesis.

Heris, M. K. (2015). *Binary and Real-Coded Genetic Algorithms in MATLAB*. Retrieved 06/07, 2018, from http://yarpiz.com/23/ypea101-genetic-algorithms

Heris, S. M. K. (2015). *CMA-ES in MATLAB*. Retrieved 09/10, 2020, from https://yarpiz.com/235/ypea108-cma-es

Hiller, J., & Lipson, H. (2009). Multi material topological optimization of structures and mechanisms*ACM.* Symposium conducted at the meeting of the Proceedings of the 11th Annual conference on Genetic and evolutionary computation

Hiller, J., & Lipson, H. (2010). Tunable digital material properties for 3D voxel printers. *Rapid Prototyping Journal*(4), 241. https://doi.org/10.1108/13552541011049252

Hiller, J., & Lipson, H. (2012). Automatic design and manufacture of soft robots. *IEEE Transactions on Robotics, 28*(2), 457-466.

Hiller, J. D., & Lipson, H. (2009). Multi material topological optimization of structures and mechanisms*ACM.* Symposium conducted at the meeting of the Proceedings of the 11th Annual conference on Genetic and evolutionary computation

Hoang, N., Fujino, Y., & Warnitchai, P. (2008). Optimal tuned mass damper for seismic applications and practical design formulas. *Engineering Structures, 30*(3), 707-715.

Howell, L. L. (2013). Compliant mechanisms. In *21st century kinematics* (pp. 189-216): Springer.

Hu, L., Feng, P., Meng, Y., & Yang, J. (2021). Buckling behavior analysis of prestressed CFRP-reinforced steel columns via FEM and ANN. *Engineering Structures, 245*, 112853. https://doi.org/https://doi.org/10.1016/j.engstruct.2021.112853

Huang, X., & Xie, Y. (2010). Evolutionary topology optimization of continuum structures with an additional displacement constraint. *Structural and Multidisciplinary Optimization, 40*(1-6), 409.

Huang, X., & Xie, Y. M. (2007). Convergent and mesh-independent solutions for the bi-directional evolutionary structural optimization method. *Finite Elements in Analysis and Design, 43*(14), 1039-1049. https://doi.org/https://doi.org/10.1016/j.finel.2007.06.006

Huang, X., & Xie, Y. M. (2008). A new look at ESO and BESO optimization methods. *Structural and Multidisciplinary Optimization, 35*(1), 89-92. Huang2008. https://doi.org/10.1007/s00158-007-0140-4

Huang, X., Zuo, Z. H., & Xie, Y. M. (2010). Evolutionary topological optimization of vibrating continuum structures for natural frequencies. *Computers & structures, 88*(5), 357-364. https://doi.org/https://doi.org/10.1016/j.compstruc.2009.11.011

Jain, A. K., Mao, J., & Mohiuddin, K. (1996). Artificial neural networks: A tutorial. *Computer*(3), 31-44.

Jakiela, M. J., Chapman, C., Duda, J., Adewuya, A., & Saitou, K. (2000). Continuum structural topology design with genetic algorithms. *Computer methods in applied mechanics and engineering, 186*(2-4), 339-356.

Jin, Y. (2005). A comprehensive survey of fitness approximation in evolutionary computation. *Soft computing, 9*(1), 3-12.

Jonathan, H., & Hod, L. (2010). Tunable digital material properties for 3D voxel printers. *Rapid Prototyping Journal*(4), 241. https://doi.org/10.1108/13552541011049252

Jung, G.-P., Choi, H.-C., & Cho, K.-J. (2017). The effect of leg compliance in multi-directional jumping of a flea-inspired mechanism. *Bioinspiration & biomimetics, 12*(2), 026006.

Kandemir, V., Dogan, O., & Yaman, U. (2018). Topology optimization of 2.5D parts using the SIMP method with a variable thickness approach. *Procedia Manufacturing, 17*, 29-36. https://doi.org/https://doi.org/10.1016/j.promfg.2018.10.009

Kasabov, N. K. (1996). *Foundations of neural networks, fuzzy systems, and knowledge engineering*: Marcel Alencar.

Kawamura, H., Ohmori, H., & Kito, N. (2002). Truss topology optimization by a modified genetic algorithm. *Structural and Multidisciplinary Optimization, 23*(6), 467-473. https://doi.org/10.1007/s00158-002-0208-0

Kaynia, A. M., Biggs, J. M., & Veneziano, D. (1981). Seismic effectiveness of tuned mass dampers. *Journal of the Structural Division, 107*(8), 1465-1484.

Kern, S., Hansen, N., & Koumoutsakos, P. (2006). Local meta-models for optimization using evolution strategies. In *Parallel Problem Solving from Nature-PPSN IX* (pp. 939-948): Springer.

Kim, T., Kwon, O.-S., & Song, J. (2019). Response prediction of nonlinear hysteretic systems by deep neural networks. *Neural Networks, 111*, 1-10. https://doi.org/https://doi.org/10.1016/j.neunet.2018.12.005

Kong, Y. L., Tamargo, I. A., Kim, H., Johnson, B. N., Gupta, M. K., Koh, T.-W., . . . McAlpine, M. C. (2014). 3D printed quantum dot light-emitting diodes. *Nano letters, 14*(12), 7017-7023.

Koprinkova-Hristova, P., Mladenov, V., & Kasabov, N. K. (2014). *Artificial neural networks: methods and applications in bio-/neuroinformatics* (Vol. 4): Springer.

Krishna, L. S. R., Mahesh, N., & Sateesh, N. (2017). Topology optimization using solid isotropic material with penalization technique for additive manufacturing. *Materials Today: Proceedings, 4*(2), 1414-1422.

Kumar, S., & Kruth, J.-P. (2010). Composites by rapid prototyping technology. *Materials & Design, 31*(2), 850-856.

Launey, M. E., Buehler, M. J., & Ritchie, R. O. (2010). On the mechanistic origins of toughness in bone. *Annual review of materials research, 40*, 25-53.

Lee, S., Ha, J., Zokhirova, M., Moon, H., & Lee, J. (2018). Background Information of Deep Learning for Structural Engineering. *Archives of Computational Methods in Engineering, 25*(1), 121-129. https://doi.org/10.1007/s11831-017-9237-0

Lee, S., Kim, H., Lieu, Q. X., & Lee, J. (2020). CNN-based image recognition for topology optimization. *Knowledge-Based Systems, 198*, 105887. https://doi.org/https://doi.org/10.1016/j.knosys.2020.105887

Li, K., Yu, Y., He, J., & Lin, Y. (2018). An integrated beam-plate structure multi-level optimal design framework based on bi-directional evolutionary structural optimization and surrogate model. *Advances in Engineering Software, 115*, 230-247. https://doi.org/https://doi.org/10.1016/j.advengsoft.2017.09.011

Ling, M., Howell, L. L., Cao, J., & Chen, G. (2020). Kinetostatic and dynamic modeling of flexure-based compliant mechanisms: a survey. *Applied Mechanics Reviews, 72*(3), 030802.

Liu, X., Yan, Z., & Zhong, Z. (2021). Predicting elastic modulus of porous La0.6Sr0.4Co0.2Fe0.8O3-δ cathodes from microstructures via FEM and deep learning. *International Journal of Hydrogen Energy, 46*(42), 22079-22091. https://doi.org/https://doi.org/10.1016/j.ijhydene.2021.04.033

Liu, Y., Cai, Y., Zhang, Y., Tovstopyat, A., Liu, S., & Sun, C. (2020). Materials, Design, and Characteristics of Bulk Acoustic Wave Resonator: A Review. *Micromachines, 11*(7), 630.

Loshchilov, I., & Hutter, F. (2016). CMA-ES for hyperparameter optimization of deep neural networks. *arXiv preprint arXiv:1604.07269*.

Loshchilov, I., Schoenauer, M., & Sebag, M. (2012). Self-adaptive surrogate-assisted covariance matrix adaptation evolution strategy Symposium conducted at the meeting of the Proceedings of the 14th annual conference on Genetic and evolutionary computation

Loshchilov, I., Schoenauer, M., & Sèbag, M. (2013). *Bi-population CMA-ES agorithms with surrogate models and line searches*. presented at the meeting of the Proceedings of the 15th annual conference companion on Genetic and evolutionary computation, Amsterdam, The Netherlands. Retrieved from https://doi.org/10.1145/2464576.2482696

Lyons, B. (2014). Additive manufacturing in aerospace: Examples and research outlook. *The Bridge, 44*(3).

Mahfouf, M., Chen, M., & Linkens, D. (2005). MULTI-OBJECTIVE PARTICLE SWARM OPTIMISATION FOR ALLOY TOUGHNESS DESIGN USING A FUZZY PREDICTIVE MODEL. *IFAC Proceedings Volumes, 38*(1), 211-216.

Menig, R., Meyers, M., Meyers, M., & Vecchio, K. (2000). Quasi-static and dynamic mechanical response of Haliotis rufescens (abalone) shells. *Acta Materialia, 48*(9), 2383-2398.

Meshram, N. A., & Pawar, V. S. (2015). Analysis of crack detection of a cantilever beam using finite element analysis. *International Journal of Engineering Research & Technology, 4*(04).

Ming, L., Hai, H., Aimin, Z., Yingde, S., Zhao, L., & Xingguo, Z. (2012). Modeling of mechanical properties of as-cast Mg-Li-Al alloys based on PSO-BP algorithm. *China Foundry, 9*(2).

Mohammed, M., Tatineni, J., Cadd, B., Peart, P., & Gibson, I. (2016). Applications of 3D topography scanning and multi-material additive manufacturing for facial prosthesis development and production Symposium conducted at the meeting of the Proceedings of the 27th Annual International Solid Freeform Fabrication Symposium

Momeni, F., Liu, X., & Ni, J. (2017). A review of 4D printing. *Materials & design, 122*, 42-79.

Mueller, B. (2012). Additive manufacturing technologies–Rapid prototyping to direct digital manufacturing. *Assembly Automation, 32*(2).

Naik, G. N., Gopalakrishnan, S., & Ganguli, R. (2008). Design optimization of composites using genetic algorithms and failure mechanism based failure criterion. *Composite structures, 83*(4), 354-367.

Ngo, T. D., Kashani, A., Imbalzano, G., Nguyen, K. T., & Hui, D. (2018). Additive manufacturing (3D printing): A review of materials, methods, applications and challenges. *Composites Part B: Engineering, 143*, 172-196.

Nguyen, T., Kashani, A., Ngo, T., & Bordas, S. (2019). Deep neural network with high-order neuron for the prediction of foamed concrete strength. *Computer-Aided Civil and Infrastructure Engineering, 34*(4), 316-332. https://doi.org/https://doi.org/10.1111/mice.12422

Nvida.com. (2022, 19/04). *CUDA Toolkit*. Retrieved 19/04, 2022, from https://developer.nvidia.com/cuda-toolkit

Osiander, R., Darrin, M. A. G., & Champion, J. L. (2018). *MEMS and microstructures in aerospace applications*. NY, US: CRC press.

Pais, A., Alves, J. L., & Belinha, J. (2021). Design of functionally graded gyroid foams using optimization algorithms and the finite element method. *The International*

Journal of Advanced Manufacturing Technology, 114(3), 725-739. https://doi.org/10.1007/s00170-020-06542-w

Palermo, E. (2013, September 19, 2013). *Fused Deposition Modeling: Most Common 3D Printing Method*. Retrieved 25/02, 2019, from https://www.livescience.com/39810-fused-deposition-modeling.html

Petković, D., Pavlović, N. D., Shamshirband, S., & Anuar, N. B. (2013). Development of a new type of passively adaptive compliant gripper. *Industrial Robot: An International Journal*.

Phatak, A. M., & Pande, S. (2012). Optimum part orientation in rapid prototyping using genetic algorithm. *Journal of manufacturing systems, 31*(4), 395-402.

Picelli, R., Vicente, W., Pavanello, R., & Xie, Y. (2015). Evolutionary topology optimization for natural frequency maximization problems considering acoustic–structure interaction. *Finite Elements in Analysis and Design, 106*, 56-64.

Pohtongkam, S., & Srinonchat, J. (2016). Object recognition from human tactile image using artificial neural network*IEEE.* Symposium conducted at the meeting of the 2016 13th International Conference on Electrical Engineering/Electronics, Computer, Telecommunications and Information Technology (ECTI-CON)

Poli, R. (2008). Analysis of the publications on the applications of particle swarm optimisation. *Journal of Artificial Evolution and Applications, 2008*.

Poli, R., Kennedy, J., & Blackwell, T. (2007). Particle swarm optimization. *Swarm intelligence, 1*(1), 33-57.

Querin, O., Young, V., Steven, G., & Xie, Y. (2000). Computational efficiency and validation of bi-directional evolutionary structural optimisation. *Computer methods in applied mechanics and engineering, 189*(2), 559-573.

Rao, C., & Liu, Y. (2020). Three-dimensional convolutional neural network (3D-CNN) for heterogeneous material homogenization. *Computational Materials Science, 184*, 109850. https://doi.org/https://doi.org/10.1016/j.commatsci.2020.109850

Richards, D. C., Abram, T. N., & Rennie, A. E. W. (2017). Designing digital materials with volumetric gradients Symposium conducted at the meeting of the 15th Rapid Design, Prototyping & Manufacturing Conference (RDPM2017)

Saha, C., O'donnell, T., Wang, N., & McCloskey, P. (2008). Electromagnetic generator for harvesting energy from human motion. *Sensors and Actuators A: Physical, 147*(1), 248-253.

Santos, I., Nieves, J., Penya, Y. K., & Bringas, P. G. (2009, 18-21 Aug. 2009). Machine-learning-based mechanical properties prediction in foundry production Symposium conducted at the meeting of the 2009 ICCAS-SICE

Sciaky. (2019). *The EBAM® 300 Series Produces the Largest 3D Printed Metal Parts & Prototypes in the Additive Manufacturing Market*. Retrieved 27/02, 2019, from http://www.sciaky.com/largest-metal-3d-printer-available

SD3D.COM. (2022). *PLA Technical data sheet*. Retrieved 03/03, 2022, from https://www.sd3d.com/wp-content/uploads/2017/06/MaterialTDS-PLA_01.pdf

Shabani, M., Mazahery, A., Rahimipour, M., Tofigh, A., & Razavi, M. (2012). The most accurate ANN learning algorithm for FEM prediction of mechanical performance of alloy A356. *Kov. Mater, 50*, 25-31.

Shabani, M. O., & Mazahery, A. (2011). The ANN application in FEM modeling of mechanical properties of Al–Si alloy. *Applied Mathematical Modelling, 35*(12), 5707-5713. https://doi.org/https://doi.org/10.1016/j.apm.2011.05.008

Shepherd, M. K., & Rouse, E. J. (2017). The VSPA foot: A quasi-passive ankle-foot prosthesis with continuously variable stiffness. *IEEE Transactions on Neural Systems and Rehabilitation Engineering, 25*(12), 2375-2386.

Sigmund, O. (2007). Morphology-based black and white filters for topology optimization. *Structural and Multidisciplinary Optimization, 33*(4), 401-424. https://doi.org/10.1007/s00158-006-0087-x

Sigmund, O., & Torquato, S. (1997). Design of materials with extreme thermal expansion using a three-phase topology optimization method. *Journal of the Mechanics and Physics of Solids, 45*(6), 1037-1067. https://doi.org/https://doi.org/10.1016/S0022-5096(96)00114-7

Singh, M., Haverinen, H. M., Dhagat, P., & Jabbour, G. E. (2010). Inkjet printing—process and its applications. *Advanced materials, 22*(6), 673-685.

Singh, V., & Gu, N. (2012). Towards an integrated generative design framework. *Design studies, 33*(2), 185-207.

Standards, U. S. N. B. o., & Nicodemus, F. E. (1977). *Geometrical considerations and nomenclature for reflectance* (Vol. 160): US Department of Commerce, National Bureau of Standards.

Stanford, B. K., & Dunning, P. D. (2015). Optimal topology of aircraft rib and spar structures under aeroelastic loads. *Journal of Aircraft, 52*(4), 1298-1311.

Stanley, K. (2014, 12/12/2014). *The NeuroEvolution of Augmenting Topologies (NEAT) Users Page*. Retrieved 04/04, 2020, from http://www.cs.ucf.edu/~kstanley/neat.html

Stanley, K. O. (2007). Compositional pattern producing networks: A novel abstraction of development. *Genetic programming and evolvable machines, 8*(2), 131-162.

Stanley, K. O. (2015, 5/6/2015). *The Hybercube-based NeuroEvolution of Augmenting Topologies (HyperNEAT) Users Page*. Retrieved 04/04, 2020, from http://eplex.cs.ucf.edu/hyperNEATpage/HyperNEAT.html

Stanley, K. O., D'Ambrosio, D. B., & Gauci, J. (2009). A hypercube-based encoding for evolving large-scale neural networks. *Artificial life, 15*(2), 185-212.

Stanley, K. O., & Miikkulainen, R. (2002). Evolving neural networks through augmenting topologies. *Evolutionary computation, 10*(2), 99-127.

Stansbury, J. W., & Idacavage, M. J. (2016). 3D printing with polymers: Challenges among expanding options and opportunities. *Dental Materials, 32*(1), 54-64.

Stappenbelt, B., & Cooper, P. (2010). *Mechanical model of a floating oscillating water column wave energy conversion device*. Retrieved 01/12/2021, 2021,

Sun, J., Jolly, M. R., & Norris, M. (1995). Passive, adaptive and active tuned vibration absorbers—a survey. *Mech. Des., 117*(B), 234-242.

Taj, S., Munawar, M. A., & Khan, S. (2007). Natural fiber-reinforced polymer composites. *Proceedings-Pakistan Academy of Sciences, 44*(2), 129.

Tang, Y., Dong, G., Zhou, Q., & Zhao, Y. F. (2018). Lattice Structure Design and Optimization With Additive Manufacturing Constraints. *IEEE Transactions on Automation Science and Engineering, 15*(4), 1546-1562. https://doi.org/10.1109/TASE.2017.2685643

Tanskanen, P. (2002). The evolutionary structural optimization method: theoretical aspects. *Computer methods in applied mechanics and engineering, 191*(47), 5485-5498. https://doi.org/https://doi.org/10.1016/S0045-7825(02)00464-4

Tarng, Y., Kao, J., & Lee, E. (2000). Chatter suppression in turning operations with a tuned vibration absorber. *Journal of materials processing technology, 105*(1-2), 55-60.

Tcherniak, D. (2002). Topology optimization of resonating structures using SIMP method. *International Journal for Numerical Methods in Engineering, 54*(11), 1605-1622.

Teimouri, M., & Asgari, M. (2019). Multi-objective BESO topology optimization for stiffness and frequency of continuum structures. *Structural Engineering and Mechanics, 72*(2), 181-190.

Tsai, T. D., & Cheng, C. C. (2013). Structural design for desired eigenfrequencies and mode shapes using topology optimization. *Structural and Multidisciplinary Optimization, 47*(5), 673-686. Tsai2013. https://doi.org/10.1007/s00158-012-0840-2

Tyflopoulos, E., Tollnes, F. D., Steinert, M., & Olsen, A. (2018). State of the art of generative design and topology optimization and potential research needs. *DS 91: Proceedings of NordDesign 2018, Linköping, Sweden, 14th-17th August 2018*.

Udupa, G., Rao, S. S., & Gangadharan, K. V. (2014). Functionally Graded Composite Materials: An Overview. *Procedia Materials Science, 5*, 1291-1299. https://doi.org/https://doi.org/10.1016/j.mspro.2014.07.442

Utela, B., Storti, D., Anderson, R., & Ganter, M. (2008). A review of process development steps for new material systems in three dimensional printing (3DP). *Journal of Manufacturing Processes, 10*(2), 96-104.

Venetis, J., & Sideridis, E. (2015). Approximate solution to three point bending equation for a simply supported beam. *Scientific Research and Essays, 10*(9), 339-347.

Verma, A., Singh, T., Chauhan, N. K., & Sarkar, K. (2016). A hybrid FEM–ANN approach for slope instability prediction. *Journal of The Institution of Engineers (India): Series A, 97*(3), 171-180.

Vicente, W., Zuo, Z., Pavanello, R., Calixto, T., Picelli, R., & Xie, Y. (2016). Concurrent topology optimization for minimizing frequency responses of two-level hierarchical structures. *Computer methods in applied mechanics and engineering, 301*, 116-136.

Vijaya Kumar, S. D., Lo Yin Kai, M., Arumugam, T., & Karuppanan, S. (2021). A Review of Finite Element Analysis and Artificial Neural Networks as Failure Pressure Prediction Tools for Corroded Pipelines. *Materials (Basel), 14*(20). https://doi.org/10.3390/ma14206135

Vonflotow, A. H., Beard, A., & Bailey, D. (1994). *Adaptive tuned vibration absorbers: tuning laws, tracking agility, sizing, and physical implementations*. presented at the meeting of the Inst. of Noise Control Engineering, VA, US.

Wang, S. Y., & Tai, K. (2005). Structural topology design optimization using Genetic Algorithms with a bit-array representation. *Computer methods in applied mechanics and engineering, 194*(36), 3749-3770. https://doi.org/https://doi.org/10.1016/j.cma.2004.09.003

Wizel, S., Margel, S., Gedanken, A., Rojas, T., Fernandez, A., & Prozorov, R. (1999). The preparation of metal–polymer composite materials using ultrasound radiation: Part II. Differences in physical properties of cobalt–polymer and iron–polymer composites. *Journal of materials research, 14*(10), 3913-3920.

Wong, K. V., & Hernandez, A. (2012). A review of additive manufacturing. *ISRN Mechanical Engineering, 2012*.

Wu, P., Wang, J., & Wang, X. (2016). A critical review of the use of 3-D printing in the construction industry. *Automation in Construction, 68*, 21-31.

X. Gu, G., Su, I., Sharma, S., Voros, J. L., Qin, Z., & Buehler, M. J. (2016). Three-Dimensional-Printing of Bio-Inspired Composites. *Journal of Biomechanical*

Engineering, 138(2), 021006-021006-021016. https://doi.org/10.1115/1.4032423

Xiao, A., Wang, B., & Jin, Y. (2013). Evolutionary truss layout optimization using the vectorized structure approach*IEEE.* Symposium conducted at the meeting of the 2013 IEEE Congress on Evolutionary Computation

Xie, Y. M., & Steven, G. P. (1993). A simple evolutionary procedure for structural optimization. *Computers & structures, 49*(5), 885-896.

Xie, Z., Qiu, L., & Yang, D. (2020). Analysis of a novel variable stiffness filleted leaf hinge. *Mechanism and Machine Theory, 144*, 103673. https://doi.org/https://doi.org/10.1016/j.mechmachtheory.2019.103673

Xu, Q. (2015). Design and development of a novel compliant gripper with integrated position and grasping/interaction force sensing. *IEEE Transactions on Automation Science and Engineering, 14*(3), 1415-1428.

Yang, W., Calius, E., Huang, L., & Singamneni, S. (2020). Artificial Evolution and Design for Multi-Material Additive Manufacturing. *3D Printing and Additive Manufacturing, 7*(6).

Yang, X., Xei, Y., Steven, G., & Querin, O. (1999). Bidirectional evolutionary method for stiffness optimization. *AIAA journal, 37*(11), 1483-1488.

Yang, X., Xie, Y., Steven, G., & Querin, O. (1999). Topology optimization for frequencies using an evolutionary method. *Journal of Structural Engineering, 125*(12), 1432-1438.

Yang, X. Y., Xie, Y. M., & Steven, G. P. (2005). Evolutionary methods for topology optimisation of continuous structures with design dependent loads. *Computers & structures, 83*(12), 956-963. https://doi.org/https://doi.org/10.1016/j.compstruc.2004.10.011

Yap, C. Y., Chua, C. K., Dong, Z. L., Liu, Z. H., Zhang, D. Q., Loh, L. E., & Sing, S. L. (2015). Review of selective laser melting: Materials and applications. *Applied physics reviews, 2*(4), 041101.

Yu, C.-H., Qin, Z., & Buehler, M. J. (2019). Artificial intelligence design algorithm for nanocomposites optimized for shear crack resistance. *Nano Futures, 3*(3), 035001.

Zhai, Y., Lados, D. A., & LaGoy, J. L. (2014). Additive Manufacturing: Making Imagination the Major Limitation. *JOM, 66*(5), 808-816. Zhai2014. https://doi.org/10.1007/s11837-014-0886-2

Zhang, Y., Bernard, A., Harik, R., & Karunakaran, K. (2017). Build orientation optimization for multi-part production in additive manufacturing. *Journal of Intelligent Manufacturing, 28*(6), 1393-1407.

Zhang, Y., Xiao, M., Gao, L., Gao, J., & Li, H. (2020). Multiscale topology optimization for minimizing frequency responses of cellular composites with connectable graded microstructures. *Mechanical Systems and Signal Processing, 135*, 106369. https://doi.org/https://doi.org/10.1016/j.ymssp.2019.106369

Zissis, D., Xidias, E. K., & Lekkas, D. (2015). A cloud based architecture capable of perceiving and predicting multiple vessel behaviour. *Applied Soft Computing, 35*, 652-661.

Appendix A

Genetic algorithm main loop

Initialisation

```
clc;

clear;

close all;

global model

%Importing the COMSOL MATALB Livelink

import com.comsol.model.*

import com.comsel.model.util.*

disp('111');

% load COMSOL file

model = mphload('test_block.mph');

disp('222');

%disable saving history files

model.hist.disable

n = 1;

lb = [4.5794, 23.002, 28.443, 28.853, 73.382, 79.891];

ub = [183.64, 1134.6, 1144.7, 1366.3, 3203.7, 3557.4];

% targets = Gen_target(n, ub, lb);

%targets = [10,60,110,160,210,260];
```

Problem Definition

```
CostFunction=@(x) CalcNatFreq(x);      % Cost Function
```

```
nVar=400;           % Number of Decision Variables



VarSize=[1 nVar];   % Decision Variables Matrix Size
```

GA Parameters

```
MaxIt= 100;      % Maximum Number of Iterations

Tol = 10;

nPop=50; % Population Size

pc=0.6;                 % Crossover Percentage

nc=2*round(pc*nPop/2);  % Number of Offsprings (also Parnets)

pm=0.08;                 % Mutation Percentage

nm=round(pm*nPop);      % Number of Mutants

mu=0.08;                % Mutation Rate

ANSWER=questdlg('Choose selection method:','Genetic Algorith',...

    'Roulette Wheel','Tournament','Random','Roulette Wheel');

UseRouletteWheelSelection=strcmp(ANSWER,'Roulette Wheel');

UseTournamentSelection=strcmp(ANSWER,'Tournament');

UseRandomSelection=strcmp(ANSWER,'Random');

if UseRouletteWheelSelection

    beta=8;         % Selection Pressure

end

if UseTournamentSelection

    TournamentSize=3;   % Tournamnet Size

end
```

```
% Array to Hold Best Cost Values

BestCost=zeros(MaxIt,n);

j = 1;

% for j = 1:n
```

Initialisation Algorithm

```
%target = targets(j,:);

tic;

empty_individual.Position=[];

empty_individual.Cost=[];

pop = create_population(nPop, CostFunction);

% Sort Population

Costs=[pop.Cost];

[Costs, SortOrder]=sort(Costs, 'descend');

pop=pop(SortOrder);

% Store Best Solution

BestSol(j)=pop(1);

BestSolSoFar(j)  = BestSol(j);

% Store Cost

WorstCost=pop(end).Cost;
```

Main Loop

```
it = 1;

prevsol = 0;
```

```
rep = 1;
restart = 1;
% for it=1:MaxIt
hold on
figure();
h = animatedline('Marker','o');
axis([0 50 -inf inf])
xlabel('Iterations')
ylabel('Fitness Value')
while it <= MaxIt && restart <= 1
    % Calculate Selection Probabilities
    if UseRouletteWheelSelection
        P=exp(-beta*Costs/WorstCost);
        P=P/sum(P);
        P=fliplr(P);
    end

    % Crossover
    popc=repmat(empty_individual,nc/2,2);
    for k=1:nc/2
        % Select Parents Indices
        if UseRouletteWheelSelection
            i1=RouletteWheelSelection(P);
            i2=RouletteWheelSelection(P);
```

```
        end
        if UseTournamentSelection
            i1=TournamentSelection(pop,TournamentSize);
            i2=TournamentSelection(pop,TournamentSize);
        end
        if UseRandomSelection
            i1=randi([1 nPop]);
            i2=randi([1 nPop]);
        end
        % Select Parents
        p1=pop(i1);
        p2=pop(i2);
        % Perform Crossover
        [popc(k,1).Position,
popc(k,2).Position]=Crossover(p1.Position,p2.Position);
        % Evaluate Offsprings
        popc(k,1).Cost=CostFunction(popc(k,1).Position);
        popc(k,2).Cost=CostFunction(popc(k,2).Position);

    end
    popc=popc(:);
    % Mutation
    popm=repmat(empty_individual,nm,1);
    for k=1:nm
```

```
        % Select Parent

        i=randi([1 nPop]);

        p=pop(i);

        % Perform Mutation

        popm(k).Position=Mutate(p.Position,mu);

        % Evaluate Mutant

        popm(k).Cost=CostFunction(popm(k).Position);

    end



    % Create Merged Population

    pop=[pop

        popc

        popm]; %#ok

    % Sort Population

    Costs=[pop.Cost];

    [Costs, SortOrder]=sort(Costs, 'descend');

    pop=pop(SortOrder);

    % Update Worst Cost

    WorstCost=max(WorstCost,pop(end).Cost);

    % Truncation

    pop=pop(1:nPop);

    Costs=Costs(1:nPop);

    % Store Best Solution Ever Found

    BestSol(j)=pop(1);
```

```
    % Store Best Cost Ever Found

    BestCost(it,j)=BestSol(j).Cost;

    % Show Iteration Information

    fprintf('Iteration %d : Best Cost = %.5f\n',it, BestCost(it,j));



    if prevsol == BestSol(j).Cost

        rep = rep + 1;

    else

        rep = 1;

    end

    if BestSol(j).Cost < BestSolSoFar(j).Cost

        BestSolSoFar(j) = BestSol(j);

    end

    if rep > 20

        pop = create_population(nPop, CostFunction);

        restart = restart + 1;

    end

    prevsol = BestSol(j).Cost;

    addpoints(h,it,BestCost(it,j))

    s = sprintf('Current Iteration: %d, Current fitness Value:%.2f Best Fitness Value: %.2f', it, BestCost(it,j), BestSolSoFar(j).Cost);

    title(s)

    if it > 30

        axis([0 inf, -inf, inf]);
```

```
    end

    drawnow;

    it= it+1;

end

% end
```

Results

```
figure;

plot(BestCost,'LineWidth',2);

xlabel('Iteration');

ylabel('Cost');

grid on;
```

Appendix B

Covariance matrix adaptation evolution strategy (CMA-ES) main loop

Initialisation

```
CostFunction=@Ackley;   % Cost Function

nVar=72;                % Number of Unknown (Decision) Variables

VarSize=[1 nVar];       % Decision Variables Matrix Size

VarMin=0.5;             % Lower Bound of Decision Variables

VarMax=10;             % Upper Bound of Decision Variables
```

CMA-ES Settings

```
% Maximum Number of Iterations

MaxIt=20;

% Population Size (and Number of Offsprings)

lambda=200;

% Number of Parents

mu=round(lambda/2);

% Parent Weights

w=log(mu+0.5)-log(1:mu);

w=w/sum(w);

% Number of Effective Solutions

mu_eff=1/sum(w.^2);
```

```
% Step Size Control Parameters (c_sigma and d_sigma);

sigma0=0.3*(VarMax-VarMin);

cs=(mu_eff+2)/(nVar+mu_eff+5);

ds=1+cs+2*max(sqrt((mu_eff-1)/(nVar+1))-1,0);

ENN=sqrt(nVar)*(1-1/(4*nVar)+1/(21*nVar^2));

% Covariance Update Parameters

cc=(4+mu_eff/nVar)/(4+nVar+2*mu_eff/nVar);

c1=2/((nVar+1.3)^2+mu_eff);

alpha_mu=2;

cmu=min(1-c1,alpha_mu*(mu_eff-2+1/mu_eff)/((nVar+2)^2+alpha_mu*mu_eff/2));

hth=(1.4+2/(nVar+1))*ENN;
```

Initialisation Algorithm

```
ps=cell(MaxIt,1);

pc=cell(MaxIt,1);

C=cell(MaxIt,1);

sigma=cell(MaxIt,1);

ps{1}=zeros(VarSize);

pc{1}=zeros(VarSize);

C{1}=eye(nVar);

sigma{1}=sigma0;

empty_individual.Position=[];

empty_individual.Step=[];

empty_individual.Cost=[];
```

```
M=repmat(empty_individual,MaxIt,1);

M(1).Position=unifrnd(3,5,VarSize);

M(1).Step=zeros(VarSize);

M(1).Cost=CostFunction(M(1).Position);



BestSol=M(1);

BestCost=zeros(MaxIt,1);
```

CMA-ES Main Loop

```
for g=1:MaxIt

    % Generate Samples

    pop=repmat(empty_individual,lambda,1);

    for i=1:lambda

        pop(i).Step=mvnrnd(zeros(VarSize),C{g});

        pop(i).Position=M(g).Position+sigma{g}*pop(i).Step

        for ii=1:24

            if pop(i).Position(ii)>10

                pop(i).Position(ii)=10;

            end

            if pop(i).Position(ii)<0.25

                pop(i).Position(ii)=0.25;

            end

        end

         for ii=25:48
```

```
        if pop(i).Position(ii)>6
            pop(i).Position(ii)=6;
        end
        if pop(i).Position(ii)<2
            pop(i).Position(ii)=2;
        end
     end
    for ii=49:72
        if pop(i).Position(ii)>8
            pop(i).Position(ii)=8;
        end
        if pop(i).Position(ii)<4
            pop(i).Position(ii)=4;
        end
    end

    pop(i).Cost=CostFunction(pop(i).Position);
    % Update Best Solution Ever Found
    if pop(i).Cost<BestSol.Cost
        BestSol=pop(i);
    end
end
% Sort Population
Costs=[pop.Cost];
```

```
    [Costs, SortOrder]=sort(Costs);
    pop=pop(SortOrder);
    % Save Results
    BestCost(g)=BestSol.Cost;
    % Display Results
    disp(['Iteration ' num2str(g) ': Best Cost = ' num2str(BestCost(g))]);

    % Exit At Last Iteration
    if g==MaxIt
        break;
    end
    % Update Mean
    M(g+1).Step=0;
    for j=1:mu
        M(g+1).Step=M(g+1).Step+w(j)*pop(j).Step;
    end
    M(g+1).Position=M(g).Position+sigma{g}*M(g+1).Step;
    for iii= 1:24
        if M(g+1).Position(iii)>10
            M(g+1).Position(iii)=10;
        end
        if M(g+1).Position(iii)<0.25
            M(g+1).Position(iii)=0.25;
        end
```

```
    end

    for iii= 25:48

        if M(g+1).Position(iii)>6

            M(g+1).Position(iii)=6;

        end

        if M(g+1).Position(iii)<2

            M(g+1).Position(iii)=2;

        end

    end

    for iii= 49:72

        if M(g+1).Position(iii)>8

            M(g+1).Position(iii)=8;

        end

        if M(g+1).Position(iii)<4

            M(g+1).Position(iii)=4;

        end

    end

    M(g+1).Cost=CostFunction(M(g+1).Position);

    if M(g+1).Cost<BestSol.Cost

        BestSol=M(g+1);

    end

    % Update Step Size

    ps{g+1}=(1-cs)*ps{g}+sqrt(cs*(2-cs)*mu_eff)*M(g+1).Step/chol(C{g})';

    sigma{g+1}=sigma{g}*exp(cs/ds*(norm(ps{g+1})/ENN-1))^0.3;
```

```
    % Update Covariance Matrix

    if norm(ps{g+1})/sqrt(1-(1-cs)^(2*(g+1)))<hth

        hs=1;

    else

        hs=0;

    end

    delta=(1-hs)*cc*(2-cc);

    pc{g+1}=(1-cc)*pc{g}+hs*sqrt(cc*(2-cc)*mu_eff)*M(g+1).Step;

    C{g+1}=(1-c1-cmu)*C{g}+c1*(pc{g+1}'*pc{g+1}+delta*C{g});

    for j=1:mu

        C{g+1}=C{g+1}+cmu*w(j)*pop(j).Step'*pop(j).Step;

    end

    % If Covariance Matrix is not Positive Defenite or Near Singular

    [V, E]=eig(C{g+1});

    if any(diag(E)<0)

        E=max(E,0);

        C{g+1}=V*E/V;

    end

end
```

Display Results

```
figure;

% plot(BestCost, 'LineWidth', 2);

semilogy(BestCost, 'LineWidth', 2);
```

```
xlabel('Iteration');

ylabel('Best Cost');

grid on;
```